Developing Ringdown Oscillation Monitoring Techniques using Synchrophasor Data with Applications to New Zealand Network

Jimmy Chih-Hsien Peng

A thesis submitted in partial fulfilment of the requirements for the degree of Doctor of Philosophy in Electrical and Computer Engineering, the University of Auckland, 2012.

For My Family,
thanks for all the support

Abstract

This thesis improves the performance of Kalman Filter and Prony Analysis for tracking multiple ringdown oscillations in stressed transmission networks. Prior to the start of this research, there were no detailed comparisons between both methods. Hence, detailed investigations were first conducted to address the merits of each technique. Subsequently, a number of modifications for enhancing the approximation accuracy of each method have been outlined. Developments were primarily conducted using synthetic signals and, assumed the ambient noise of the applied systems is white.

As a result, a sampling scheme has been integrated to traditional Prony Analysis resulting into an Enhanced Prony procedure. Instead of using a fixed sampling interval, the Enhanced Prony Analysis continuously selects a sampling interval appropriate to the network. This was achieved by utilizing a proposed condition number as a quality control index. Unlike the existing relative error approach, the condition number examines the adequacy of the sampling interval without prior knowledge of the values of the modal parameters. Overall, the Enhanced Prony Analysis has been shown to provide more reliable modal estimations.

In addition to monitoring the dominant oscillation, the functionality of Kalman Filter was extended to detect multiple modes. By, firstly, redefining the state variables to directly represent the modal contents and, secondly, Hankel Singular Value Decomposition was applied to provide more accurate estimates of the initial state variables. Since network dynamics are not linear, the use of Extended Kalman Filter was also adopted. The improved Kalman Filter is subsequently known as Extended Complex Kalman Filter (ECKF). Unlike Kalman Filter, ECKF is designed to operate in a non-linear non-predetermined operational environment. Its monitoring performance was also verified using a New Zealand case study.

Overall, the proposed ECKF technique provided an estimation accuracy at par with Prony Analysis while retaining Kalman's recursive nature of implementation. Although both improved methods are suitable for tracking multiple oscillations simultaneously,

ECKF is considered to be the more attractive option for the New Zealand operation. Meanwhile, parallel-processing was applied to both detection methods. Compared with the traditional sequential computation, parallelizing the monitoring algorithms was able to achieve faster computing speeds. Hence, it was identified as a suitable implementation solution for realizing future monitoring algorithms.

Lastly, this thesis investigated the operation of Power System Stabilizers (PSS) to damp the inter-area oscillations when utilizing the remote synchrophasor measurements. The objective was to examine the degradation of the damping performance under different load characteristics. Overall, the use of the remote phasor data offered a better observability for the controller. Damping performance was improved when compared with conventional design. PSS, using a combination of remote and local signals, are less affected by the attributes of the load. The worst damping performance was identified under constant power load while the best damping performance occurred under the constant impedance.

Acknowledgments

This thesis represents a truly enormous investment for me. The contents cover my work between March 2008 to July 2011 and perhaps will be the most rewarding accomplishment in my life. However, it is not only my effort that has been required to get to this point; there are many people that I need to thank. Each of these people has provided me with something, and without them it would have been much more difficult to slog my way through.

Firstly, I'd like to thank my supervisor, Dr. Nirmal Nair. His ability to endlessly proof read draft papers and his research suggestions have been a huge amount of help. Nirmal is a limitless source of ideas and wisdom, both in regards to electrical power systems and myriad other topics. In addition, I really appreciated the guidance provided by my provisional PhD committee. Their advices have helped me avoid several unnecessary detours during my research.

Secondly, a big thanks goes to the University of Auckland Scholarship Office for their financial support over the course of this thesis. Life would indeed have been a struggle without it.

Thirdly, I would also like to thank my peers and friends: Michael Kissin, Prem Kumar, Andrew Meads, Janet Meads, Waqar Qureshi, Ao Qian, Craig Smith, Akshya Swain, Feng Wu, Hunter Wu, Jian Zhang and Stephen Zhao. Each person has helped me provide technical and moral support throughout the process of researching and writing this thesis. Thanks everyone for accompanying me on this great and memorable journey.

Finally, but by no means least, I would like to thank both of my parents, Kevin and Stacey, as well as my brother Andrew. Their ability to stay positive even when my completion date slipped for what seemed like the ten thousandth time was invaluable. Don't worry guys; it's finally done.

- Jimmy Peng
January, 2012

Contents

List of Figures

List of Tables

Nomenclature

Acronyms

AR	Autoregressive
ARMA	Autoregressive Moving Average
BPA	Bonneville Power Administration
CPU	Central Processing Unit
DAE	Differential-Algebraic Equation
DFT	Discrete Fourier Transform
ECKF	Extended Complex Kalman Filter
EU	European Union
FACT	Flexible AC Transmission devices
GPS	Global Positioning System
HTLS	Hankel Total Least Square
HHT	Hilbert-Huang Transform
HSVD	Hankel Singular Value Decomposition
HVDC	High Voltage Direct Current
LP	Linear Prediction
MIMD	Multiple-Instruction Multiple-Data
PDC	Phasor Data Concentrators
PE	Processing Element
PMS	Phasor Measurement System
PMU	Phasor Measurement Unit
PNNL	Pacific Northwest National Laboratory

PSS	Power System Stabilizer
R3LS	Regularized Robust Recursive Least Square
RLS	Recursive Least Square
RMS	Root-Mean-Square
RTU	Remote Terminal Unit
SCADA	Supervisory Control and Data Acquisition
SIMD	Single-Instruction Multiple-Data
STT	Small Tactical Terminal
SVC	Static Var Compensator
SVD	Singular Value Decomposition
TCP/IP	Transmission Control Protocol/Internet Protocol
USA	United States of America
WAMS	Wide Area Monitoring Systems
WACS	Wide Area Control Systems
WECC	Western Electricity Coordinating Council
WSCC	Western Systems Coordinating Council
WT	Wavelet Transform

Symbols

A	The data matrix of the Linear Prediction model
a	The autoregressive coefficients representing the poles
b	The autoregressive coefficients representing the zeros
C	The Covariance constant for Kalman Filter
D	The rows of Hankel Singular Value data matrix
E	The column/rank of Hankel Singular Value data matrix

F	The truncated rank of Hankel Singular Value data matrix
det	The determinant of a matrix
f	The oscillatory frequency
g	The Kalman Filter gain
H	The observation vector for ECKF
I	The identity matrix
J	The cost function
K	The covariance matrix
k	The current time instance
L	The estimated system order (much larger than m)
Mag	The magnitude of the sinusoidal waveform
m	The system order of the signal
N	The total number of extracted data
n	The number of oscillatory modes in the signal
P	The covariance matrix for ECKF
p	The vector containing the AR coefficients for Kalman Filter
Q_m	The correlation factor of the measurement noise
Q_p	The correlation matrix of the process noise
R	The residue
S	The left eigenvector matrix of HTLS
T	The right eigenvector matrix of HTLS
tr	The trace of a matrix
U	The left eigenvector matrix of SVD
u	The input signal
V	The right eigenvector matrix of SVD

v	The noise component
X	The state vector
y	The measured signal
Z	The Discrete-time pole
α	The local weighting constant for WACS-based PSS
β	The remote weighting constant for WACS-based PSS
ε	The estimation/prediction error
ζ	The damping ratio
κ	The condition number
λ	The eigenvalue
σ	The damping factor
τ	The time constant
Φ	The phase angle of the Sine wave
Ψ	The mother wavelet or the phase function for R3LS
ω	The angular frequency

Operators

+	The Moore-Penrose pseudoinverse operator
H	The conjugate transpose operator
^	The estimated value
|| ||	Absolute value

1 Introduction

The first operating power grid was built by Thomas Edison in September 1882. It marked the beginning of the modern electricity infrastructure. Due to technological limitations in the late 19th century, distributed generation was considered the practical way to supply electricity. However, as the generation capacity of turbo generators increased to megawatts range combined with the use of alternating current for distant power transmission, the ability to have large generation plants supplying remote load centres became economically feasible. As a result, the use of electricity as a substitute for steam became widely adopted in many industrial applications.

In the 1920s, local governments constructed large-scale transmission lines to link industrial parks. The initial motivation was for military purposes such as ammunition production, but civil loads were gradually connected to the power grid. As the use of electricity continues to grow in the industrial, commercial and residential sectors, the demand for reliable and secure power transfer becomes ever more crucial. Therefore, managing the power grid has become a critical part of the economic infrastructure for nations.

In order to provide secure and economical power transfer between regions, interconnection of neighbouring utilities was established. Benefits include providing emergency support between the networks, optimizing the installed equipments at strategic locations, enhanced the operating security, and reducing the capital investment in the modern grid. During the 1950s and 1960s, the developed countries saw vast expansion in the transmission infrastructure. They linked the surrounding utilities together in a continuous expanding transmission web of enormous complexity.

Within an interconnected grid, the equipment settings and the control actions are no longer self-contained. They interact with each other. Varying one device can potentially affect the parameters or operations of others. Analyzing the operational

reliability of such a network is a very intensive computational task. Thus, it naturally evolved to becoming a centralized operation centre to provide a global supervision of the power grid [1, 2].

With the boom of electronics in the 1970s, personal computers in the 1980s, telecommunication in the 1990s and the internet in the 2000s, the daily power usages have increased rapidly. Therefore, the ability to manage the grid and maintain a secure supply is becoming increasingly more important in industrialized nations.

1.1 *Overview of the New Zealand Grid*

The New Zealand power grid can be regarded as a mature but stressed system. Its total generation capacity in 2009, was 8700 MW. Around 5300 MW were in the North Island, and 3400 MW in the South Island. That made an average total energy production of 42,000 GWhr [3]. The main generation source in New Zealand is hydro; accounting for 54% of the country's total generation [4]. The pursuit for sustainable green energy has resulted in thermal generation based on coal decreasing in the past two decades. It currently occupies around 15% of generation. On the other hand, renewable sources like geothermal and wind farms are rapidly being deployed around the country. They respectively occupy around 8% and 3% of the generation capacity [4, 5]. These percentages are expected to increase in the near future as part of the government's 2050 energy strategy, with the target of 90 per cent of electricity to be generated from renewable sources by 2025. Many of the new sustainable generations will be situated at sites which are remote from load centres. Compared with existing generating stations that is a significant change in terms of the system operation [6].

Although the generation capacity is sufficient to meet the nation's peak demand of 7000 MW, the distribution of power demand is significantly unbalanced. According to the government census conducted in 2006, approximately 76% of the total population lived in the North Island and about 43% of that population are in Auckland city which is located in the northern half of the North Island [7]. Consequently, power generated in the middle of South Island is transferred across the Cook Strait via 350 kV HVDC

cable to supply the daily demand of the North Island. The interlink HVDC transfers around 1050 MW during peak demand and that is expected to rise in the future. New Zealand's transmission infrastructure is based on 220 kV and 110 kV lines, which were mostly constructed in the 1950s and 60s [5]. Presently, the entire grid consists of 11,800 km of lines and 178 substations and switchyards. They are owned and operated by Transpower New Zealand Limited. Many of these assets are older than 40 years and several have been in service for over 70 years. Hence, transmission upgrades are inevitable. As a result, Transpower has recently changed its strategy to a concentrated period of high reinvestment in its assets. Major projects underway include building 192 km long 400 kV lines in the North Island and upgrading existing HVDC cables and transmission framework. An estimate value of at least $2 billion NZD will be spent in transmission projects within this decade [8].

1.1.1 Challenges in the System Operations

Despite the physical infrastructure upgrades, the rate of increase of the annual power demand is faster. As a result, the system operation is becoming more pressured to maintain the operational security. Given that new transmission infrastructure takes a longer time to commission, it will not address any immediate transmission capacity shortages. Additionally, the establishment of the wholesale electricity market operation in 1996 has caused the system to experience new power flow patterns. The power flow patterns affecting the grid operation are becoming less predictable.

Therefore, an alternative monitoring architecture is needed to track the growing transmission capacity in the short/medium term and also to provide sufficient observability of the system dynamics when the future infrastructure upgrades are completed. The recently proposed Wide Area Monitoring Systems (WAMS) is regarded as a feasible solution [9].

1.2 *The Dawn of the Wide Area Monitoring Systems*

Conventional SCADA systems are unable to measure the phase angles or provide fast, reliable, network data oriented to the monitoring of the system dynamics. Additional limitations of SCADA systems can be referred to Appendix A. Therefore, designing a new architecture will be very useful.

In summary, the desired improvements to the present supervising systems include: upgrading from a static to a dynamic supervision; from an offline to an online; from a conservative to an optimized operation, from an isolated to a cooperative system; and from consideration of a single contingency to that of multiple cascading contingencies. These improvements can be realized by utilizing the data collected from the Phasor Measurement Units (PMUs) that are installed across the grid. The infrastructure is known as Wide Area Monitoring System (WAMS) [10]. In simple terms, the motivation of WAMS is to provide a high flexibility in the operation and the control in a close-to-real-time environment.

Unlike the existing RTU/SCADA systems, PMU/WAMS systems can extract both the magnitudes and the associated phase angles in an unified time-stamped manner using Global Positioning System (GPS), and at a faster sampling rate. Hence, the operators are able to assess the system performance instantaneously. That has reshaped the view of conventional grid management. A visual illustration of a general WAMS infrastructure is shown in Figure 1-1.

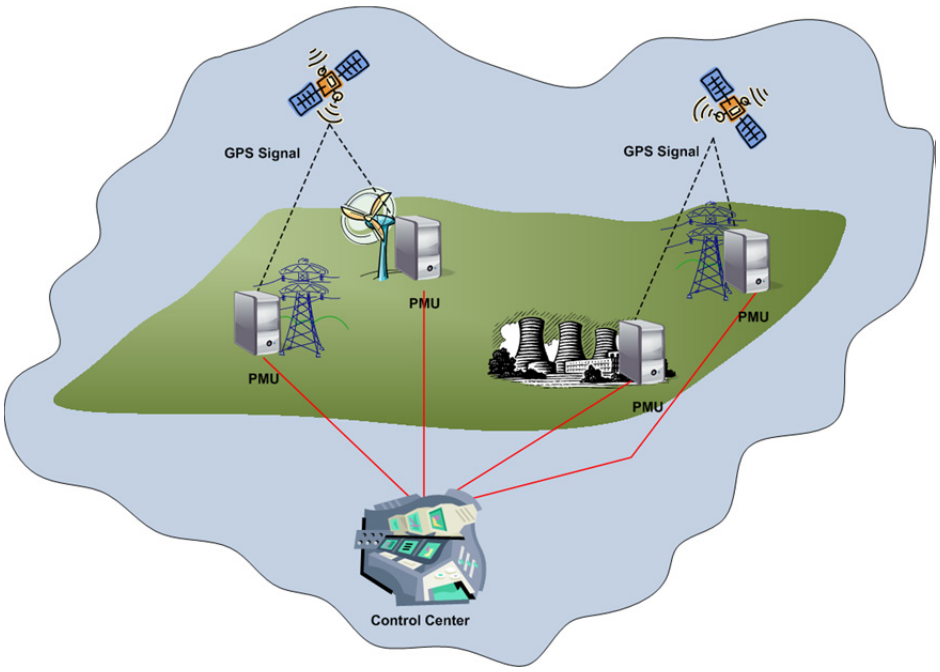

Figure 1-1 Overview of a simple WAMS infrastructure

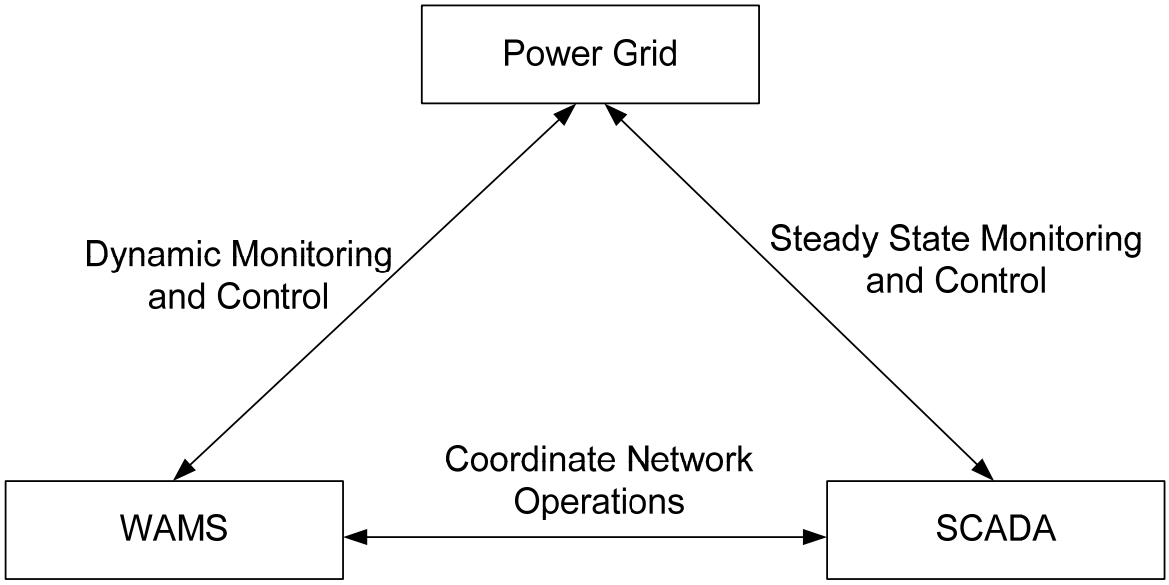

Figure 1-2 Outline of the projected WAMS role in the existing infrastructure

Instead of being embedded inside the SCADA systems, the proposed WAMS framework will operate alongside it and supervise the dynamic operations such as online estimation of the stability limits, and the online optimization for the decision-making [11, 12]. Additionally, the independency between the two infrastructures will make it much easier to expand them in the future. A visual illustration of WAMS role is shown in Figure 1-2.

1.2.1 The Birth of the Phasor Measurement Unit (PMU)

The first commercial PMU, shown in Figure 1-3, was launched in 1991 by Virginia Tech, USA. The first generation was much larger than a modern PMU, which is typically a module card inside a protection relay or any monitoring device. As the name suggests, the principle function of PMUs is to measure the positive sequence voltages and the currents from the secondary side of the transformers [13, 14]. These are represented by a complex number called a Phasor, which can be computed by Discrete Fourier Transform (DFT). If the measured signal is not a pure sinusoid, the phasor would correspond to its fundamental frequency.

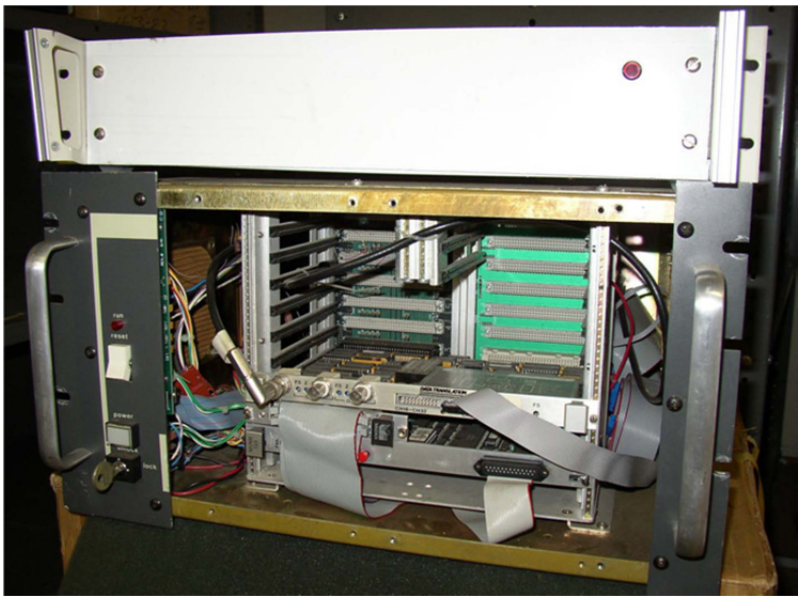

Figure 1-3 First commercial PMU developed by Virginia Tech [15]

The phase angle can only be extracted if the monitoring instruments are tuned to a common time that is independent of geographical position. That is achieved by synchronizing all PMUs to a universal time with the aid of GPS. Thus, the phase angle at any node can be computed by comparing it to the phase angle at a reference bus.

Most PMUs are capable of providing 6 to 60 measurements per second, which is considered adequate for capturing the system dynamics. However, it should be noted that different sampling rates are used depending on the intended operation. For example, a slower sampling is needed for tracking inter-area dynamics; faster rates are needed for monitoring the local behaviours. The performance requirements of PMU are outlined in the IEEE synchrophasor standard (C37.118), [16].

Since all the phasors are GPS time-stamped, the progression of any network dynamics can be tracked with high precision by analyzing the system-wide phasors. Subsequently, validation of the system models and their parameters, as well as extraction of the information related to the aspects such as power quality and the dynamic security of the grid, can be assessed. Network uncertainties can be minimized, which will aid towards the potential increase in the transmission capacities by being able to optimize security constraints.

1.2.2 A Brief History of Wide Area Monitoring System

The idea of tracking the state of the power grid online based on real-time measurements began after the 1965 blackout in the North Eastern power grid in North America [13, 17]. Nevertheless, due to technological limitations, it was not until 1976 that the first successful attempt at extracting the real-time measurements took place. At Hydro Quebec, the shift in the voltage angle between Arnaud and Boucherville was measured at a sampling rate of 1 Hz. The monitoring devices were installed at two 735 kV substations which were separated by more than 1000 km. In order to arrange the data into a timely order, Loran C-based clocks and STT satellites were used to provide the time synchronization. Since the late 1980s, other utilities, such as Bonneville Power Administration (BPA) also began investigating WAMS. Among all involved parties there is a common interest: collect the dynamic data to monitor the operational stress of long-distance transmission lines. To be specific, the common objective is to track the undesired inter-area oscillations that are prone in the long power lines. Such a concern is classified under small-signal stability. It is increasingly threatening the network operation since the 1980s. The simplest resolution is to restrict the transmission capacity, but the resultant effect is major bottlenecks in the transmission grids to meet the power demand. Especially in the modern deregulated market condition, reducing the power transfer equates with a loss of money due to increased constraint rentals.

Nonetheless, in the 1970s and 1980s, the rapid deployment of this technology to provide dynamic monitoring capability was not practical due to technological constraints. Although the first commercialized PMU was launched by Virginia Tech in 1991, few were deployed due to their implementation cost [18]. Hence, it was not until the mid 1990s that implementation of WAMS began to take place. That was made possible as powerful computing tools and the high speed telecommunication broadband became more mature and economical.

Interest in establishing WAMS were again raised after the massive breakup of the western interconnection in USA on August 10, 1996. The cause was that analyzed results based on inaccurate or out-dated models give erroneous conclusions. Such issues could have been resolved by analyzing time stamped phasor data instead of

those of the SCADA. As a result, in 1997, BPA began redesigning its measurement systems to facilitate WAMS functionalities [18]. Unfortunately, this was not followed by the other grid operators. In the late 1990s, the WAMS deployments were limited. Nevertheless, a worldwide interest in WAMS has been continuously increasing since then.

Although more WAMS applications were explored and deployed in the 21th century, the final push for WAMS technology was determined in 2009. The announcement of a multi-billion dollar stimulus program towards renewable energy, and establishing a new electricity “smart grid” in the USA encouraged many utility companies around the world to invest in the WAMS technology. Additionally, a number of WAMS extensions, amongst the neighbouring utilities, provide a greater awareness of the system operation across the whole grid. As of 2010, WAMS has been operating in:

- Australia [19-22]
- Brazil [21, 23-25]
- Canada [26]
- China [23, 27-30]
- Colombia [31]
- European Union [9, 21, 32-34]
- India [23, 35, 36]
- Japan [37-39]
- Korea [40]
- Mexico [23, 41, 42]
- New Zealand [43-47]
- USA [9, 23, 48-53]

Presently, WAMS is predominately deployed in mature electricity networks due to their aging infrastructure and high growth potential in power consumption. Although the modern PMUs are capable of achieving a sampling rate of 60 Hz, it is only possible with the presence of adequate communication bandwidths. Hence, the fundamental assumption of WAMS is that the installed power systems already have a fibre-optic, or equivalent, based communication network. Despite the great progress made on proposing PMU/WAMS applications; there is still plenty of work to be done

before there is full utilization of the phasor data and extraction of effective information using them [9]. As a result, most of the dynamic operating decisions are still being dispatched by SCADA. More decision making roles may be given in the future as WAMS becomes more mature.

1.2.3 The WAMS Infrastructure

The primary objective of the WAMS deployment was to take a step away from existing steady-state of SCADA systems to a fast dynamic view of the entire grid. Similar to the SCADA systems, the Wide Area Monitoring Systems also uses a hierarchy-based infrastructure as shown in Figure 1-4. Although there are commercial devices that offer dedicated phasor monitoring, most of the operators integrate the phasor applications into their existing line protection relays. That is a more cost effective solution which can be easily installed by inserting an additional module into the relay. Note that the protection and the monitoring operations are independent to each another. Similar to RTUs, measurements are collected at the secondary side of the transformer and each PMU acts as a node in the monitoring framework.

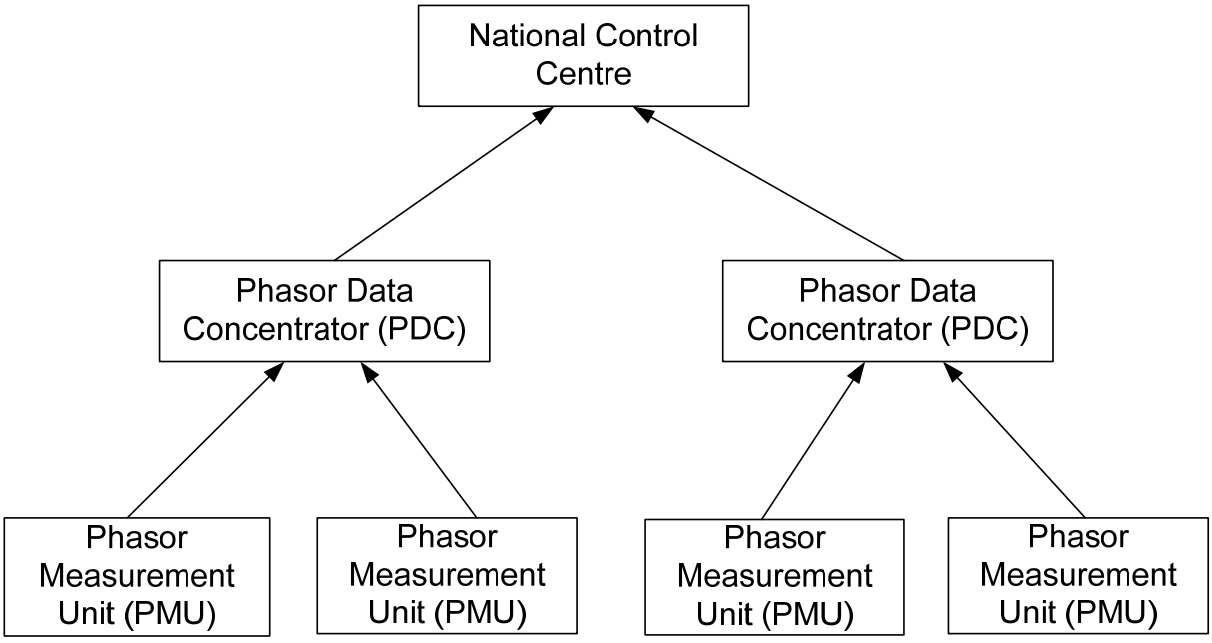

Figure 1-4 Outline of the WAMS framework [12]

Because of differences in the geographical distances and the communication equipment, the phasor data that are simultaneously measured from the various remote devices may arrive at their designated location in different times. Each measurement is time-stamped, but sorting and dispatching them to their intended destinations tends to be an involved processing task. The sheer volume and the speed of the incoming phasor measurements can be described as a never-ending flow of data [18]. In order to coordinate the incoming phasors, Phasor Data Concentrators (PDCs) are used to supervise the regional PMUs. They act as an intermediate processing station, and manage the data distribution for the monitoring applications. In order to preserve the past data, for planning or training purposes, PDC also provide data archiving features.

Depending on the complexity of the grid, and the number of PMUs, there may be several layers of PDCs between PMUs and the national control centre. Amongst the presently published WAMS developments, Hydro Quebec has the most sophisticated framework which consists of two PDC layers.

The main purpose of the national control centre level is to evaluate the network dynamic behaviours after disturbances, such as changes in the line loading or, the generation dispatch following a fault. They are computed from the phasor data collected from many geographical locations in the grid. Compared to the conventional SCADA's scan rate in the 2 to 10 second range [54], the typical 30 Hz sampling rate of WAMS provides the system operators with faster alerts to any growing global instabilities caused by factors like, inter-area oscillation, or, islanding.

1.2.4 Outline of the New Zealand WAMS Infrastructure

The current and the near-future characteristics of New Zealand transmission grid can be characterised as follows:

1) An increasing power demand from distant load centres.
2) Stressed transmission assets from the growing power transfers between the regions.
3) A strategic shift towards a large scale integration of renewable energy, like the wind, to reduce the carbon footprint from the electricity generations.

They all contribute to the challenges of maintaining the security of the supply [3, 4]. Consequently, the resultant growing dynamic complexity has made it much more involved to sustain a reliable operation with the current SCADA monitoring system. Any failed detection of the disturbances can potentially trigger a wide-spread blackout [8, 46].

Thus, the idea of Wide Area Monitoring System (WAMS) based on Phasor Measurement Units (PMU) was explored by Transpower. The primary motivations for Transpower to install PMU and subsequently establish the WAMS framework were:

1) To enhance the transmission capacity by using PMU data to detect any abnormal dynamic behaviours like poorly damped oscillations.
2) To improve the operational confidence by regularly validating the power system models based on the field data.
3) To elevate situational awareness by conducting the time-domain analysis at a close-to-real-time environment.

The proposed system is known Phasor Measurement System (PMS) and is presently under the Grid Model Validation project [43]. In the near future, WAMS will be incorporated into the Transmission 2040 project, which was launched in the winter of 2008 [55].

Based on these criteria, in 2007, Transpower have located 10 substations that are suitable for installing PMUs: 5 in the North Island and 4 in the South. They are: Huntly (HLY), Whakamaru (WKM), Stratford (SFD), Bunnythorpe (BPE), Haywards (HAY), Islington (ISL), Twizel (TWZ), Roxburgh (ROX), North Makarewa (NMA) and Tiwai (TWI). All PMUs were installed for monitoring the 220 kV lines and a geographical mapping of these locations are shown in Figure 1-5.

Figure 1-5 The operational PMU sites within New Zealand since 2008

The red circles refer to PMU sites; the black triangles and the orange squares represent the main generation reserves and Phasor Measurement System major load centres respectively. The solid and the blue dash lines correspond to the 220 kV lines and the HVDC link. The installation procedures and the tests are conducted based on the guidelines outlined in [16, 56, 57]. More details regarding to the development of the New Zealand WAMS infrastructure can be referred to Appendix B.

1.3 *A Summary of the Current WAMS Applications*

Due to technological and economic limitations, Phasor Measurement Units are not able to be installed at all buses. Thus, the variety of the available WAMS functions vary depending on the grid's PMU allocation. A brief description of the currently operational WAMS applications is as follows:

1) Corridor monitoring [21, 27, 34, 35, 53, 58]:
   Determines the present transmission strength by calculating the corresponding voltage phase angle differences.
2) Frequency and power plant outage detection [9, 31, 59]:
   Identifies the forced unit outage, due to severe disturbances, by continuously tracking the system frequency gradient. The warnings are also issued in the event of a frequency deviation [60].
3) Line thermal loading [9, 21, 61]:
   Evaluates the present line temperature by measuring the power losses and monitoring the changes in the line resistance due to thermal balance.
4) Island detection [62-64]:
   Notifies the operators when an islanding occurred due to operating instability. Subsequently, it dynamically determines the appropriate islanding boundaries for the island-specific loads and the generation balances.
5) Oscillation detection [28, 30, 46, 48, 65-67]:
   Detects any lightly-damped or unstable inter-area oscillations. They usually occur due to the lack of the damping torque at the generator rotors.
6) Voltage stability assessment [9, 21, 52, 68, 69]:
   Estimates the load characteristics after a contingency, and evaluates the potential of any long term voltage instability.
7) Commercial Operation [9]:
   Offers detailed dynamic information to predict the future energy pricings.
8) Model validation and fine-tuning [59, 70-73]:
   Assesses the adequacy of the present simulating models by comparing the computed results with the actual field data.

9) Post-mortem study of major events [15, 34, 53, 74-77]:
   Recorded network behaviours are analyzed for planning purposes such as, future infrastructure investment.

Applications 1) to 6) are conducted online. They are updated within seconds or minutes, depending on the application and the experienced disturbances. Referring to Pourbeik *et al.* in [9], the data collection time for some of the popular WAMS applications are summarized in Table 1-1. A communication time below 200 ms can be achieved with TCP/IP system while anything below 20 ms is almost impossible even with TCP/IP dedicated channels. With the aid of powerful modern computing hardware, the update time of any WAMS applications are mainly based on data acquisition procedure, while the associated computational time is usually negligible in comparison [78]. The alarms are then raised in the steady-state SCADA system by referring to the computed WAMS results.

Applications 8) and 9) are carried out in an offline environment. In this case, their aim is to provide the network planners with the ability to identify the trend of the future grid operations. Thus, better coordination of the infrastructure investments and designing better control strategies can be realized. Operational planning requires accurate static and dynamic system data. The generation and the load models have a strong influence on the oscillatory behaviour, the voltage stability, and the transient stability. Therefore, by providing constant updates of the existing simulation models, blackouts, such as the one in August 1996, could be prevented in the future.

Table 1-1 The estimated data acquisition time for some of the popular WAMS applications

Applications	Sampling window needed for the Intended Algorithm
Thermal Monitoring	20 ms
Oscillation Monitoring	≈ 10 s (ringdown), ≈ 10 min (ambient)
Voltage Stability	20 ms ~ 300 s

Apart from improving the existing WAMS applications, more monitoring and control features are currently being investigated or tested. Some of the promising future WAMS functions include:

1) Online state estimation [79-83]:
   Enhances the state estimation accuracy and the speed by using time-stamp measurements.
2) Oscillation damping control [21, 71, 84-86]:
   Improves the inter-area damping performance by using the remote and the local Phasor signals.
3) Power flow control [9, 87, 88]:
   Provides better utilization of the transmission capacity while maintaining the system integrity. This is closely related to the market profits in any deregulated networks.
4) Load shedding [42, 53, 89-91]:
   Minimizes the overshedding in the event of a frequency or a voltage instability. This is achieved by modelling the load online and subsequently analyzing the required margins.
5) Reactive compensation [26, 92]:
   Allows better coordination of the compensation equipments to enhance the operating margins.
6) Voltage stability assessment [12, 26, 40, 90, 91, 93-95]:
   Conducts online sensitivity analysis to monitor the long term voltage instabilities. Constructing P-V curves to analyze the operating region is also considered.

Most of these projected functions are associated with incorporating the global signals into the local controllers. This is a feasible option for solving the inter-regional problems. These control applications are classified as Wide Area Control System (WACS). Compared to WAMS, WACS is still relatively at the "*drawing board"* phase and will only be considered when WAMS has become more mature following more widespread deployments. Nevertheless, the growing research publications in

formulating the WACS applications have clearly strengthened the motivation for establishing WAMS in most of the modern power grids.

Amongst all the published Wide Area Monitoring Applications, detecting the inter-area oscillation is one of its most widely adopted functions. It has been integrated into the system operation in many grids and has helped the operators to enhance the reliability of the long distance transmission capacity. However, the oscillation monitoring aspect has only been recently considered, and tested offline, in the New Zealand grid. Unlike other developed nations, the WAMS development only began in 2007. It was always a great interest for system operators to track dynamic behaviours in real-time. As a result, the oscillatory detection was selected as the first dynamic application to be monitored by WAMS in real-time.

1.3.1 Monitoring the Oscillations in the New Zealand Network

The New Zealand network is a longitudinal power grid with the major load centres and the generation sources located at its physical extremities. It is also prone to electromechanical oscillations, like those experienced by WSCC. Currently, the New Zealand grid transfers around a peak power of 1,000 MW over a distance of more than 1,000 km from the central South Island to the upper North Island. That has resulted in the occurrence of one local and two Inter-Area oscillations. They are:

- 1.6 Hz local mode that exists in the main generation reserve situated in the middle of the North Island.
- 1.1 Hz inter-area mode that is present in the middle of the South Island. The exact participating groups of the generators are not known as the generation plant status reports are not shared with system operators in the deregulated market. The inter-area is speculated to involve with the hydro generations in the middle of South Island and the generation reserves in the North Island.
- 0.7 Hz inter-area mode is at the bottom of the South Island. It exists in the two double circuit tie-lines which supply the aluminium smelter plant in Tiwai.

Unlike those experienced in the North American or the European power grids, the frequency of the electromechanical oscillations are widely apart. Although the power grid was able to tolerate these oscillations in the past, their presence can no longer

be ignored as the recent peak transmission capacity and the load centres continue to grow. Therefore, using the PMU data to track the lightly damped or unstable oscillatory behaviours is identified as another application for the system operation.

Presently, commercial Psymetrix software is applied to extract the oscillatory information from the collected PMU data. Furthermore, Transpower uses PI Soft data acquisition system to collect the phasor measurements, as shown in Figure 1-6. They are exported in Microsoft Excel or MATLAB formats [45]. Thereafter, cross validations of the estimated oscillatory parameters using Prony Analysis can be conducted. However, these systems are presently operating in an offline environment and their results are applied mainly for the planning purposes. Hence, there are currently no industry standardized online monitoring methods for tracking the oscillations in the New Zealand network [46].

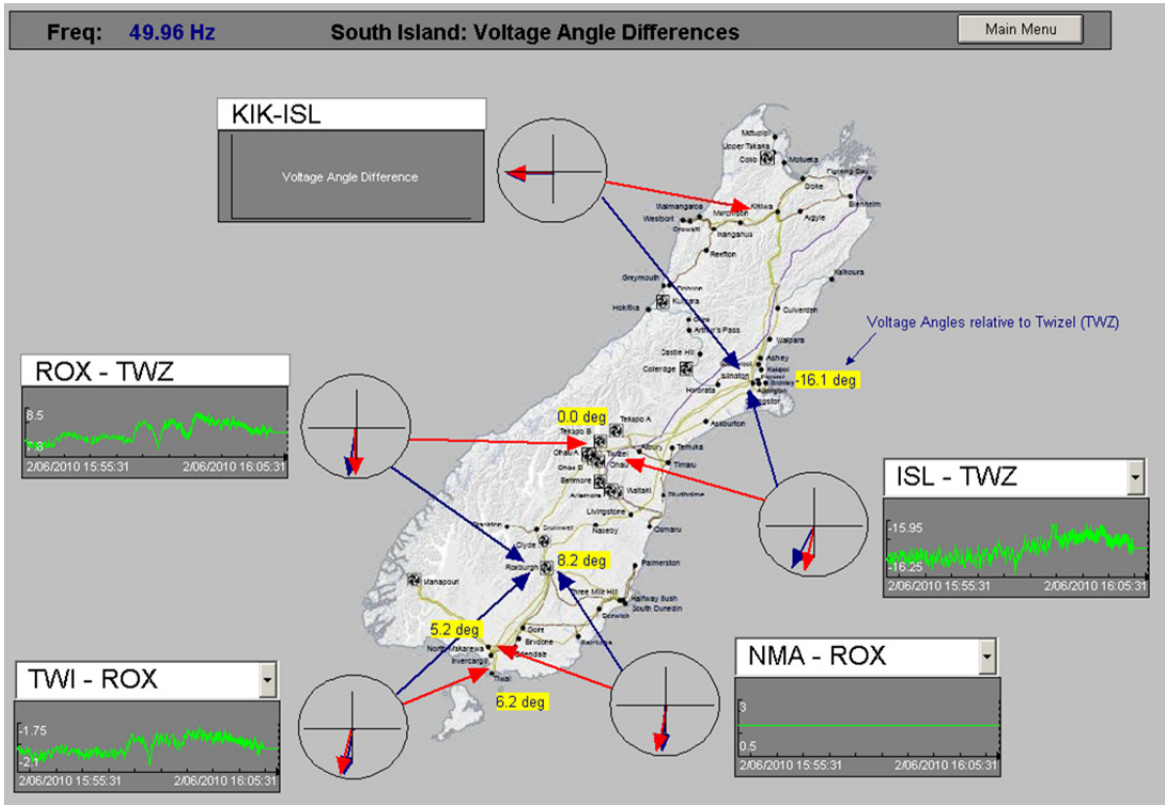

Figure 1-6 A visual representation of the South Island Phasor data in PI Soft platform

1.4 *Motivation for the thesis*

After learning the lessons from many blackouts around the world, there is a growing consensus in New Zealand to upgrade the local solutions to a more cooperative defence framework in order to effectively minimize blackouts. This research is proposed in the context of the emerging concerns regarding to the power system performance and its impact on the real-time system security assessment due to the various factors stressing the electrical network operation. Since PMUs are being installed into the New Zealand grid for the very first time, the number of initial Wide Area Monitoring System applications is limited. Presently, WAMS are implemented and tested on a central computer at Transpower. Only mature and passive WAMS applications that have been tested are considered for the New Zealand system. Thus, monitoring multiple electromechanical oscillations using synchrophasor data is identified as the primary focus of this dissertation.

However, presently deployed oscillation monitoring techniques are still in the early stage of their operations. For this reason, this thesis investigates and develops oscillation monitoring algorithms that meet the needs of the New Zealand power grid, and those with a similar dynamic nature. The scope of this research is to formulate detection schemes, and evaluate their capabilities using synthetic synchrophasor signals. Implementation issues such as hardware integration or, field tests using real measurements are beyond the scope of this thesis.

1.5 *Contributions of the Thesis*

This dissertation has identified and improved two monitoring techniques to be applied into the New Zealand grid operation. In addition, these methods are later implemented in a parallelized manner to provide faster computing performance. Although the primary scope was towards the monitoring aspect, the impact of the load characteristics towards a WACS-based damping strategy has also been investigated.

In total, one journal and twelve conferences, of which three are invited papers, have been published as a direct result of the work carried out for this thesis. In addition to

these, three more journal papers are currently under review, or, are being written. A complete list of these publications is presented in Subsection 8.2 of Chapter 8.

In summary, this dissertation has made five original contributions. They are summarized as follows:

1) Provided guidelines for using Prony and Kalman Filter techniques:
   Referring to the literature prior to the start of this thesis; despite several publications discussing the effectiveness of Prony and Kalman Filter individually, none have compared both of them qualitatively. Consequently, deciding which detection scheme to apply for a particular power grid can be a challenging task for the operators. Therefore, the contribution of this work is to supply a guide for the users to determine the method that better suits their needs. This is achieved by exhaustively analyzing the characteristics of each technique from many simulated studies. The results were published in [96] and [97].

2) Minimized the sampling errors within the Prony solutions:
   The accuracy of Prony solutions are dependent on the adequacy of the constructed data matrix, which is influenced in turn, by the appropriateness of the selected sampling interval. Furthermore, it has been observed in [98] that the adequacy of the selected interval in a fixed monitoring window condition will change depending on the signal's contents. Therefore, the traditional approach of using a fixed sampling interval can incur additional sampling errors under some operating situations. Hence, a sampling method was developed to assess, and then select a sampling interval that was adequate for the monitoring situation. As a result, the sampling errors within the estimated solutions were minimized. Thus, there was an increase in the reliability of the extracted estimated solutions. Three papers were published based on this research; [99] and [100].

3) Enhanced Kalman Filter's functionality:

Kalman Filter was originally derived to monitor the dominant mode in the network. In order to apply Kalman Filter into New Zealand, several extensions were applied and the modified method is known as the Extended Complex Kalman Filter (ECKF). As the name suggests, ECKF was able to extend the functionality of Kalman Filter to monitor multiple modes. Unlike its predecessor, the states of the ECKF represents the actual modal parameter; instead of the AR coefficients. Furthermore, Hankel Singular Value Decomposition (HSVD) was embedded within ECKF to improve its detection accuracy. The work was published in [44], [45], [46], [47], [101] and [102].

4) Evaluated the potential of parallel-processing:

The computing time is regarded as a crucial factor for realizing the online oscillatory monitoring application. Multi-core computers are now widely available, and parallelizing the monitoring algorithms was considered as feasible option. The contribution of this work is in outlining the potential benefits of using the parallel-processing implementation compared with the classic sequential computing. Such an investigation has not yet been carried out for the monitoring operation and therefore, is identified as one of the important aspects to consider when implementing the detection methods. In addition, the effectiveness of the parallel-processing procedure using different hardware specifications is investigated. The observations made in this chapter can also act as a reference for parallelizing other power system operations. They were presented in [102] and [103].

5) Examined the impact load characteristics for damping oscillations:

As more synchrophasor data are made available for the operators, the idea of using a remote signal for the local controllers is being revisited by many researchers in recent years. According to the existing literature, the impact of the load behaviour on the operating effectiveness of these strategies has not been thoroughly investigated. Inspired by the work published in [104], the effect of the load characteristics on the damping performance of a simple

remote signal controller, used in [105], is assessed. The thesis evaluates the benefits of using the remote signal by comparing it with the classic local signal control design. Two papers were published based on this work, [106] and [107].

1.6 *Thesis Overview*

This thesis is organized into eight chapters and is summarized as follow:

Chapter 1 presents an overview of WAMS and its intended applications. In addition, the current state of the New Zealand grid is summarized. The primary motivation of this dissertation is to develop oscillation monitoring methods for the New Zealand grid.

Chapter 2 provides an overview of the previous work published in the area of oscillatory monitoring. Several popular techniques have been outlined and explained. Amongst them, Kalman Filter and Prony Analysis are chosen as suitable candidates applicable to the New Zealand transmission network.

Chapter 3 focuses on understanding the fundamental traits of Kalman Filter and Prony Analysis. Based on the simulation results, the merits of each method are discussed.

Chapter 4 addresses the influence of the sampling interval on estimated Prony solutions. Subsequently, a proposed sampling scheme is recommended to examine the sampling adequacy. The modified method is termed as the Enhanced Prony Analysis in this thesis.

Chapter 5 outlines the derived ECKF method. This is accompanied by evaluating its performance against other monitoring techniques. These include Kalman Filter, Prony and Robust RLS methods.

Chapter 6 investigates the benefits of implementing parallel-processing for the Enhanced Prony Analysis and the ECKF techniques. The evaluations are carried out by comparing its processing speed with that of traditional sequential computing.

Chapter 7 explores the effectiveness of a remote signal based damping controller when subjected to different load characteristics. The obtained results are then compared with those from the local signal based controller.

Chapter 8 concludes the work presented in this dissertation. The summaries of each chapter are also provided along with their potential future research directions.

2 Analyzing Power System Oscillations

2.1 *Background of Power System Oscillations*

2.1.1 What are they?

The generators in an interconnected grid are synchronized to the same frequency. The power is shared between the generators by the ratio of their individual ratings. The definition of synchronism is: the ability to minimize the speed deviation of one generator when it deviates from its set speed by transferring the power from the other generators in the system. Such an action provides an improved system security, and an economy to the operation [1]. By interconnecting the neighbouring utilities, the mutual emergency assistance enhances the security of one's own network. Furthermore, individual utilities need to invest less on the generation reserve within their systems and thus, provide a more overall economical operation. Since power can be transferred anywhere in an interconnected grid, utilities are able to take advantage of the most economical sources of power generation.

Due to synchronization, the generators are no longer isolated, but instead, they interact with each other [85]. The dynamic of the power transfer between the generators can be characterised as electromechanical oscillations and are inherent in an interconnected network.

From an operational perspective, the power oscillations are acceptable as long as they decay [108]. Any lightly, or negatively damped oscillations need to be promptly addressed as they threaten the reliability of transferring power between regions.

2.1.2 The nature of the Oscillations

An interconnected power grid contains many modes of oscillation as a consequence of the interactions of its components. Power system oscillations are complex in nature and difficult to analyze. In order to provide a better understanding, the electromechanical oscillations are usually classified by the system components they

affect. Referring to [1] and [109], these can be categorized into five categories, namely:

1) Intra plant mode oscillations:

Generating units within the same plant oscillate against each other at a frequency of 2 to 3 Hz. The exact magnitude is dependent on the unit's rating and the reactance connecting them.

2) Local plant mode oscillations:

This mode is associated with the swinging of units at a generating station, with respect to the rest of the power network. The impact is localized to the plant and the line connecting it to the grid. The typical frequency is 1 to 2 Hz. Studies on the dynamic behaviour can be conducted by modelling the rest of the system as a constant voltage source whose frequency is assumed to remain constant [109].

3) Inter-area mode oscillations:

The oscillation is between groups of generators swinging against other machines in a distant part of the grid. The cause is due to two or more groups of closely coupled machines being interconnected by weak tie-lines. The frequency is usually less than 1 Hz. Unlike the first two modes of oscillation, the inter-area mode involves many components in the system. The damping characteristics are closely related to factors like: the tie-line strength, the nature of the loads, the power flow behaviours, and the implemented control strategies [110, 111]. Due to increased number of variables required to model inter-area oscillation, it is much more complex and difficult to analyze compared with local modes.

4) Control mode oscillations:

The oscillation is caused when the controllers, such as the exciters, the governors or the FACT devices, are poorly tuned. The frequency range is typically between 0.2 Hz to 2.5 Hz.

5) Torsion mode oscillations:

This mode is associated with the turbine–generator shaft system rotational components. Instability can be caused by: interaction with excitation controls, speed

governors, or series compensated lines. The oscillatory frequency is greater than 2 Hz.

The electromechanical oscillations can be characterized as the dynamic power transfer behaviour between synchronous generators in an interconnected network. They are generated due to a variety of disturbances such as; changing the load magnitude and the transmission capacity, or, tripping the lines due to system faults. These oscillations, ranging between 0.1 Hz to 2 Hz, can be grouped into two main categories; local and inter-area oscillations. As these names suggest, the local oscillations refer to the oscillations between nearby generators, and the inter-area oscillations occur between remote generators. Because the local modes usually involve lower impedance than inter-area modes, their frequencies tend to be higher than their inter-area counterparts.

To summarize: the intra-plant, the local, the control, and the torsion modes are usually induced by the interaction between the mechanical and the electrical modes of a turbine-generator system [109]. Inter-area oscillation is influenced not only by generator interactions, but also by network parameters such as, the line and the load characteristics. When present in the system, the inter-area oscillation limits the amount of the power transfer between the regions containing the groups of coherent generators.

2.1.3 Potential Threats towards Secure Network Operation

In the early stage of the network interconnection, during the 1960s and 1970s, the electromechanical oscillations were generally local and their amplitudes easily controlled. Furthermore, several regions were established to categorized groups of generators, in terms of their geographical locations. However, as more utilities were interconnected, the physical distance between generator groups and the load centres widened. That resulted in a new paradigm of transmission operation that focused on the inter-area/distant power transfer. Consequently, modern power networks are more prone to inter-area oscillations. The potential factors contributing to poor damping resulting in an unstable inter-area oscillation are:

- The increasing line impedance in the transmission corridor connection areas tends to lower the oscillatory frequency and worsen the associated damping.
- The higher power flows in the grid between the participating regions can degrade the damping.
- The load characteristics and the geographical location from the main generation reserves can impact on the stability of inter-area oscillation.
- Inadequate setting of the generator's operating points. Both the power output and the power factor of the generators can affect their damping characteristics.
- Voltage instability in the network can reduce damping [112].

Unlike the local oscillations, the inter-area oscillations are much smaller in their frequency component (0.1 Hz~0.8 Hz) and are much harder to monitor under quasi steady-state condition [108]. Consequently, the lightly damped inter-area oscillations have caused many operational problems since the 1960s. A summary of past note worthy incidents are listed below:

Events attributed to inter-area oscillation:

1. In early 1960s, oscillations were observed when the Detroit Edison, Ontario Hydro and Hydro Quebec systems were inter-connected [113].
2. In 1964, oscillation observed in WECC. Insufficient damping caused at least hundreds of line separation between the newly interconnected Northwest and Southwest US grid [109].
3. In 1966, Saskatchewan-Manitoba Hydro-Western Ontario interconnected grid experienced oscillation [109].
4. In 1969, oscillations were observed under several operating conditions in the Scandinavian interconnected grid (Finland, Sweden, Norway and Denmark) [113].
5. Between 1971 and 1972, over 70 incidents of unstable inter-area oscillations occurred in the mid continent area power pool (MAAP) in North America [113].
6. During 1971 – 1974, oscillations were presented in the interconnected grid of Italy-Yugoslavia-Austria [109].

7. In 1975, unstable oscillation of 0.6 Hz were encountered on the interconnected power system of New South Wales and Victoria [113].
8. Between 1975 and1980s, Southern Brazil showed oscillations with a range of 0.15 to 0.25 Hz [109, 113].
9. In 1978, Scotland-England interconnected grid experienced inter-area oscillations [109].
10. Between 1982 and 1983, the state energy commission of Western Australia experienced lightly damped oscillation in the range of 0.2-0.3 Hz [113].
11. In 1985, Taiwan first experienced poorly damped inter-area oscillation in the north between its nuclear and thermal power plants [109, 114].
12. In 1985, lightly damped inter-area oscillations were encountered in Ghana-Ivory Coast [109].
13. On August 10, 1996 the Pacific AC Inter-tie (PACI) in WECC experienced unstable low frequency inter-area oscillations following the outage of four 400kv lines [108].

A visual timeline of these events is shown in Figure 2-1. Most of these incidents (especially the early ones) caused much system separation but few wide scale blackouts (mainly the later ones). The lesson learnt from these events is those oscillation problems are moving from the local to the inter-area as the dependency on the distant power transfer continuous to increase in a stressed network.

The electromechanical oscillations can be regarded as the characteristics of a system, which means the oscillatory modes and the associated oscillatory parameters are dependent to the physical infrastructure. Since each power grid is unique in physical nature, the presence of electromechanical oscillations varies significantly between different networks.

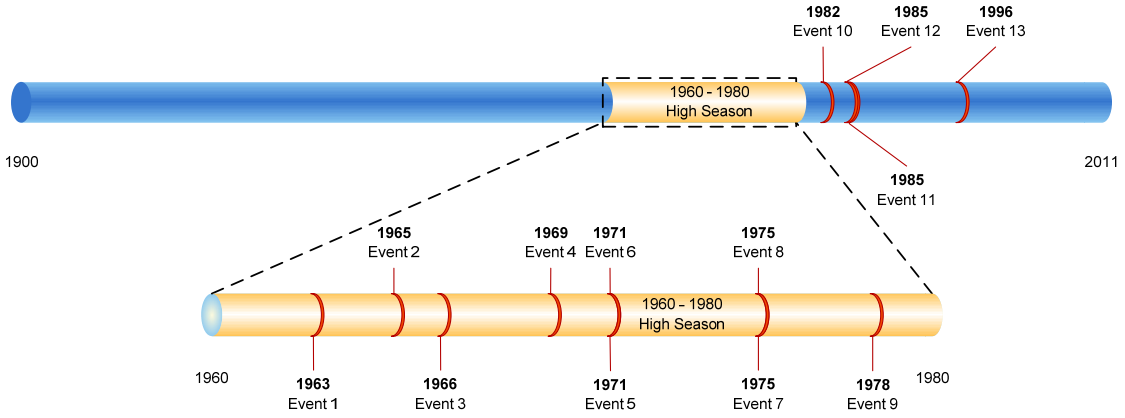

Figure 2-1 History of the past inter-area oscillation occurrences

Although these oscillations are linked with the generator interactions and can be triggered after the contingencies, they are generally rare cases. More often the lightly damped or the unstable oscillations are caused by the normal change in the system loads [115]. These are more deadly as there are no warnings to the operators when the new operating condition can cause the oscillation amplitudes to rise.

2.2 *Analysis Tools*

2.2.1 Power System Analysis: Basic Concepts

In network analysis, calculations such as: the voltage drop, the power flow, and the short-circuit currents are usually carried out using phasor representation. It is a complex number that contains both the magnitude and phase angle of the sinusoidal waveforms found in electricity. A visual illustration of the phasor transposition is provided in Figure 2-2, [13].

Here, the magnitude (Mag) refers to the root-mean-square (RMS) value of the measured waveforms, rather than the peak amplitude. The magnitude, in most cases, represents the positive sequence voltage or the current readings. It is useful when conducting steady-state analysis such as the load flow or the system modelling.

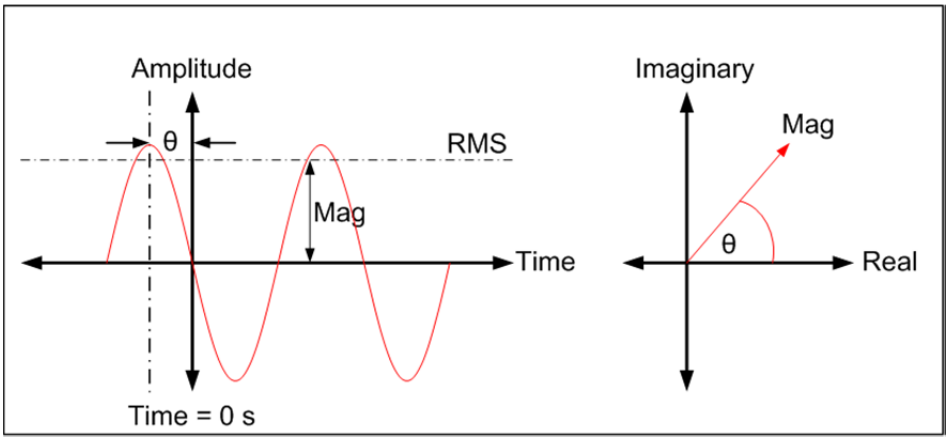

Figure 2-2 The phasor representation of a sinusoidal waveform

Furthermore, the phase angle (θ) is the angle between the peak of the sine wave and the point when the time equals to zero. In other words, the phase angle is a relative value that is computed by simultaneously comparing it to a reference phasor that is synchronized to a common time. In contrast to the magnitude attribute, the phase angle is usually associated with the grid dynamics. The reason: the active power flow in a transmission line can be considered as proportional to the Sine of the angle difference between the voltages at the two terminals of the line [116, 117]. Since the network behaviour can be referred to as the power/energy transfer between the nodes; tracking the active power flow is the key when analyzing system dynamics such as the stability limits, and estimating the instantaneous system states. Thus, monitoring the phase angle at the power network buses is important from the planning and the operational perspectives.

2.2.2 Small-Signal Analysis: Basic Concepts

The electromechanical dynamic effects in power systems usually involves analyzing the nonlinear, high system order and time-varying situations [109]. Moreover, excitation of electromechanical oscillations can be considered stochastic in nature and a typical power grid may be prone to several oscillations whose associated frequencies are close to each other.

Consistent with the conventional power system stability theories, the system is linearized about an operation point. Thus, the power system dynamics can be formulated into a set of Differential Algebraic Equations (DAE) in the following form:

$$\begin{aligned} \Delta\dot{\mathbf{x}} &= \mathbf{A}\Delta\mathbf{x} + \mathbf{b}\Delta u \\ \Delta y &= \mathbf{c}\Delta\mathbf{x} \end{aligned} \tag{2-1}$$

where $\mathbf{A}$ is the state matrix, $\Delta\mathbf{x}$ is the state vector, Δu is a single input, Δy is a single output, $\mathbf{c}$ is a row vector and $\mathbf{b}$ is a column vector. Note: y is not a direct function of u. The focus is the low frequency oscillation. Therefore, in order to simplify the problem, the high frequency network and stator transient variables are ignored.

Now, assuming the system is of m^{th} order, the state matrix will be an mxm matrix. Suppose that a linear, time-invariant dynamic system with an initial state defined by means of some test input or disturbance. If the input is an impulse, or a relatively short-term signal and it is removed with no subsequent inputs to the system, the dynamic systematic behaviour can be described as a *ringdown* with the variable Δu equals to zero [118].

For simplicity, consider the power system as a single-input-single-output (SISO) system as shown in Figure 2-3. Referring to Kundur [1], the Laplace transform transfer function $G(s)$ for the dynamic analysis is:

$$G(s) = \frac{\Delta y(s)}{\Delta u(s)} = \frac{R_1}{s-\lambda_1} + \frac{R_2}{s-\lambda_2} + \cdots + \frac{R_m}{s-\lambda_m} \tag{2-2}$$

Here, R_i is the *residue* of the function $G(s)$ at the eigenvalue (λ_i). Note that the residue contains the left and right eigenvectors corresponding to λ_i.

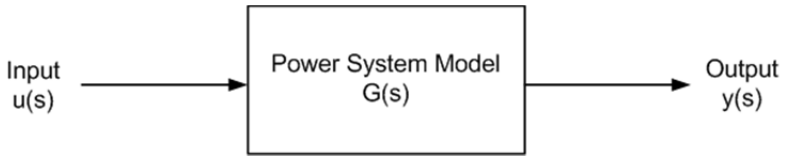

Figure 2-3 Block diagram representation of the system

In the case of the *ambient* situation, the input is assumed to be an approximately stationary white noise in the frequency band of interest over the analysis window [119]. Hence, Δu cannot be neglected and the system contains both poles and zeros as stated by Wies *et al.* [120]. The trend is that there are generally more poles than the zeros. Details related to both the ringdown and the ambient situations are given in the later subsections along with their detection algorithms.

In system analysis, the eigenvalue is expressed as:

$$\lambda = -\sigma + j\omega \tag{2-3}$$

The real part (σ), relates to the damping factor and the imaginary part (ω), corresponds to the oscillatory frequency. Conventionally, the oscillatory parameters are represented in terms of the damping ratio and frequency in Hz. These values are computed by:

$$\varsigma = \frac{\sigma}{\sqrt{\sigma^2 + \omega^2}} \tag{2-4}$$

$$f = \frac{\omega}{2\pi} \tag{2-5}$$

Note: the positive damping ratio indicates the positive damping, i.e. the oscillatory amplitudes decays over time.

2.2.3 Overview of the Existing Monitoring Techniques

There are two ways to estimate the oscillatory modes in power systems. Firstly, modelling the system using theoretical derivations and linearizing about a given operating point using Taylor series expansions. Secondly, using a mathematical fitting algorithm to optimally fit a linear model to a specified measured system response [119]. Traditionally, the modal analysis based on the first approach is used for determining the oscillatory behaviour in the power grid. In essence, the objective is to formulate and analyze the transfer function $G(s)$ of the system shown in Figure 2-3. That is regarded as the state-space approach. The oscillatory parameters are estimated by formulating the state matrix of the entire system, but modelling all components in the grid, such as the exciters and the generators, is extremely time

consuming. It is conducted offline. In addition, the constructed system matrix is obtained by linearizing the Differential-Algebraic Equation (DAE) model of a power system around an equivalent point [1]. Hence, the estimated eigenvalues from each modal analysis is only valid for one particular operating point. Since the power system operating conditions are always changing due to the fluctuations in the load and the generation, there is a need to investigate an alternative solution to the existing modal analysis. As a result, many time-domain based signal analysis techniques using the measurements collected from PMUs are popular alternatives amongst the power utilities. Different to the state space approach, these parametric methods do not build large complex system matrices to identify the oscillatory modes. Their aim is to determine the system parameters by characterizing the output response $y(s)$, shown in Figure 2-3, as accurately as possible.

The PMU data can be categorized into three types: ambient, ringdown and probing. In order to extract useful oscillatory information, two detection approaches are implemented: ambient and ringdown. Ambient detection refers to monitoring the network under an equilibrium condition, with the assumption of constant small-amplitude random load variations occurring in the system. Those changes provide enough excitation to capture the electromechanical dynamics, but due to the magnitude and randomness of those perturbations, several minutes worth of data are needed to estimate the oscillatory modes. Ringdown detection tracks the oscillatory behaviour after the system has experienced some major disturbances [121]. Since those excitations are usually distinctly noticeable, the collected measurements contain rich electromechanical information. Thus, a small timeframe of only several seconds are needed to extract modal parameters.

The types of signal processing strategy utilized are block-processing, and recursive tracking. The monitoring methods using the first approach estimate the oscillatory parameters by building a model based on all the data collected within a set time window. They are usually seen in the methods used for ringdown analysis. Alternatively, the recursive algorithm updates the detection once every sampling instance. It is mainly seen in ambient detection techniques. A list of the popular

tracking techniques along with their primary intended application are listed in Table 2-1.

Depending on the intended grid characteristics, many extensions based on these methods have also been published [28, 85, 122-124]. Note: most ambient detections are also capable of monitoring the ringdown behaviour. Perhaps the most mature techniques amongst all proposed algorithms are Prony, and Kalman Filter. Prony Analysis for oscillations was first developed by Bonneville Power Administration (BPA) in the early 1990s and is currently implemented in Brazil, Canada, China, USA and many European nations. Kalman Filter was initially proposed by ABB Switzerland in the early 2000s and is deployed in the Scandinavian countries and Thailand [9].

The structure of the remainder of this chapter is as follows. The ringdown detection methods are addressed followed by the ambient algorithms. In each case, a brief history is provided along with the past developed extensions. Furthermore, for ease of understanding, the noise component is neglected when explaining the fundamental nature of the detection method.

Table 2-1 A list of the popular oscillation monitoring techniques

Ringdown Detection	**Ambient Detection**
Prony Analysis [121]	Autoregressive Moving Average [125]
Matrix Pencil [126]	Regularized Robust RLS [127]
Hankel Total Least Square [115]	Hilbert-Huang Transform [128]
Kalman Filter [129]	
Wavelet Transform [130]	

2.2.4 Prony Analysis (PA)

The method, developed by Gaspard Riche de Prony in 1795, was first proposed by Hauer *et al.* [121], as a means of estimating the electromechanical modes in the power grid. It is a linear estimation technique that fits a sum of exponentially damped complex sinusoids to a finite number of samples of a signal spaced equally in time. Subsequently, the modal parameters such as the amplitudes (A), the damping factors (σ), the frequencies (f) and the phases (ϕ) are extracted from the observed signal. A short outline of the method is discussed here.

Consider a continuous noiseless signal $y(t)$, containing n number of oscillatory modes, to be modelled by:

$$\hat{y}(t) = \sum_{i=1}^{n} A_i e^{\sigma_i t} \cos(2\pi f_i t + \phi_i) \qquad for\ t \geq 0 \tag{2-6}$$

By manipulating Equation (2-6) using Euler's Formula, $\hat{y}(t)$ can be represented as:

$$\hat{y}(t) = \sum_{i=1}^{m} R_i e^{\lambda_i t} \tag{2-7}$$

where R_i is the output residue or the complex amplitude of the i^{th} pole. Note: the system order m is twice of n because each oscillatory mode is modelled by one complex conjugate eigenvalue pair.

Next, assume $\hat{y}(t)$ consists of N samples that are evenly spaced by Δt, Equation (2-7) can be converted into the discrete-time form as:

$$\hat{y}(k) = \sum_{i=1}^{m} R_i z_i^k, \qquad for\ k = 0,1,\ldots,N-1 \tag{2-8}$$

where $z_i^k = e^{\lambda_i \Delta t}$ is the discrete-time pole. The objective is to estimate R and z from Equation (2-8) that best approximate the actual measured signal in a least square sense, i.e. $\hat{y}(k) = y(k)$, for all k. In general, Prony Analysis can be summarized as solving two sets of linear equations with an intermediate polynomial rooting process. This can be divided into three steps:

1) Construct a Linear Prediction Model (LP) from the observed data and

approximate the Autoregressive (AR) coefficients.

2) Compute the roots (eigenvalues) of the characteristic polynomial equation generated by the AR coefficients.
3) Solve the original set of linear equations in order to estimate the exponential amplitude and the sinusoidal phase.

Firstly, suppose the present value can be approximated as a sum of weighted past values. Hence, the Linear Prediction model based on Equation (2-8) is defined as:

$$y[k] = a_1 y[k-1] + a_2 y[k-2] + \ldots + a_m y[k-m] \tag{2-9}$$

where the symbol a represents the AR coefficients. These parameters are determined by solving a set of linear equations:

$$\begin{aligned} y[k] &= a_1 y[k-1] + a_2 y[k-2] + \ldots + a_m y[k-m] \\ y[k+1] &= a_1 y[k] + a_2 y[k-1] + \ldots + a_m y[k-m+1] \\ y[k+2] &= a_1 y[k+1] + a_2 y[k] + \ldots + a_m y[k-m+1] \\ &\vdots \\ y[N] &= a_1 y[N-2] + a_2 y[N-3] + \ldots + a_m y[N-m-1] \end{aligned} \tag{2-10}$$

Alternatively, Equation (2-10) can be expressed in matrix form of ($\boldsymbol{y} = \boldsymbol{Ax}$):

$$\begin{bmatrix} y(m) \\ y(m+1) \\ \vdots \\ y(N-1) \end{bmatrix} = \begin{bmatrix} y(m-1) & y(m-2) & \cdots & y(0) \\ y(m) & y(m-1) & \cdots & y(1) \\ \vdots & \vdots & & \vdots \\ y(N-2) & y(N-3) & \cdots & y(N-m-1) \end{bmatrix} \begin{bmatrix} a_1 \\ a_2 \\ \vdots \\ a_m \end{bmatrix} \tag{2-11}$$

In most cases the total number of discrete samples (N) will be greater than $2m$, which means the data matrix $\boldsymbol{A}$ is an overdetermined matrix. The column size of $\boldsymbol{A}$ is determined by the system order. Hence, the coefficients a can be computed by using pseudo-inverse approach. Note that the appropriateness of the constructed data matrix is dependent on: 1) the spread of the measured data, and 2) the number of available samples. Since the monitoring window is usually predefined and fixed, care is needed for selecting the sampling interval.

Once these parameters are found, the eigenvalues can be calculated by solving the following characteristic polynomial equation in Least Squares sense:

$$z^m - (a_1 z^{m-1} + a_2 z^{m-2} + \ldots + a_m) = 0 \tag{2-12}$$

The primary advantage of Prony is that it does not require any prior knowledge of the system models to conduct its approximation. However, it is a time-invariant method, i.e. the network dynamics are assumed to be constant within the same sampling time window. Singular Value Decomposition (SVD) is often used to filter the noise component. In brief, the SVD decomposes the data matrix of the LP model into:

$$\mathbf{A} = \mathbf{U}\Sigma\mathbf{V}^H \tag{2-13}$$

The $\boldsymbol{U}$ and $\boldsymbol{V}$ matrices are the left and right eigenvectors of $\boldsymbol{AA}^H$ respectively, where $\boldsymbol{A}^H$ is the conjugate transpose of $\boldsymbol{A}$. In addition, the singular values of $\boldsymbol{A}$ are stored in the diagonal entries of $\boldsymbol{\Sigma}$ matrix. Under noiseless condition, the overdetermined data matrix will contain many zero singular values. However, when subjected to noise, these entries are corrupted and become nonzero. Hence, by inspecting the singular values of the data matrix, those with small magnitudes can be regarded as being perturbed by noise, and need to be removed. Furthermore, the associated columns of the $\boldsymbol{U}$ and $\boldsymbol{V}$ matrices also need to be deleted. Therefore, the processed truncated data matrix becomes:

$$\hat{\mathbf{A}} = \mathbf{U}_p \mathbf{U}_p^H \Sigma_p = \Sigma_p \mathbf{V}_p \mathbf{V}_p^H \tag{2-14}$$

The index p represents the order/rank of the matrix. The terms $\boldsymbol{U_p U_p}^H$ and $\boldsymbol{V_p V_p}^H$ act like a *Wiener Filter* for minimizing the noise effects in the data matrix [131]. In the past two decades, several extensions have been proposed for enhancing the noise resistance and the estimation accuracy. Notable modifications include:

- Improving the noise resistance by analyzing multiple input signals simultaneously [111, 122]. That transforms Prony from SISO into MIMO.
- Enhancing the tracking of the modes which are close in frequency, by using an interleaved approach [9, 132]. As a result, the modified Prony becomes an *n* step predictor instead of the standard *one-step ahead predictor*.
- Enhancing the noise resistance by using autocorrelation to construct the Linear Prediction data matrix [28].

- Providing better automation for initiating Prony Analysis [133]. Hence, the estimated modal results can be performed in a more reliable and prompt manner.

2.2.5 Matrix Pencil (MP)

Incorporating Matrix Pencil to track the electromechanical oscillations was first used by Liu *et al.* [126]. Similar to Prony Analysis, MP is also a linear approximation technique that belongs to the pencil-of-function family. It is a relatively new technique and was first published in 1990 by Hua and Sarkar [134]. In a sense, Matrix Pencil is the simplified version of Prony. Suppose an m^{th} order signal is modelled and represented in discrete-time by Equations (2-8). The basic difference between the two techniques is that Prony Analysis is a *polynomial* based algorithm that requires two steps to compute the eigenvalues. Firstly, it needs to compute the coefficients of the polynomial characteristics equation, and secondly, find the associated roots. That can be a computationally intensive task when dealing with a higher system order, and is reflected in solving more roots.

The basic outline of Matrix Pencil is as follows. It is a one step process that approximates the eigenvalues by manipulating the data matrix. Instead of forming one matrix, two $(N-L)\times L$ ranked data matrices ($\mathbf{Y_1}$ and $\mathbf{Y_2}$) are used:

$$\mathbf{Y_1} = \begin{bmatrix} y(0) & y(1) & \cdots & y(L-1) \\ y(1) & y(2) & \cdots & y(L) \\ \vdots & \vdots & & \vdots \\ y(N-L-1) & y(N-L) & \cdots & y(N-2) \end{bmatrix} \tag{2-15}$$

$$\mathbf{Y_2} = \begin{bmatrix} y(1) & y(2) & \cdots & y(L) \\ y(2) & y(3) & \cdots & y(L+1) \\ \vdots & \vdots & & \vdots \\ y(N-L) & y(N-L+1) & \cdots & y(N-1) \end{bmatrix} \tag{2-16}$$

where the parameter L is larger than actual signal order (m). Using Equation (2-8), $\mathbf{Y_1}$ and $\mathbf{Y_2}$ matrices can be rearranged as:

$$\mathbf{Y_1} = \mathbf{Z_1 R Z_0 Z_2} \tag{2-17}$$

$$\mathbf{Y_2} = \mathbf{Z_1 R Z_2} \tag{2-18}$$

where

$$\mathbf{Z_1} = \begin{bmatrix} 1 & 1 & \cdots & 1 \\ z_1 & z_2 & \cdots & z_m \\ \vdots & \vdots & & \vdots \\ z_1^{(N-L-1)} & z_2^{(N-L-1)} & \cdots & z_m^{(N-L-1)} \end{bmatrix}_{(N-L)\times m} \tag{2-19}$$

$$\mathbf{Z_2} = \begin{bmatrix} 1 & z_1 & \cdots & z_1^{L-1} \\ 1 & z_2 & \cdots & z_2^{L-1} \\ \vdots & \vdots & & \vdots \\ 1 & z_m & \cdots & z_m^{L-1} \end{bmatrix}_{mxL} \tag{2-20}$$

$$\mathbf{Z_0} = \operatorname{diag}[z_1, z_2, \ldots, z_m] \tag{2-21}$$

$$\mathbf{R} = \operatorname{diag}[R_1, R_2, \ldots, R_m] \tag{2-22}$$

Note that the notation $\operatorname{diag}[\ldots]$ refers to a diagonal matrix. In this case, the problem of solving z can be treated as an ordinary eigenvalue problem,

$$\mathbf{Y_1^{+} Y_2} - \lambda \mathbf{I} \tag{2-23}$$

where the subscript $+$ refers to the Moore-Penrose pseudoinverse operator and matrix $\boldsymbol{I}$ is an identity matrix. Since no polynomial equation is needed, the computational speed is generally quicker than Prony. Additional noise enhancement can be achieved by integrating SVD into MP. Details related to the mathematical formulation can be viewed in [134, 135].

2.2.6 Hankel Total Least Square (HTLS)

Hankel Total Least Square was first implemented in 2007 to detect electromechanical oscillations by Liu *et al.* [126]. The method was proposed by Van Huffel [136] and is relatively new compared with the previous two methods. It is an enhanced version of the proposed linear prediction algorithm by Tufts and Kumaresan [137]. In brief, assuming the output signal *y(t)* is modelled as Equation (2-8), the Hankel/data matrix is constructed in the form of:

$$\mathbf{H} = \begin{bmatrix} y(0) & y(1) & \cdots & y(N-L) \\ y(1) & y(2) & \cdots & y(N+1-L) \\ \vdots & \vdots & & \vdots \\ y(L-1) & y(L) & \cdots & y(N) \end{bmatrix} \tag{2-24}$$

where the parameter L is chosen to be larger than the actual system order (m) to form an overdetermined matrix. Subsequently, the data matrix can be factorized as:

$$\begin{aligned} \mathbf{H} &= \begin{bmatrix} 1 & 1 & \cdots & 1 \\ z_1^1 & z_2^1 & \cdots & z_m^1 \\ \vdots & \vdots & & \vdots \\ z_1^L & z_2^L & \cdots & z_m^L \end{bmatrix} \begin{bmatrix} R_1 & & & \\ & R_2 & & \\ & & \ddots & \\ & & & R_m \end{bmatrix} \begin{bmatrix} 1 & z_1^1 & \cdots & z_1^{N-L} \\ 1 & z_2^1 & \cdots & z_2^{N-L} \\ \vdots & \vdots & & \vdots \\ 1 & z_m^1 & \cdots & z_m^{N-L} \end{bmatrix} \\ &= \mathbf{SRT}^T \end{aligned} \tag{2-25}$$

where $\boldsymbol{S}$ and $\boldsymbol{T}$ matrices are the left eigenvector and right eigenvectors of $\mathbf{H}$ respectively. They are known as Vandermonde Matrices, and can be found by solving Equation (2-24) using SVD operation. Prior to solving the oscillatory parameters contained in the $\boldsymbol{Z}$ matrix, the $\boldsymbol{S}$ matrix needs to be manipulated in a shift-invariant manner such that:

$$\mathbf{S}_{\downarrow}\mathbf{Z} = \mathbf{S}_{\uparrow} \tag{2-26}$$

The up and down subscript arrows refer to deleting the top or bottom row of the matrix respectively. The diagonals of the $\boldsymbol{Z}$ matrix contain the eigenvalues and can be solved by making $\boldsymbol{Z}$ the subject in Equation (2-26).

HTLS is very similar to MP and also does not require polynomial rooting. Therefore, under certain operating conditions and network characteristics, HTLS provides a faster processing speed than Prony Analysis and MP [126]. Although HTLS has a decent noise resistance, SVD is recommended to provide a better performance under noisy conditions.

2.2.7 Kalman Filter (KF)

Kalman filter is a mathematical method that was developed in the late 1950s to estimate the time-varying states of a linear dynamic system by using the measured data and the previous state approximations. It is a recursive tracking algorithm that

belongs to the recursive least square filter family [138]. KF was initially implemented as part of the navigation software in the Apollo space program and later was proven to be extremely useful in applications such as the trajectory estimation.

Depending on the formulated state model and the intended applications, several versions of KF have been proposed in the past few decades. The one that is used for oscillatory monitoring is based on the Information-Filtering Algorithm [139]. The state estimations are conducted by propagating the inverse correlation matrix of the error in the state prediction. In simple terms: the proposed Kalman filter accentuates the recursive least-square nature of the filtering process. A basic overview of KF is provided below.

Instead of using a state space approach, a linear autoregressive (AR) model with L number of time-varying coefficients (a) is implemented. Note that L must be greater or equal to the system order m. Suppose the signal at time k is formulated as:

$$\hat{y}(k \mid k-1) = \sum_{i=1}^{m} a_i(k) y(k-i) \tag{2-27}$$

where $\hat{y}(k \mid k-1)$ is the predicted value of $y(k)$ based on m past measurements. Since the tracking of the state progression is determined by the prediction errors $\varepsilon(k)$, the main objective is to acquire a set of coefficients that would minimize the sum of the squared prediction error:

$$J = \min_{a_i} \sum \varepsilon^T \varepsilon = \min_{a_i} \sum (\hat{y}(k \mid k-1) - y(k))^2 \tag{2-28}$$

A summary of KF's recursive operation is outlined in Equations (2-29) to (2-33). Note that $g(k)$ is the filter gain, $u(k)$ is the buffered measurement vector, $K(k)$ is the covariance matrix, $p(k)$ contains the estimated coefficients, Q_m is the correlation factor of the measurement noise and Q_p is the correlation matrix of the process noise.

$$g(k) = K(k-1)u(k)[u^T(k)K(k-1)u(k) + Q_m]^{-1} \tag{2-29}$$

$$\hat{y}(k) = u^T(k)\, p(k-1) \tag{2-30}$$

$$\varepsilon(k) = \hat{y}(k) - y(k) \tag{2-31}$$

$$p(k) = p(k-1) + \varepsilon(k)g(k) \tag{2-32}$$

$$K(k) = k(k-1) - g(k)u^T(k)K(k-1) + Q_p \tag{2-33}$$

To ensure adequate numerical robustness, Equation (2-33) can be enhanced by:

$$K(k) = \frac{K(k) + K^T(k)}{2} \tag{2-34}$$

$$K(k) = c_1 \frac{K(k)}{tr(K(k))} + c_2 I \tag{2-35}$$

Here, the covariance matrix $K(k)$ will remain symmetrical and thus, provide better tracking by using a regularised constant trace algorithm. The constants c_1 and c_2 are determined experimentally and has a ratio of $c_1 / c_2 \approx 10^4$ [129]. The matrix I is an unity matrix with the same rank as $K(k)$.

Meanwhile, care is needed for initializing Kalman Filter. In this case, the influence of Q_p has been minimized by enforcing the covariance matrix robustness. The ratio between the process noise Q_p and the measurement noise Q_m can affect the monitoring performance. A small Q_p or Q_m indicates whether the user trusts more towards the model or the measurements respectively [140]. Note that a zero process noise refers to the model matches the signal perfectly.

Similar to Prony Analysis, the state variables from Equation (2-32) represent the AR coefficients. Instead of solving them in a least square manner like Prony Analysis, Kalman Filter recursively predicts these coefficients when a new sample is collected. Once Kalman Filter has converged within an acceptable error range, the estimated AR coefficients (frozen at the time k) are then applied to the discrete polynomial characteristic equation as:

$$z^m - a_1(k)z^{m-1} - \ldots - a_{m-1}(k)z - a_m(k) = 0 \tag{2-36}$$

Prior to rooting the characteristic equation, Equation (2-36) is converted into the continuous time domain via Tustin approximation. Subsequently, the eigenvalues λ

are extracted from the computed polynomial roots. The damping factors and the associated frequencies are determined in the same manner as Prony Analysis by Equations (2-4) and (2-5) respectively.

2.2.8 Wavelet Transform (WT)

The first Wavelet Transform was formulated by Grossman and Morlet in the 1980s for solving signal processing problems in oil prospection [141]. It is basically a generalization of Fourier analysis, which decomposes a given signal into shifted and scaled versions of the predetermined mother wavelet $\Psi(t)$. The main purpose of the mother wavelet is to provide a source function to generate the daughter wavelets, which are, simply, the translated and the scaled versions of the mother wavelet. If the input signal is similar to a given daughter wavelet, a time-frequency analysis can be obtained.

Although WT has been used in many engineering applications, it was first adopted in tracking the oscillatory behaviours in the Italian grid in 2006 [9]. Since then WT has been proven to be an effective tool for analyzing ringdown dynamics. The general procedure of WT is outlined below.

Suppose a continuous time domain signal $y(t)$ can be modelled by WT as:

$$WT(a,\tau) = \frac{1}{\sqrt{a}} \int_{-\infty}^{+\infty} y(t).\Psi_{a,\tau}(t).dt \tag{2-37}$$

where the mother wavelet can be real or complex. The notation a and τ are the dilatation and the location parameters respectively. They are used for defining the daughter wavelet by:

$$\Psi_{a,\tau}(t) = \Psi\left(\frac{t-\tau}{a}\right) \tag{2-38}$$

Additionally, the term $1/\sqrt{a}$ refers to the energy normalization factor. Since the electromechanical oscillations are modelled as exponentially damped sinusoids, the complex Morlet mother wavelet is regarded as an adequate candidate. It is defined by:

$$\Psi(t) = \frac{1}{\sqrt[4]{\pi}}\left(e^{j\omega_0 t} - e^{-\frac{{\omega_0}^2}{2}} \right) e^{-\frac{t^2}{2}} \tag{2-39}$$

where ω_0 is the central frequency of the mother wavelet. In this case, the oscillatory frequency is related to the central frequency by the dilatation factor such that:

$$f = \frac{\omega_0}{2\pi a} \tag{2-40}$$

Furthermore, the damping factor of the time signal is computed by analyzing the wavelets of two time instants τ_1 and τ_2 :

$$\sigma = \frac{1}{(\tau_2 - \tau_1)} \ln \frac{|WT(a,\tau_1)|}{|WT(a,\tau_2)|} \tag{2-41}$$

Subsequently, the damping ratio can be computed by Equation (2-4). Further readings related to the mathematical formulation can be referred to [130, 142, 143].

2.2.9 Autoregressive Moving Average (ARMA)

ARMA was first proposed by George Box and Gwilym Jenkins in the 1970s for predicting the states of a dynamic system [144]. It combines the all-pole autoregressive (AR) and all-zero moving average (MA) models. The fundamental assumption is that the present observed value can be expressed as a finite linear combination of its own past history, plus the unpredictable component consisting of a finite linear combination of uncorrelated random variables. That can be represented in mathematical formulation as:

$$y(k) + a_1 y(k-1) + \ldots + a_m(k-m) = b_0 u(k) + b_1 u(k-1) + \ldots + b_p u(k-p) \tag{2-42}$$

where $a_1,\ldots,a_m$ and $b_1,\ldots,b_p$ are the coefficients of the characteristics equations for the poles and the zeros of the system respectively. In power system scenarios, there are generally more poles than zeros, i.e. m>p. $u(k)$ refers to the input values of the system.

For oscillatory monitoring applications, a block-processing ARMA proposed by Wies *et al.* [120], is used. Unlike the recursive KF, ARMA conducts modal estimations for

each new window of data. Further extensions, such as, adopting a modified Yule-Walker algorithm and the moving/sliding time window have also been suggested [125]. The general approach for any type of ARMA detection is to express the inputs as part of the outputs such that the model can be treated as an AR process [120, 125]. A brief outline of the ARMA is given in reminder of this subsection.

The objective of ARMA is to approximate the coefficients a by rooting the following characteristic equation:

$$0 = 1 + a_1 z^{-1} + a_2 z^{-2} + \ldots + a_m z^{-m} \tag{2-43}$$

That is achieved by firstly deriving the autocorrelation function $r(k) = E\{y(k)y(k-\tau)\}$ of the ambient data over the predefined time window, where, the variable τ is the discrete-time shift integer. Note that the right hand side of Equation (2-42) are assumed to be zero for $\tau > p$ because the output $y(k)$ is uncorrelated with the future inputs, i.e. treating the problem as an AR model [145]. Hence, after some mathematical manipulation, the autocorrelation function at τ instance can be approximated as:

$$r(k) = -\sum_{i=1}^{m} a_i r(k-i), \quad for\ k > p \tag{2-44}$$

In addition, using the autocorrelation property $r(k) = r(-k)$, q number of linear equations can be formulated to estimate the coefficients of the characteristic equation in a least square sense such that:

$$-\mathbf{r} = \mathbf{R}\mathbf{a} \tag{2-45}$$

where

$$\begin{aligned} \mathbf{r} &= \begin{bmatrix} r(p+1) & r(p+2) & \ldots & r(p+q) \end{bmatrix}^T \\ \mathbf{R} &= \begin{bmatrix} r(p) & r(p-1) & \cdots & r(p-m) \\ r(p+1) & \cdots & \cdots & r(p-m+1) \\ \vdots & \vdots & & \vdots \\ r(p+q-1) & r(p+q-2) & \cdots & r(p-m+q) \end{bmatrix} \\ \mathbf{a} &= \begin{bmatrix} a_1 & a_2 & \cdots & a_m \end{bmatrix}^T \end{aligned} \tag{2-46}$$

The derived relationship is similar to Equation (2-9) of Prony. By finding the roots of the of Equation (2-43), the associated eigenvalues can be obtained. Unlike Prony, and other ringdown methods, the use of autocorrelation provides ARMA with a better noise resistance and thus SVD is not required. However, one should keep in mind that autocorrelation not only reduces the noise content of the signals, it also minimizes those oscillatory modes with smaller residues than the dominant mode.

2.2.10 Regularized Robust Recursive Least Square (R3LS)

The foundation of R3LS is based on recursive least square. It recursively finds the coefficients that minimize a weighted linear least squares cost function related to the measured signal. It can be viewed as a special case of Kalman Filter. The parameters are predicted on a sample-by-sample basis. R3LS was developed by the same research group as the ARMA detection, and thus, can be considered as an extension to the existing detection. Unlike its predecessor; constructing the data matrix based on the autocorrelation approach was not adopted, and an autoregressive moving average exogenous (ARMAX) model was proposed to enhance noise resistance. Furthermore, a regularization term was added for improving the numerical performance [127, 146]. R3LS is relatively new compared to those previously mentioned in this chapter. It is predominantly prompted by PNNL in the USA. Like ARMA, it is still in the testing phase and has not yet been integrated into the actual system operation. A brief outline of the monitoring algorithm is as follows.

Suppose the ARMAX model at time k can be described as:

$$\begin{aligned} & y(k)+a_1 y(k-1)+a_2 y(k-2)+\ldots+a_m y(k-m) \\ & =u(k)+b_1 u(k-1)+b_2 u(k-2)+\ldots+b_p u(k-p)+ \\ & c_1 e(k-1)+c_2 e(k-2)+\ldots+c_r (k-r) \end{aligned} \tag{2-47}$$

where the additional notation c_r refers to the r^{th} order of the exogenous coefficient c while the variable e is the associated input. Therefore, the parameters to be computed can be grouped into a vector such that:

$$\theta = \begin{bmatrix} a_1 & a_2 & \ldots & a_m & b_1 & b_2 & \ldots & b_p & c_1 & c_2 & \ldots & c_r \end{bmatrix}^T \tag{2-48}$$

Once again the primary objective is to determine the coefficient a_i in order to formulate the characteristics polynomial equation of Equation (2-43). Unlike ARMA, the recursive nature of the R3LS utilizes a different update engine that is more similar to Kalman Filter. Further details regarding to the mathematical formulation can be referred to [127].

2.2.11 Hilbert-Huang Transform (HHT)

In essence, Hilbert-Huang Transform is a technique that is designed to analyze the non-linear and the non-stationary processes. Similar to Wavelet Transform, HHT decomposes a signal into a series of the amplitude and the frequency modulated components by the means of the Empirical Mode Decomposition Method. Subsequently, the modal properties can be derived by applying the Hilbert Spectral analysis. HHT was proposed by Huang *et al.* [147], in 1998. Today, HHT is applied to a wide range of applications ranging from image-processing to biomedical engineering. For power system analysis, HHT was first introduced in 2006 for detecting the electromechanical oscillations [128]. Several extensions have been developed since then and are outlined in [85, 123, 148]. An overview of the fundamental HHT operation is summarized below.

Suppose a real output $y(t)$ can be represented in the complex form as:

$$z(t) = y(t) + iy_H(t) \tag{2-49}$$

where $y_H(t)$ is the Hilbert Transform of the original output signal given by:

$$y_H(t) = \frac{1}{\pi} P \int_{-\infty}^{+\infty} \frac{y(s)}{t-s} ds \tag{2-50}$$

Here the notation P refers to the Cauchy principal value of the integral. Like all previously detection algorithms, Equation (2-49) can also be expressed in terms of the exponential form:

$$z(t) = A(t)e^{i\psi(t)} \tag{2-51}$$

where

$$A(t) = \sqrt{y(t)^2 + y_H(t)^2}$$
$$\psi(t) = \arctan\frac{y_H(t)}{y(t)} \tag{2-52}$$

The variables $A(t)$ and $\psi(t)$ are the time-dependent amplitude and the phase functions respectively. The time derivative can then be formulated as:

$$\dot{z}(t) = A(t)e^{i\psi(t)}(i\omega(t)) + e^{i\psi(t)}\dot{A}(t) \tag{2-53}$$

Where $\omega(t)$ is the instantaneous angular frequency, which is the time derivative of the instantaneous angle such that:

$$\omega(t) = \dot{\psi}(t) = \frac{d}{dt}\arctan\frac{y_H(t)}{y(t)} \tag{2-54}$$

From Equation (2-54), the oscillatory frequency can be computed by:

$$f(t) = \frac{1}{2\pi}\mathrm{Im}\left(\frac{\dot{z}(t)}{z(t)}\right) = \frac{y(t)\dot{y}_H(t) - y_H(t)\dot{y}(t)}{2\pi(y(t)^2 + y_H(t)^2)} \tag{2-55}$$

Similar to WT, the damping factor cannot be extracted simultaneously by estimating the frequency component, like those based on Linear Prediction models. Instead, the modelled signal in Equation (2-51) needs to be rearranged such that:

$$z(t) = A(t)e^{i\psi(t)} = \sum(t)e^{-\theta(t)+i\psi(t)} \tag{2-56}$$

which then the time-dependent decay function (damping factor) can be approximated as:

$$\theta(t) = -\int_0^t \sigma(t)dt \tag{2-57}$$

By manipulating Equations (2-53) and (2-56), the instantaneous damping factor be approximated as:

$$\sigma(t) = -\frac{d\theta(t)}{dt} = -\frac{\dot{A}(t)}{A(t)} \tag{2-58}$$

Further readings regarding to the mathematical formulation can be referred to [85, 147].

2.3 *Remarks*

In this chapter, the nature of the electromechanical oscillations has been defined. Due to the increasing network stress to meet the power demands, many grids, similar to New Zealand's, are becoming more prone to lightly damped oscillations. In particular, the networks are more susceptible to the inter-area oscillations. The inter-area oscillations are caused by remote generators oscillating against each other and they are difficult to detect. Consequently, those oscillations have triggered a number of wide area blackouts in the recent decades. Based on these past experiences, and with the introduction of PMUs, several monitoring methods have been formulated to track the unstable oscillatory build-ups. In general, the trend of real-time situation awareness in modern system monitoring is moving towards the time-domain analysis using synchrophasor measurements.

Since to date there are no industry standardized online algorithms for the PMU platform in New Zealand, the country has the freedom to explore various options of detection schemes. In this case, mature algorithms that are currently operating in the networks are favoured. As discussed in Chapter 1, Prony Analysis is presently adopted in many nations like China, USA and the majority of the European Union. Meanwhile, Kalman Filter has seen operation in Scandinavian countries and Thailand. Therefore, this research identifies Kalman Filter and Prony Analysis as two attractive candidates for the New Zealand operation.

In order to address the merits of each technique, exhaustive comparative studies are needed. Several comparative studies have been conducted to evaluate Kalman Filter and Prony Analysis against other new monitoring techniques, but few papers have been published to compare the two mature methods. Therefore, it is necessary to investigate their operational nature. That is the main scope of the next chapter.

3 Evaluating the Performance of Kalman Filter and Prony Analysis

3.1 *The Nature of the Monitoring Methods*

Unlike many other power networks, vast hydro generation reserves allow the New Zealand grid to ride through most ambient excited oscillations with little danger. As a result, detecting the oscillatory behaviours caused by ringdown dynamics are regarded as a higher priority than the ambient counterpart. Ringdown oscillations are usually generated by notable network disruptions such as load variation, faults, outages, or change in generation capacity.

In order to accurately detect the inter-area oscillations caused by ringdown behaviour, several linear analysis techniques have been proposed in the past. As discussed in Chapter 2, the monitoring methods can be grouped into two families: blocking-processing and recursive. In brief, methods belonging to the block-processing class are usually time-invariant; meaning: that they assume the parameters do not change throughout that time window [146]. Conversely, the recursive detections allow the time-varying parameters to be promptly addressed, but their monitoring procedures are generally more complex than the block-processing approach. Hence, the fundamental question one may ponder is "*Which one to adopt?*" That is the prime focus of this chapter. In order to identify the adequacy of a technique for the New Zealand operation, it is crucial that the characteristics of the block-processing and the recursive methods be exhaustively analyzed.

In the past two decades, many monitoring techniques based on both approaches have been proposed. Initially, research focused on developing block-processing methods, but later shifted towards their recursive counterparts. Many proposed monitoring methods have shown outstanding functionality in simulation and testing phases, but few have been integrated into actual network operation. Currently,

amongst published algorithms, Kalman Filter and Prony Analysis are considered the two mainstream methods. Prony is perhaps the most widely adopted technique, and has seen operation in Australia, Brazil, China and USA [9]. It was developed by *Bonneville Power Administration* in 1990 and was one of the earliest methods used to detect power system oscillations from a time-domain perspective [121]. Prony is a classic block-processing algorithm that shares similar characteristics to the later developed Matrix Pencil, and Hankel Total Least Square.

Kalman Filter, is a monitoring technique proposed by *ABB Switzerland Ltd. Corporate Research Group* in 2003 [129]. It was one of the earliest operational recursive techniques and is currently deployed in Scandinavian countries and Thailand [9, 66]. Recent recursive algorithms, such as, Yule-Walker and Regularized Robust Least Square are developed on similar principles to Kalman Filter.

Therefore, in terms of the development timeframe, both Prony and Kalman Filter can be considered as the founding fathers of most modern oscillation detection schemes. They serve as excellent representatives for the block-processing and the recursive detection respectively. Hence, as discussed in Chapter 2, both methods have been selected as suitable candidates for the New Zealand network.

Although several publications have attempted to assess the performance and applicability of each method, there is no significant publication that compares them qualitatively. Since the characteristics of each country's networks are unique; neither method should be regarded as the optimal, or, the universal approach for online monitoring application. Therefore, the focus of this chapter is to provide the system operator with a guide for choosing a parameter estimation technique that better suits their need. The investigation was motivated by two aspects:

1) The estimation accuracy
2) The operational robustness

These were achieved by studying the behaviours of both techniques when subjected to:

- Changing oscillatory activities
- Different noise levels
- Various sampling intervals

The main objective was to address the merits and applicability of each method for estimating power oscillations. Based on those findings, potential enhancements for each technique can be subsequently addressed.

3.2 *The Initialization and Tuning Procedures*

3.2.1 Variable Initialization

In order to effectively detect oscillations from noise contaminated measurements, both Kalman Filter and Prony Analysis require calibration prior to implementation. Although the recursive nature of the Kalman Filter is more attractive than Prony Analysis, it comes with a cost. Lists of variables that require initializing for both methods are shown in Table 3-1.

Table 3-1 A list of initialization variables for Prony and Kalman Filter

Kalman Filter	**Prony Analysis**
Estimated parameters, $p(k)$	System order, m
Kalman gain, $g(k)$	
Correlation matrix of estimation error, $K(k)$	
Covariance constant, C_1	
Covariance constant, C_2	
Correlation of measurement noise, Q_m	
Correlation matrix of process noise, Q_p	
System order, m	

For Kalman Filter, inadequate initialization of $p(k)$, $g(k)$, Q_m and Q_p can cause slow convergence or, may even lead to convergence failure. In addition, $K(k)$ is a unity matrix that is multiplied by a large constant. It determines the tracking ability of Kalman Filter and its performance is reflected by C_1 and C_2 constants. Unfortunately, there are no definite formulae for calculating those values. Instead, it has been suggested that they are experimentally selected through systematic examination [129]. Due to the number of parameters and their associated initializing procedures, calibrating Kalman Filter is an exhaustive task. Furthermore, retuning the variables is necessary when the network dynamics have changed significantly because the performance of Kalman Filter relies on the knowledge of the system characteristics. Nevertheless, once these variables are initialized or retuned, Kalman Filter is extremely effective in tracking and extracting useful modal information.

Compared with Kalman Filter, Prony Analysis is a non-recursive and curve-fitting technique. It approximates modal contents without any prior knowledge of the system operating conditions. Therefore, it is much simpler to implement than Kalman Filter in the context of the variable initializations. For Prony Analysis, the only variable that needs to be predefined is the system order m. That also applies to Kalman Filter.

3.2.2 System Order

Both Kalman Filter and Prony Analysis require selection of the order of the estimated model. The model order of the system represents the number of oscillatory modes in the captured signal. If the order is set less than the actual value, a highly smoothed spectrum is obtained. Consequently, inaccurate dynamic information of the network is generated. Alternatively, if the order chosen is too large, overfitting the model to noise would occur. Since the oscillatory modes occurring in power systems in any instance is unknown, estimating the actual model is not practical. Nevertheless, a good engineering practice is to allow overfitting instead of underfitting [149]. When a larger order is used, spurious noise modes are introduced from overfitting. However, those modes usually contain frequencies much higher than the generator oscillations and can be subsequently filtered out. Such a procedure is adopted by both Kalman Filter and Prony Analysis.

The approach taken by Kalman Filter [129], was to implement *Akaike Information Criteria* (AIC) followed by a systematic tracking procedure to identify the system order m. The order is found by minimizing the following criteria:

$$AIC(m) = \ln \hat{\sigma}_{wL}^2 + \frac{2m}{N} \tag{3-1}$$

where $\hat{\sigma}_{wL}$ is the estimated variance of the linear prediction error and *N* is the data size. Lower $\hat{\sigma}_{wL}$ would refer to higher m. However, $2m/N$ term would also increase as the order becomes larger. Therefore, searching for a balance between $\hat{\sigma}_{wL}$ and m is needed to achieve minimum AIC [150]. Unfortunately, under certain conditions, the performance of AIC is questionable. Since Kalman Filter contains adaptive characteristics; the data may exhibit time-varying property and thus violate the statistically independent assumption of successive data vectors. Additionally, AIC is proven to be sensitive to variations in Signal to Noise Ratio (SNR) and the data size [139]. Therefore, one can state:

- Under high SNR and larger samples, AIC can easily lead to overdetermined system order.
- For low SNR and small data size, AIC provides more reliable estimates. However, the trade-off is these approximations are highly sensitive to statistical variations. Consequently, it may not be a practical option.
- As a result, careful interpretations of the oscillatory information are needed.

In contrast, Prony Analysis searches for the model order by starting with an exaggerated initial guess of the magnitude m. That value is subsequently reduced to a more appropriate order by SVD. An approach to reduce the initial excessively large order was proposed in [151] and is formulated as:

$$K(i) = \left[\frac{\delta_1^2 + \delta_1^2 + \cdots + \delta_m^2}{\sum_{i=1}^{m} \delta_i^2} \right]^{\frac{1}{2}} \tag{3-2}$$

where δ are the singular values obtained from SVD. Since the singular values are ranked as:

$$\delta_1 \geq \delta_2 \geq \cdots \geq \delta_L \geq \delta_{L+1} = \cdots = \delta_m = 0 \tag{3-3}$$

When index i approaches the real order, the monotonically increasing function $K(i)$ will converge towards 1. In practice, the operator needs to predefine a threshold for $K(i)$. That is usually done through a trial-and-error approach.

Although the order estimation methods used in Prony Analysis are different to Kalman Filter, they all require trial-and-error. Consequently, extra computation time is needed to search for the model order. Prony Analysis approach is less effective in terms of calculation time. The use of high order results in a higher matrix dimension for the data matrix. Such an action will cause matrix operations, like pseudo-inverse and SVD technique, to become more computationally intensive.

3.2.3 Data Pre-processing

In order to provide accurate solutions, data pre-processing has been adopted for both algorithms. In the case of Kalman Filter, a band-pass filter is implemented to remove measurement noise. Although Kalman Filter can still operate without the aid of filters, faster convergence and better accuracy are achieved with them.

In contrast, pre-filtering is not implemented in Prony Analysis. Nevertheless, the applied SVD operation itself acts like a Wiener Filter. Hence, one can conclude that both methods apply filtering technique. Compared to Kalman Filter, the accuracy of Prony Analysis is more sensitive to data offsets. Since Prony Analysis is based on the assumption that the system is constantly undergoing small changes, it would not work under steady-state condition. Hence, de-trending the measured samples is necessary. However, de-trending the data (removing signal offsets) under the noisy condition is a difficult task as, the offsets are not clearly visible, and may be non-linear [144]. Due to the additional de-trending stage, Prony Analysis is more computationally intense and complex than Kalman Filter in terms of data pre-processing.

3.3 *The Impact of the Modal Contents*

To prevent confusion, the rest of this chapter will address sampling in terms of sampling interval/period instead of sampling rate. Here, the sampling interval, or the

sampling period, refers to the time between two consecutive measurements. The timeframe used to collect the data is referred as the sampling window, or, the sampling timeframe.

3.3.1 Tracking Fixed and Time-Varying Oscillatory Modes

In a modern power grid, there are often multiple electromechanical oscillations occurring simultaneously. Their dynamic behaviours are usually embedded inside the measured signal. Hence, the ability to approximate multiple oscillations is essential. In order to examine the monitoring performance of Kalman Filter and Prony Analysis, two test cases are formulated:

1) Monitoring multiple fixed oscillatory parameters
2) Monitoring time-varying oscillations

To distinctly outline the operational characteristics of both methods, all studies are conducted by examining each method in its most fundamental form. Hence, a synthetic signal similar to Equation (2-6) is used to simulate the ringdown behaviour in the form of:

$$y(t) = \sum_{i=1}^{n} A_i e^{-\sigma_i t} \cos(2\pi f_i t + \phi_i) + v(t) \tag{3-4}$$

where the extra variable *v(t)* refers to the white noise component. Using the known model parameters ensures the simulations are conducted in a more controlled manner. Therefore, a synthetic signal containing three oscillations is selected as the primary test bench for this chapter. Its modal parameters are listed in Table 3-2, and the corresponding time-domain behaviour is shown in Figure 3-1.

Table 3-2 Oscillatory parameters of the synthetic signal

Mode	Amplitude	Damping Factor	Frequency (Hz)
1	1.5	0.1	0.5
2	0.5	0.3	0.9
3	0.7	0.5	1.5

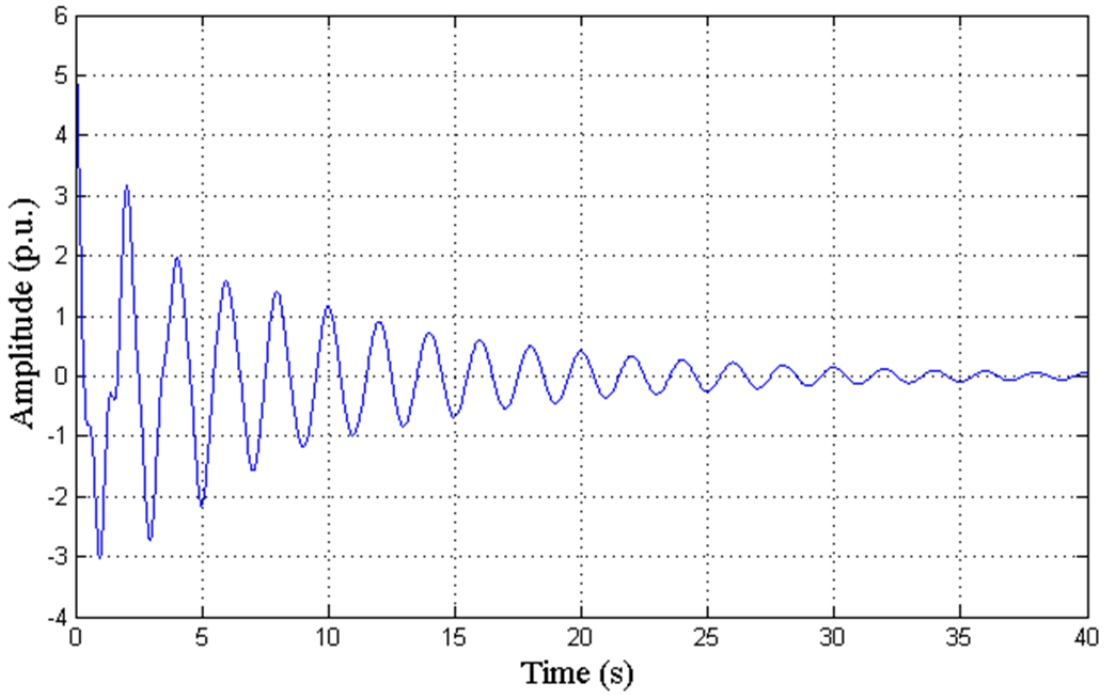

Figure 3-1 The time domain behaviour of the simulated synthetic signal

3.3.1.1 Test Case 1: Monitoring Fixed Modal Parameters

The main aim of this study is to assess the capability of each technique to detect the dominant Mode 1. The secondary objective is to examine the ability to monitor other less-dominant oscillations because networks like New Zealand's can have multiple oscillations occurring simultaneously. For this test case, the sampling interval was fixed 0.1 second and a 10 second sampling window was used. A component noise, with a Signal to Noise Ratio (SNR) of 40 dB, was added to both signals. For this research, uncorrelated white noise is added into the synthetic signals to simulate the ambient/background operational dynamics. Note that the ambient noise of actual power grids may not be white. The initial conditions of all variables are listed in Table 3-3. To provide a detailed assessment, 100 independent Monte Carlo simulations were conducted. Note: the noise behaviour was investigated in the later example but was not the emphasis for this study. In order to establish a common comparison platform, the monitoring results are updated at the end of the 10 second window. However, due to the recursive characteristics of Kalman Filter, its solutions were calculated by averaging the results from all the iterations within each sampling

window. Moreover, the results from the initial convergence process in the first few iterations were not included as part of the mean.

Firstly, the ability to monitor a single ringdown oscillation was examined. The performance of both detection schemes is outlined in Table 3-4. Note: STD stands for the standard deviations of the 100 computed results. As expected, both Kalman Filter and Prony Analysis were able to track the dominant oscillation accurately. Other modal contents had little effect in causing significant estimation inaccuracies.

Next, the effectiveness of monitoring the other two oscillations is presented in Table 3-5. According to these results, Prony Analysis was able to approximate Mode 2 and 3 with similar precisions as with Mode 1. Hence, it is an ideal algorithm for tracking multiple oscillations simultaneously.

Even though Kalman Filter is primarily designed to only track the dominant mode, it was used to test the detection of the other two oscillatory modes. Unsurprisingly, higher errors were introduced in the less dominant oscillations, especially, when approximating the damping factors. Nevertheless, it was still able to detect them with less than 20% errors.

Table 3-3 Initial conditions of Kalman Filter and Prony Analysis

Variable	**Value**
Estimated parameter, $p(k)$	0 for all elements
Correlation matrix of estimation error, $K(k)$	10000 (for the diagonal elements)
Correlation matrix of process noise, Q_p	0.01 (for the diagonal elements)
Correlation of measurement noise, Q_m	0.9
Covariance constant, C_1	100
Covariance constant, C_2	0.01
Kalman gain, $g(k)$	0 for all elements
System order (Kalman Filter)	20
System order (Prony Analysis)	20
Reduced SVD order (Prony Analysis)	18

Table 3-4 Monitoring the Dominant Mode 1 Oscillation

Mode	Kalman Filter				Prony Analysis			
	Damping Factor		Frequency (Hz)		Damping Factor		Frequency (Hz)	
	Mean	STD	Mean	STD	Mean	STD	Mean	STD
1	0.101	$3.2\text{x}10^{-4}$	0.499	$3.6\text{x}10^{-5}$	0.100	$2.1\text{x}10^{-4}$	0.500	$3.0\text{x}10^{-5}$

Table 3-5 Tracking Performance of the less Dominant Modes 2 and 3

Mode	Kalman Filter				Prony Analysis			
	Damping Factor		Frequency (Hz)		Damping Factor		Frequency (Hz)	
	Mean	STD	Mean	STD	Mean	STD	Mean	STD
2	0.359	$2.3\text{x}10^{-3}$	0.925	$3.5\text{x}10^{-4}$	0.300	$2.0\text{x}10^{-3}$	0.900	$2.8\text{x}10^{-4}$
3	0.527	$3.3\text{x}10^{-3}$	1.50	$4.2\text{x}10^{-4}$	0.501	$2.8\text{x}10^{-3}$	1.50	$4.0\text{x}10^{-4}$

Table 3-6 Percentage Error of Kalman Filter's Computed Eigenvalues

Mode	**Real** (Damping Factor)	**Imaginary** ($2\pi f$)	**Absolute**
1	2.9	0.3	0.4
2	8.0	1.0	1.0
3	5.2	0.7	0.7

Although the overall performance of Kalman Filter was less attractive than Prony Analysis, it was able to approximate the frequency components (i.e. imaginary part of the eigenvalues) with reasonable accuracies. This was indeed an interesting behaviour. To understand such phenomena, further examinations in terms of monitoring errors were conducted and are listed in Table 3-6. These results can be interpreted as:

- The estimation error of the real part increases for modes that are less dominant.
- The detection accuracy of the imaginary part can be regarded as not affected by the number of modes in the signal.
- The absolute of the complex eigenvalue has similar approximation precision as its corresponding imaginary part because $\omega >> \sigma$.

Those observations can be explained by the formulation of the state variable of Kalman Filter. In essence, the state variables of Kalman Filter are used to approximate the autoregressive AR coefficients of the characteristic equation as shown in Equation (2-36). Subsequently, the eigenvalues are extracted by rooting the formulated polynomial equation in the continuous domain. Finally, the damping factors and the oscillatory frequencies are computed from the obtained Eigen solutions. Hence, Kalman Filter from [129] can be considered as estimating the modal parameters in an indirect manner.

State variables are not formulated to model the individual damping factors and their matching frequency components. Therefore, distinguishing them from the eigenvalues is a challenging task. The reason; the significantly larger magnitude of the imaginary part shadows the relatively smaller real component of the eigenvalue, i.e. $\mathrm{Re}\{\lambda\} << \mathrm{Im}\{\lambda\}$. Although Kalman Filter is able to estimate AR coefficients with high precisions, any minute errors in the coefficients could, potentially, magnify into greater inaccuracies when extracting the damping factors. Furthermore, the use of *Tustin* approximation, to transform the transfer function from the discrete to the continuous domain, also introduces additional estimation inaccuracies. In other words, the ability to detect multiple damping factors and their associated frequencies, is challenging when using the state variables to passively approximate the

eigenvalues. Nevertheless, according to Table 3-4, one should note the recursive engine of Kalman Filter is sound. With some modifications to the modelling of the state variables, it is possible to improve its performance to monitor multiple oscillations.

3.3.1.2 Test Case 2: Monitoring Time-Varying Parameters

To simulate a time-varying behaviour, Mode 1 experienced a change in its damping factor from 0.1 to 0.2 after 5 seconds into the simulation. Note that a change in the system dynamics during a ringdown event may occur when the network is subjected to severe disturbances. Such abrupt change is not often encountered during normal operations. In addition, a larger monitoring window of 15 seconds was used in this study. The rest of the parameters were kept unchanged. The obtained results from 100 Monte Carlo simulations are summarized in Table 3-7.

According to the table, both methods are able to track the final modal contents accurately. However, Prony was unable to identify that the original damping factor of Mode 1 was in fact, 0.1 instead of 0.2. Being a time invariant block-processing technique, Prony is only able to update modal parameters once every sampling window. Consequently, the initial content of Mode 1 was unable to be monitored. Theoretically, Prony should not be able to track the changed damping factor with suitable precision when the data batch is contaminated by different modal characteristics. However, that was not the case in this situation. That is because there were more measurements containing the changed modal parameter, than those containing the original oscillatory contents. Prony solutions are highly dependent on the adequacy of the constructed Linear Prediction data matrix, and tend to approximate the dynamics present in the majority of the collected data. Nevertheless, owing to modal contamination, Prony still incurred higher inaccuracies compared with Test Case 1.

Table 3-7 Modal Estimations of the Time-Varying Mode 1

	Kalman Filter				Prony Analysis			
	Damping Factor		Frequency (Hz)		Damping Factor		Frequency (Hz)	
	Mean	STD	Mean	STD	Mean	STD	Mean	STD
Before Change	0.101	1.2×10^{-3}	0.500	2.4×10^{-4}	0.191	7.2×10^{-4}	0.500	9.4×10^{-5}
After Change	0.204	1.7×10^{-4}	0.502	5.3×10^{-4}				

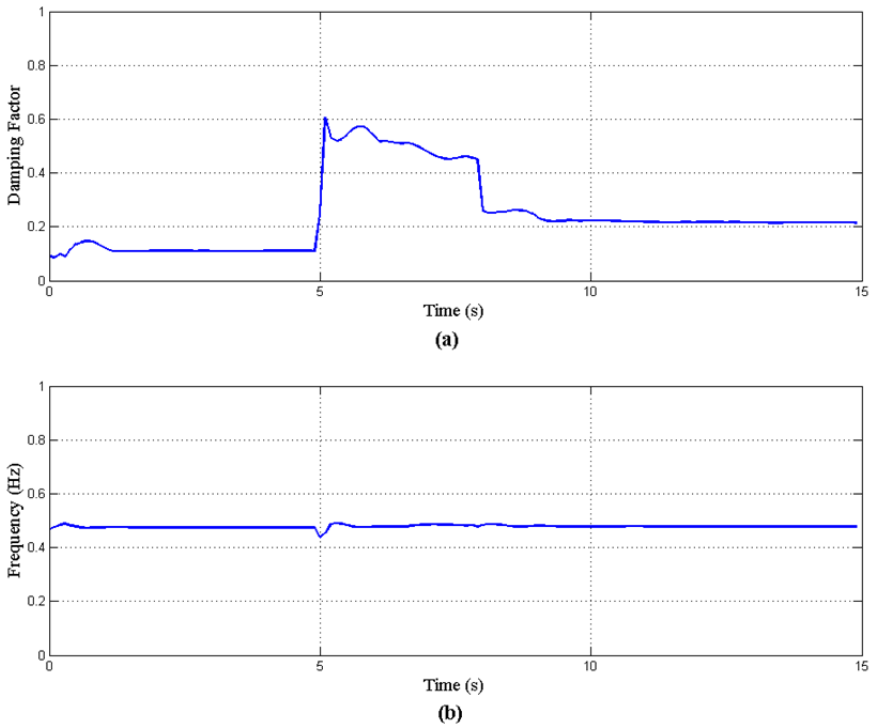

Figure 3-2 Performance of Kalman Filter to track the time-varying Mode 1: (a) damping factor, (b) oscillatory frequency

On the contrary, the recursive Kalman Filter had little trouble in detecting the time-varying behaviour of Mode 1 and its time-domain performance is illustrated in Figure 3-2. In addition, referring to Table 3-7 and comparing that with Test Case 1, the higher standard deviations in the approximated results were caused by the recursive tracking characteristics. Due to Monte Carlo simulations, the mean values obtained from the recursive iterations also varied each time. As a result, Kalman Filter would generate a slightly larger population spread when estimating the changed modal parameters. That would not be an issue for block-processing techniques.

3.4 *The Effect of the Operating Environments*

3.4.1 The Impact of the Noise on Monitoring Performance

The signal noise caused by the system dynamics, the measurement devices, or the communication channels, are major obstacles to providing accurate modal parameters extraction. The use of large overdetermined data matrix in Prony Analysis is known to be weak towards noise [126]. Nevertheless, the integration of Singular Value Decomposition (SVD) into modern Prony approximation has helped to improve its noise resistance capability [129]. The presence of noise is also an issue for Kalman Filter. Its convergence accuracy and speed is dependent on the noise level [96, 140].

3.4.1.1 Test Case 3: Monitoring under Different Noise Levels

In order to investigate the effects of the noise on Kalman Filter and Prony Analysis, three different SNR levels (20 dB, 30 dB and 40 dB) were added into the synthetic signal outlined in Table 3-2. The waveform corrupted by the 20 dB noise is illustrated in Figure 3-3. For continuation purposes, the sampling interval, the sampling window and the initial conditions were kept the same as those in Subsection 3.3.1.

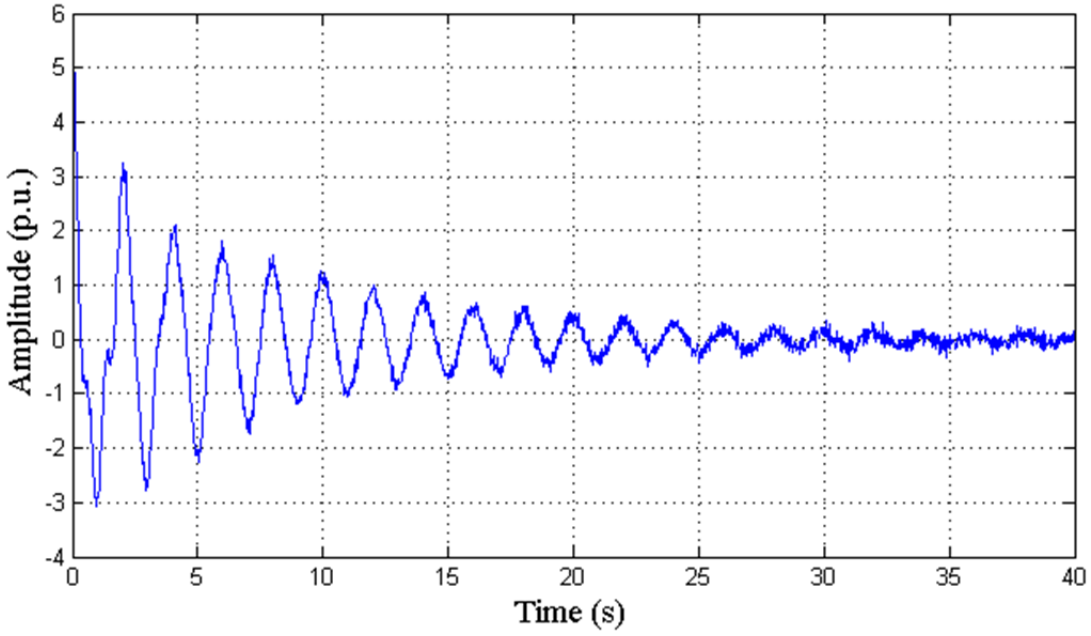

Figure 3-3 Signal waveform corrupted by 20 dB noise

The diversity of estimated modal parameters over 1000 Monte Carlo simulations are illustrated in Figure 3-4 and Figure 3-5. Each point on the plot corresponds to one estimated solution and the cyan coloured '+' symbol points to the true modal value. In addition, the colours red, blue and green represent the solutions obtained from 40 dB, 30 dB and 20 dB respectively. Referring to those plots, and inspecting Mode 1 (0.5 Hz), it is suggested that both methods are able the extract modal parameters with suitable accuracy. However, Prony Analysis was slightly more accurate than Kalman Filter under the noisy conditions. A proposed explanation is that in the presence of the noise, it is more difficult to identify the convergence direction, and thus, Kalman Filter was unable to detect with similar precision as Prony Analysis. If the correct convergence direction was provided to Kalman Filter at the start of the simulation, the tracking performance would be enhanced.

As noted in the previous studies, Kalman Filter was developed to monitor the dominant mode. Therefore, the approximation errors of Modes 2 and 3 were further amplified when noise was applied. Overall, it is clear that Prony Analysis was superior to Kalman Filter when tracking multiple oscillations under noisy conditions.

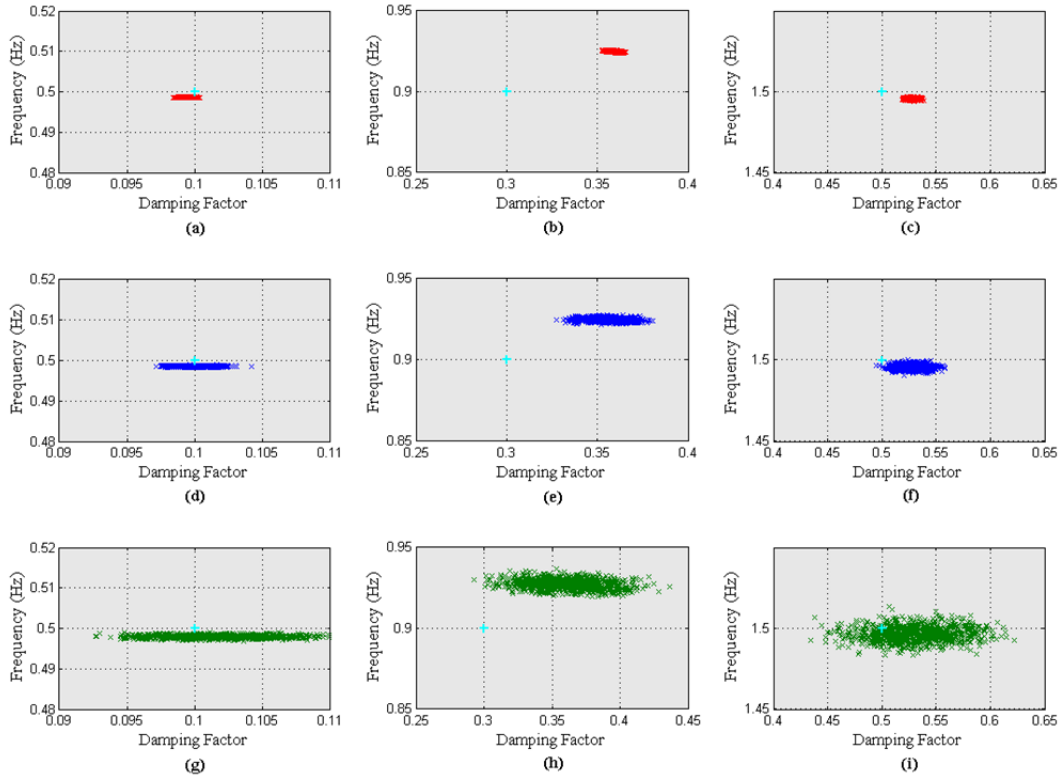

Figure 3-4 Kalman Filter estimations under various noise levels: (a)~(c) under SNR 40dB, (d)~(f) under SNR 30 dB, (g)~(i) under 20 dB

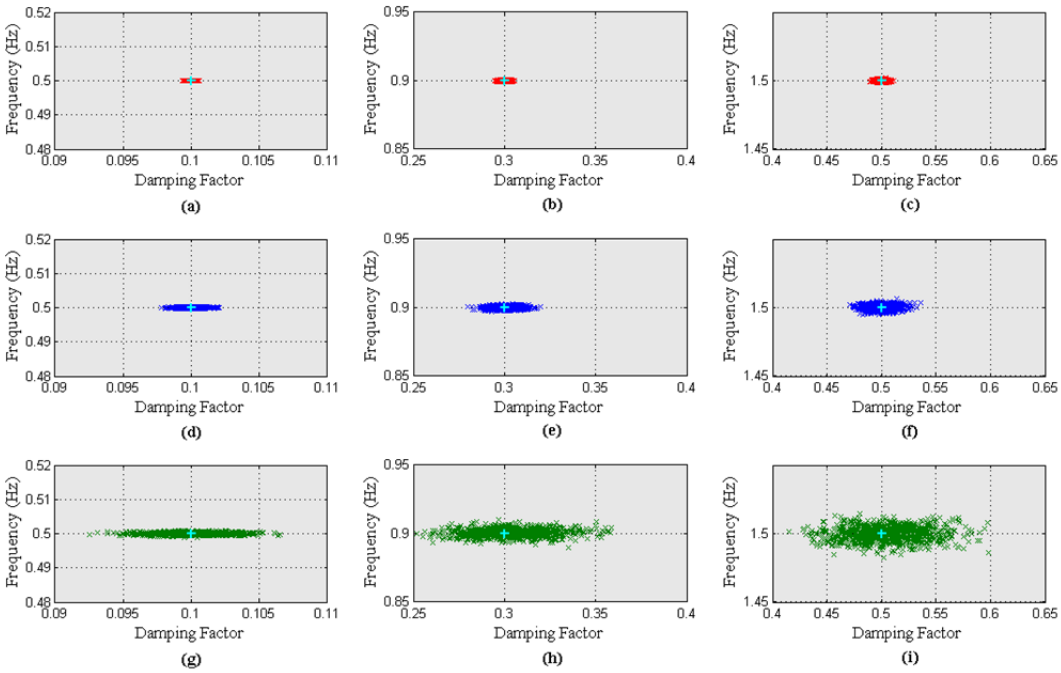

Figure 3-5 Prony estimations under various noise levels: (a)~(c) under SNR 40dB, (d)~(f) under SNR 30dB, (g)~(i) under 20 dB

3.4.2 The Impact of the Sampling Interval/Rate

The oscillatory detection techniques, using the discrete synchrophasor data, may subject to sampling issues if not setup properly. This refers to the fact that high-frequency components in the continuous function can impersonate low frequencies when the selected sampling rate is too low. Nevertheless, the aliasing effects can be prevented if Nyquist-Shannon sampling theorem is applied. That keeps the sampling frequency higher than twice the largest frequency component in the signal. Theoretically, it should be as fast as possible to minimize the loss of continuous information during the digitalization [139, 144]. However, in practice, the sampling rate of any system is limited due to the bandwidth of the installed hardware. Although Phasor Measurement Units are able to provide a typical sampling rate of 50 Hz, the collected synchrophasor measurements are usually down-sampled to a much lower rate for the oscillatory monitoring application. Note: the sampling process addressed in this thesis refers to the re-sampling procedure.

According to Korba [129], the sampling rate for Kalman Filter should be about 10 times greater than the highest frequency component. Being a recursive technique, there is no need to analyze large batch of data. Thus, the risk of encountering a numerically ill-conditioned problem during the estimation process is low. In fact, the effect of the sampling rate is less significant when compared with other sensitive factors such as the variable initialization. On the contrary, since Prony uses a large batch of measurements to construct its data matrix, its resultant monitoring accuracy is more dependent on the selected sampling interval. Recent literatures have indicated that an inappropriate sampling interval can cause Prony Analysis to give inaccurate solutions [98, 99, 152]. Therefore, a small variation in the sampling rate can cause a significant change in the obtained waveform and thus, the calculated eigenvalues. Presently, the typical sampling rate is around 10 Hz [9, 151]. Based on these observations, the performance of both methods using different sampling intervals needs to be investigated.

3.4.2.1 Test Case 4: Monitoring Sensitivity under Various Sampling Intervals

The purpose of this test case is to observe the impact of the sampling interval on modal estimation accuracy. Because Kalman Filter is not designed for tracking multiple oscillations, the synthetic signal used in this study only contained Mode 1 and its parameters as listed in Table 3-2. Furthermore, a high SNR level of 40 dB was applied. Any inaccuracies caused by the sampling interval could be easily accentuated from those caused by the method's limitations and the noise components. In total, three different sampling intervals were tested: 0.005 second, 0.1 second, and 0.2 second. Those intervals correspond to a sampling rate of 200 Hz, 10 Hz and 5 Hz. In this experiment, the initial conditions of both techniques were kept the same as all previous studies. A fixed monitoring window of 10s was adopted.

The results showing the average of 100 Monte Carlo runs are outlined in Table 3-8. According to the computed mean values; operating under different sampling intervals had little impact on the detection accuracy of Kalman Filter. However, a closer look shows Kalman Filter's dependency on the sampling interval, as observed in the corresponding standard deviations in Figure 3-6. Note that the green dash line represents the true value. The Monte Carlo solutions at 0.005 interval is significantly higher than the other two intervals.

Table 3-8 Mode 1 Estimation Using Different Sampling Intervals

Interval (s)	Kalman Filter				Prony Analysis			
	Damping Factor		Frequency (Hz)		Damping Factor		Frequency (Hz)	
	Mean	STD	Mean	STD	Mean	STD	Mean	STD
0.005	0.101	$3.7\text{x}10^{-3}$	0.500	$3.9\text{x}10^{-4}$	0.104	$3.5\text{x}10^{-3}$	0.500	$2.2\text{x}10^{-3}$
0.10	0.100	$2.7\text{x}10^{-4}$	0.500	$3.8\text{x}10^{-5}$	0.100	$1.6\text{x}10^{-4}$	0.500	$2.9\text{x}10^{-5}$
0.20	0.101	$3.1\text{x}10^{-4}$	0.500	$2.0\text{x}10^{-5}$	0.101	$3.6\text{x}10^{-4}$	0.500	$1.2\text{x}10^{-4}$

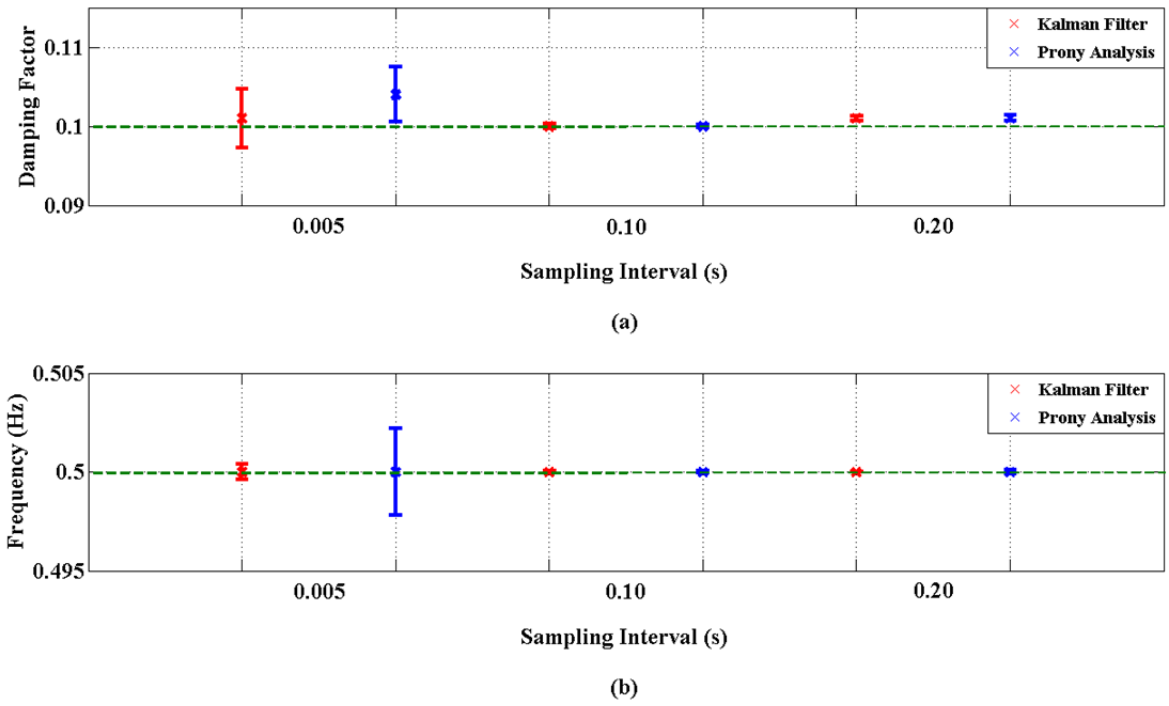

Figure 3-6 Standard deviations of the estimated Mode 1 parameters: a) damping factor and b) oscillatory frequency

Compared with Kalman Filter, the precision of Prony Analysis was found to be more dependent on the selected sampling intervals. According to Table 3-8, the computed modal solutions when operating at 0.005 second interval was found to be less accurate. That is also reflected in the standard deviations illustrated in Figure 3-6. At close inspection, it appears that higher errors are introduced at smaller sampling intervals.

Based on these observations, the dependency of the sampling interval for each method has been analyzed. The next step was to further examine the monitoring accuracy of Prony Analysis under smaller sampling intervals. Using the same simulated signal, the subsequent tracking performance is listed in Table 3-9.

According to these results listed in Table 3-9, the approximation accuracy of Prony Analysis distinctly degraded when operating at smaller sampling intervals. It failed to approximate the oscillatory parameters at a more extreme sampling interval of 0.001 second. That is also shown in Figure 3-7 by the constant increase in the standard

deviations at smaller intervals. Therefore, in a fixed monitoring window condition, the effectiveness of Prony Analysis is dependent on the selected sampling interval.

Table 3-9 Performance of Prony Analysis under Various Sampling Intervals

Sampling Interval (s)	Prony Analysis			
	Damping Factor		Frequency (Hz)	
	Mean	STD	Mean	STD
0.001	–	–	–	–
0.004	0.107	$3.2\text{x}10^{-3}$	0.500	$2.2\text{x}10^{-3}$
0.005	0.104	$3.5\text{x}10^{-3}$	0.500	$2.6\text{x}10^{-3}$
0.02	0.101	$1.9\text{x}10^{-4}$	0.500	$4.5\text{x}10^{-4}$
0.10	0.100	$1.6\text{x}10^{-4}$	0.500	$2.9\text{x}10^{-5}$

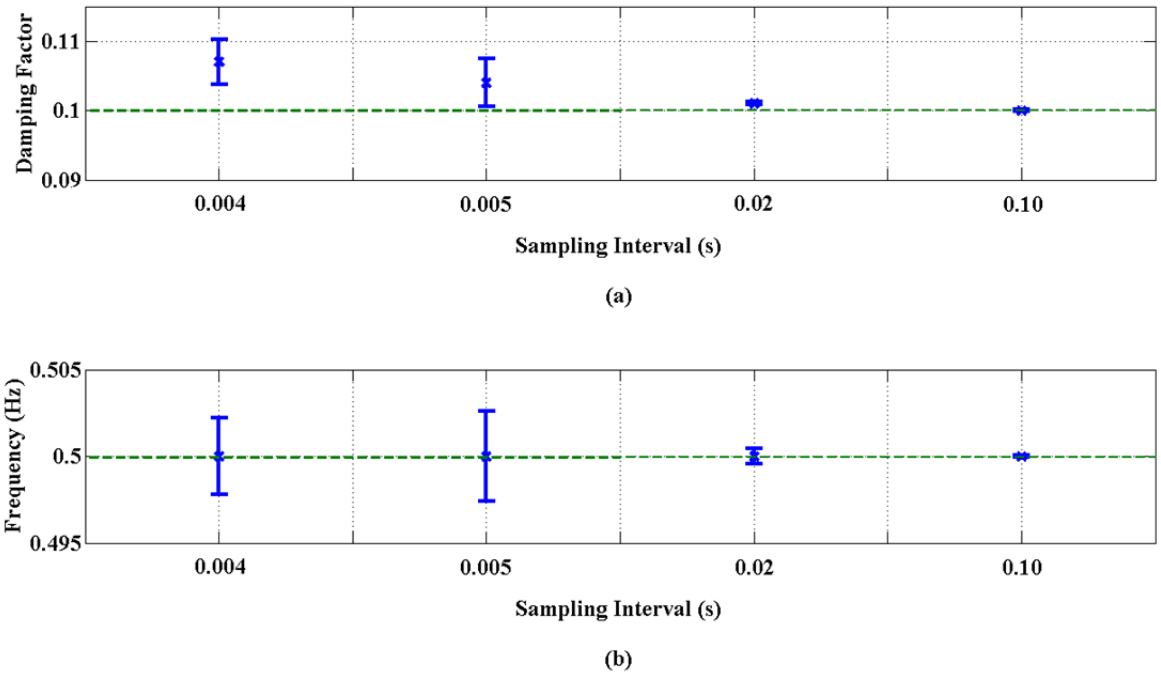

Figure 3-7 Standard deviations of Prony solutions under various sampling intervals: a) damping factor and b) oscillatory frequency

In summary, the observations indicate that the performance of Prony Analysis was more sensitive to the sampling interval than Kalman Filter. That is mainly related to the formulation of each technique. Since Prony Analysis is a fitting method that is dependent on the constructed data matrix, as shown in Equation (2-11), inappropriate sampling interval would affect the matrix's reliability. The inadequate interval provided measurements that were unable to capture the true signal dynamics. In contrast, being a recursive detection technique, Kalman Filter estimated the modal parameters by predicting current dynamics based on a small finite past measurement. Unlike block-processing Prony, Kalman Filter is not a fitting method that relies on a large data matrix. Instead, its effectiveness is dependent on the established system knowledge.

3.5 *Discussion*

The merits of Kalman Filter and Prony Analysis are summarized in Table 3-10. The symbol ↑ represents more attractive, ↓ means less favourable, and ≈ means the same. For larger power networks, the actual dynamic system parameters may be less identifiable related to factors such as infrastructure modifications, near-random changes in system load, or operating the network at a new stress level. Therefore, the estimated post-contingency initial conditions could be unreliable. Under such situations, Prony Analysis is more suitable to implement as the method is less dependent on prior knowledge of the system and is able to monitor multiple oscillatory behaviours.

In contrast, Kalman Filter is more adequate for designated monitoring. Instead of being an all-purpose oscillation tracking algorithm like Prony Analysis, Kalman Filter can be designed to detect a particular inter-area mode. Its recursive nature provides a higher refresh rate and allows Kalman Filter to accurately identify modal parameters quicker than Prony Analysis, and track time-varying parameters. However, the convergence speed and the estimation accuracy have been observed to be dependent on the initial condition settings [9, 96, 98, 99, 139, 140, 151].

Table 3-10 Merits of Kalman Filter and Prony Analysis

Criteria	Kalman Filter	Prony Analysis
Variable Initializations Process	↓	↑
System Order Determination	≈	≈
Data Pre-Processing	↑	↓
Estimate Dominant Mode	≈	≈
Estimate Multiple Modes	↓	↑
Capture Time-Varying Dynamics	↑	↓
Noise Sensitivity	↓	↑
Sampling Rate Sensitivity	↑	↓
Sampling Window/Refresh Rate	↑	↓
Operation Flexibility	↓	↑

3.6 *Identified Potential Enhancements*

In most cases, detecting the dominant oscillation is sufficient to ensure system security. However, in New Zealand's narrow, longitudinal networks, there are often multiple oscillations that need to be monitored simultaneously. Therefore, the ability to detect multiple lightly damped oscillations is highly desired. Although there are multiple electromechanical oscillations in the New Zealand grid, their frequency magnitudes are widely apart [43]. Therefore, the need to track oscillations with similar frequency values is not a necessity.

Before implementing either of the mature monitoring schemes into the New Zealand grid, the following issues, associated with each method, need to be addressed. They are:

Kalman Filter:

- Increasing its ability to detect multiple oscillations
- Reducing the influence of initial conditions on estimation performance
- State variables needed to represent the modal parameters instead of the autoregressive coefficients

Prony:

- Improving the estimation confidence under various sampling settings. In particular, assessing the adequacy of the selected sampling interval

For Kalman Filter, the primary objective is to enhance its capability to monitor multiple modes. This is potentially feasible. The present method can already track less dominant oscillations with an error of less than 20%. Referring to Test Case1, the use of Tustin approximation, and the indirect estimation of modal parameters are the primary suspects of causing inaccuracies. Therefore, enhancing Kalman Filter to operate in the discrete domain and reformulating the state representation would help to extend the functionality to track multiple oscillations. Kalman Filter is able to detect time-varying parameters. However, the convergence of Kalman Filter is dependent on the adequacy of the initial conditions. Notably, inadequate selection of the initial state variables for Kalman Filter can produce biased results, and affect its convergence performance. Nevertheless, such concern can be minimized if the modal parameters are approximated beforehand. Therefore, equipping Kalman Filter with the ability to estimate prior signal properties would enhance the method's convergence performance.

Prony is a more mature method than Kalman Filter, and many improvements to it have already been published. The main goal of those researchers was associated with resolving Prony's weakest aspect, namely noise resistance. Hence, many of the existing publications focused on addressing this aspect [122, 131, 151, 153]. Assessing the impact of the sampling procedure on monitoring accuracy has been less investigated. Despite Kulp [98] and Van Blaricum *et al.* [154] mentioning that using inadequate sampling settings could result in estimation errors, no clear

evaluation procedure of selecting the sampling interval has been established. Therefore, to ensure that the extracted modal parameters are indeed trustworthy, a quality index for examining the adequacy of selected sampling intervals for Prony Analysis is desired.

3.7 *Remarks*

In this chapter, detailed assessments of Kalman Filter and Prony Analysis have been presented. In general, Kalman Filter is identified as an algorithm that is capable of monitoring the time-varying behaviour of the dominant oscillatory mode. In contrast, Prony Analysis is credited for its ability to accurately detect multiple modes under unknown parameters.

Related to experimental observations, several enhancements for each technique have been noted. For Prony Analysis, integrating a sampling scheme to a select suitable sampling interval has been recommended. Such a modification will be explored in Chapter 4. Extending the application of Kalman Filter to monitor multiple oscillations is proposed. The development in realizing this goal will be outlined in Chapter 5.

4 The Enhanced Prony Analysis

4.1 *Introduction*

In Chapter 2, Prony Analysis and Kalman Filter were identified as the two potential oscillation detection schemes for the New Zealand grid operation. Potential enhancements were noted in Chapter 3. The focus of this chapter is improving the performance of Prony Analysis. The primary aim is improving the sampling procedure by continuously assessing the adequacy of the sampling interval.

When monitoring in a digital environment, the accuracy and the reliability of the modal solutions are dependent on the adequacy of the chosen sampling interval. For oscillation detection application, the sampling interval is fixed and recommended to be at least 5 times higher than the largest known frequency component in the system [28, 129]. A fixed sampling window of 10 to 20 seconds has been suggested [9, 30]. Since the network conditions are continuous and changing due to its demands, the impact of the sampling process will be different under each situation. Consequently, fixed sampling settings may not be suitable for a specifically encountered disturbance. Prony Analysis is a block-processing technique, and its performance is dependent on the formulation of its data matrix as shown in Equation (2-11). Inappropriate sampling intervals could introduce additional sampling errors and demand more measurements. That would cause a drop in estimation accuracy and increase the data acquisition time. Such behaviour was observed in Subsection 3.4.2 and in other publications [98, 152]. Compared to the noise immunity aspect; enhancing the sampling procedure for Prony Analysis has been less investigated.

To resolve potential issues, redesign of the established guidelines can be explored. In the past, several sampling interval selection techniques have been developed [98, 152, 155, 156]. However, those methods were primarily designed for scenarios where the processing time was not crucial, and for non-power system applications.

Hence, they may not be suitable for tracking power oscillations in a close to real-time environment.

Therefore, the motivation of this chapter is to propose a technique that could be integrated into Prony Analysis to continuously select an adequate sampling interval. The improved method is known as the Enhanced Prony Analysis in this dissertation. The goal was to move away from a conservative fixed sampling approach, based on the worst case scenario to a more flexible data acquisition procedure that continuously adapts to changing operating conditions.

4.2 *The Resultant Impact of Sampling Errors: Data Matrix Formulation*

The nature of the block-processing technique is to extract the desired information by manipulating Linear Prediction-based data matrix. It contains the measurements collected within a predefined and fixed sampling/monitoring window. The sampling window/timeframe is defined as the number of historical measured data required to conduct a Prony Analysis. A typical monitoring window is around 10 seconds [9, 151].

Referring to Kulp [98], apart from the noise and measurement errors, a suspect for causing additional inaccuracy is the impact of the sampling interval on the formulation of the data matrix. Hence, poor selection of the sampling interval could cause the data matrix to become singular, or contain incorrect oscillatory dynamics because a small variation in the sampling interval implies a change in the obtained waveform and thus, the calculated eigenvalues [96, 99, 152]. Generally, the more suitable sampling rate is dependent on the predicted system order, and the size of the data matrix as shown in Figure 4-1. According to Nyquist-Shannon Sampling Theorem [144], it lies in the range of $[f_{\text{Nyquist}},\infty]$, where f_{Nyquist} refers to the minimum Nyquist sampling frequency. However, in an actual operation, the upper bound is restricted to the data acquisition speed of the implemented hardware specifications.

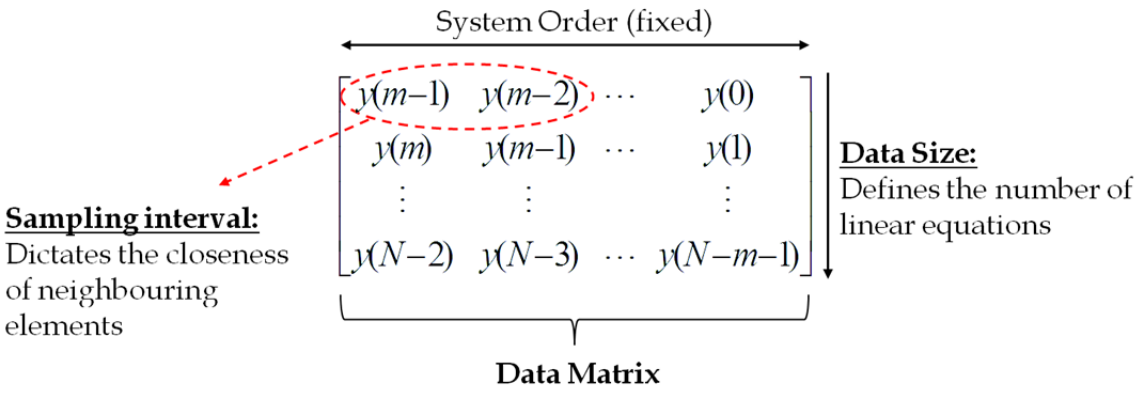

Figure 4-1 Characteristics of constructed data matrix for Prony Analysis

According to Figure 4-1, inadequate sampling not only results in poor capture of the modal contents, but it often increases the risk of matrix deficiency of A [157]. The deficiency refers to the data matrix becoming singular due to the closeness of measurements. Furthermore, one should note that using excessively overdetermined data matrix accompanied by a fast sampling rate, can increase the risk of having an ill-conditioned matrix [98]. In the contrary, operating at a larger sampling interval in a fixed monitoring window condition could also introduce sampling errors. The corresponding small batch of collected data may be insufficient to produce a reasonable set of linear equations.

Consequently, in both situations, the approximated Autoregressive coefficients from Equation (2-10) may be incorrect. Subsequently, errors are incurred in the computed oscillatory parameters due to the inaccurate characteristic equation from Equation (2-12). Since Prony Analysis does not rely on any system knowledge, the reliability of the estimated modal parameters when subjected to sampling errors is difficult to verify.

4.3 *Outline of the Proposed Sampling Scheme for the Enhanced Prony Analysis*

Assuming a disturbance has occurred, the sampling process of the existing Prony Analysis is formulated based on the maximum potential oscillating frequency of the network. Although this is a conservative approach, it does ensure that all oscillations can be detected. However, the trade off is that optimisation of the sampling procedure to address all disturbances may not be achieved. In this study, the appropriateness of the sampling process is addressed by examining the sampling interval.

In brief, the developed sampling procedure consists of two main objectives: the sampling interval selection, and the sampling adequacy verification. Based on these objectives, the proposed method can be summarized into the following three stages:

1. Conduct Prony Analysis
2. Verify the accuracy of the sampling constraints
3. Re-select and set new sampling parameters if required

A flowchart illustrating the above steps is shown in Figure 4-2. The condition number is implemented as a quality control indicator for checking the adequacy of the sampling interval. To provide an unbiased evaluation, the column size of Prony's data matrix was fixed for all sampling interval assessments. Details related to the condition number are discussed in the subsequent subsection.

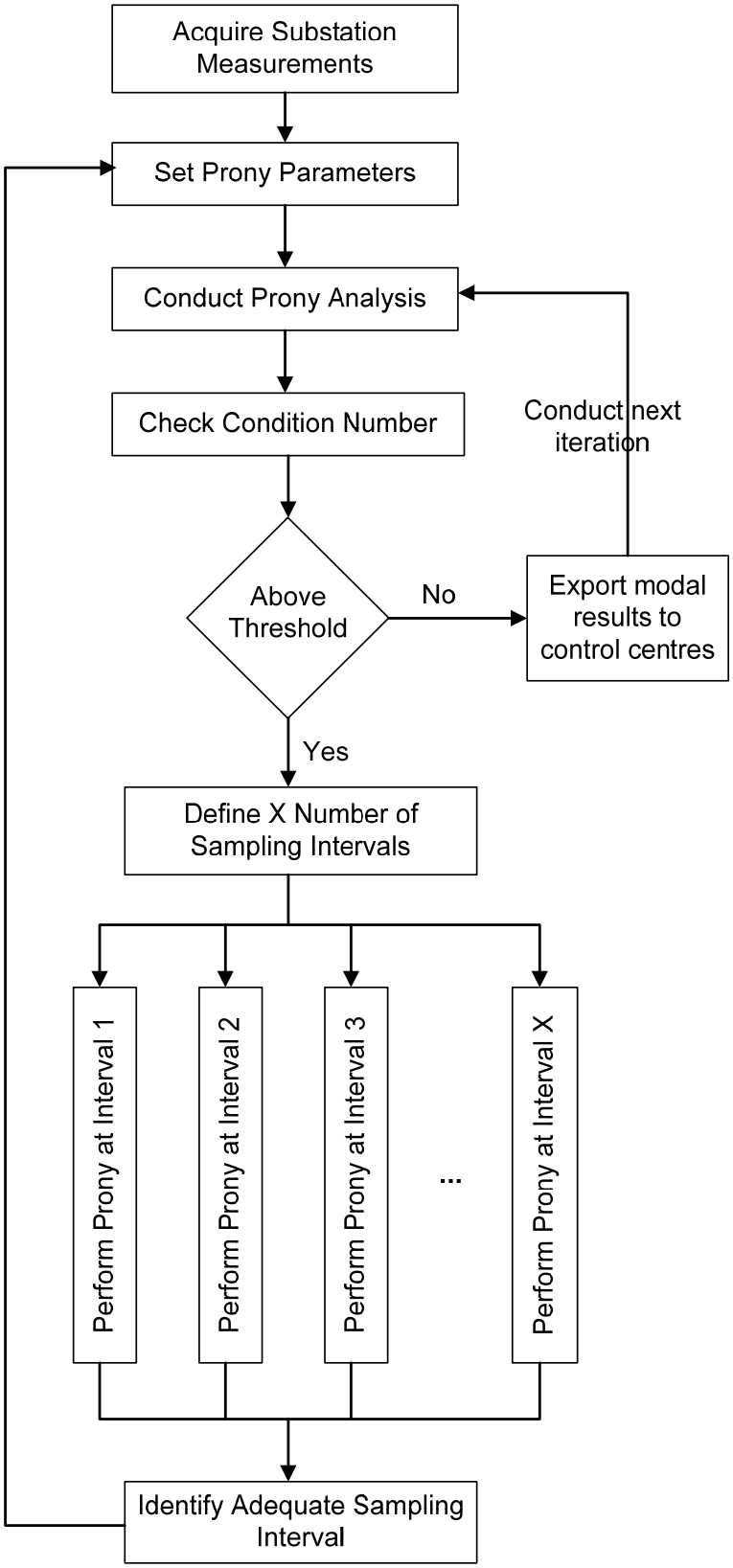

Figure 4-2 Outline of the proposed Prony sampling scheme

4.3.1 The Proposed Quality Evaluation Index – Condition Number

According to [98] and [152], two methods: the relative error, and the condition number have been recommended to assess the performance of the sampling process. Currently, two variations of relative error technique have been suggested as incorporations into power systems applications [151, 156]. In essence, the relative errors examine the appropriateness of the sampling interval by simply comparing the estimated solutions with their true values such as:

$$relative\ error = \sum_{i=1}^{m} \frac{|\lambda_i - \hat{\lambda}_i|}{|\lambda_i|} \tag{4-1}$$

where the header ^ represents the approximated eigen solutions. However, since oscillating frequencies are dependent on the grid dynamics, their true theoretical values are often unknown to the operators. Therefore, the relative error approach may not be appropriate for most power networks.

Alternatively, the condition number approach evaluates the significance of the sampling errors by indirectly assessing the status of the constructed data matrix. Such an option has been suggested and briefly described [152] for a communication application. Because the nature of the power system operation, the condition number is considered as a more attractive candidate than, the relative error. The ability of the condition number to reflect the impact of the sampling errors was not addressed mathematically in [152]. It is addressed and discussed in the reminder of this section.

Given that Prony Analysis is a polynomial fitting method, frequencies are computed from the coefficients of the approximated polynomial equation. However, due to the finite data size, and the rich information contained in PMU measurements, extracting oscillatory frequencies of interest from a signal could be a numerical problem. A small perturbation of the estimated solutions would result in an increase of relative errors. Since the condition number quantifies the amount of perturbations in the estimated solutions; it will possess similar characteristics to the relative error for determining the ideal sampling interval [152]. If the calculated condition number is above a predetermined threshold, doubts related to the accuracy of the solution are raised.

The derivations of how the condition number reflects inadequate sampling intervals are discussed below.

Generally, the condition number κ is introduced to passively monitor the quality of the sampling interval of the measured data. It acts as an error magnification factor, which is the ratio between the maximum and minimum singular values of the data matrix. The relationship between the condition number and the relative error in a linear system of $\mathbf{Ax} = \mathbf{b}$ is defined as:

$$\frac{\| \mathbf{x} - \hat{\mathbf{x}} \|}{\| \mathbf{x} \|} \leq \kappa(\mathbf{A}) \frac{\| \mathbf{R} \|}{\| \mathbf{b} \|} \tag{4-2}$$

$$\kappa(\mathbf{A}) = \| \mathbf{A} \| \quad \| \mathbf{A}^{+} \| \tag{4-3}$$

where $\mathbf{R}$ is the residue vector ($\mathbf{R} = \mathbf{b} - \mathbf{A}\hat{\mathbf{x}}$) and $\hat{\mathbf{x}}$ is the approximated solution vector. Furthermore, the symbol $\mathbf{A}$ represents the data matrix and the symbol $+$ refers to the pseudo-inverse operator [157]. Similar derivation can be achieved to model the behaviour of the condition number in the presence of the uncertainties. Suppose now the extracted signal incurs an error *e(k)* such that:

$$\hat{y}(k) = y(k) + e(k) \tag{4-4}$$

The linear algebra equation $\mathbf{Ax} = \mathbf{b}$ becomes:

$$\hat{\mathbf{A}}(x + \Delta x) = \hat{\mathbf{b}} \tag{4-5}$$

where

$$\begin{aligned} \hat{\mathbf{A}} &= \begin{bmatrix} y(m-1)+e(m-1) & y(m-2)+e(m-2) & \cdots & y(0)+e(0) \\ y(m)+e(m) & y(m-1)+e(m-1) & \cdots & y(1)+e(1) \\ \vdots & \vdots & & \vdots \\ y(N-2)+e(N-2) & y(N-3)+e(N-3) & \cdots & y(N-m-1)+e(N-m-1) \end{bmatrix} \\ &= \mathbf{A} + \mathbf{E} \end{aligned} \tag{4-6}$$

and

$$\hat{\mathbf{b}} = \begin{bmatrix} y(m)+e(m) \\ y(m+1)+e(m+1) \\ \vdots \\ y(N-1)+e(N-1) \end{bmatrix} = \mathbf{b}+\mathbf{e} \tag{4-7}$$

Note that Equation (4-5) is a general representation for any linear algebra problems and the vector $\boldsymbol{x}$ represents the coefficient vectors for the linear prediction monitoring methods. To recap from Chapter 2, the symbol m represents the system order while *N* is the amount of analyzed data. Assuming the error is small in the sense:

$$\left\|\mathbf{E}\right\| \left\|\mathbf{A}^{+}\right\| < 1 \tag{4-8}$$

then the maximum relative error of Equation (4-5) in a least square sense is:

$$\frac{\left\|\Delta\mathbf{x}\right\|}{\left\|\mathbf{x}\right\|} \le \frac{\kappa}{1-\left\|\mathbf{E}\right\| \left\|\mathbf{A}^{+}\right\|}\left[\frac{\left\|\mathbf{E}\right\|}{\left\|\mathbf{A}\right\|}+\frac{\left\|\mathbf{e}\right\|}{\left\|\mathbf{b}\right\|}\right] \tag{4-9}$$

Therefore, a data matrix with a large condition number, could reflect the presence of an estimation inaccuracy of the AR coefficients [98]. Further readings on the applied principles can be referred to [144, 157, 158]. The condition number can be used as a threshold logic for screening bad modal approximations. Subsequently, warnings would be issued when the computed condition number of the data matrix has exceeded the pre-set value.

The characteristics of the condition number when operating at an inadequate sampling interval is described in the following subsections. Noise components are not considered in the derivation because the objective was to highlight the relationship between the condition number and sampling interval. The mathematical examination here focuses on the more extreme scenarios in order to distinctly show the true nature of the sampling characteristics.

4.3.1.1 Effects of large Sampling Interval

When sampling at the minimum Nyquist interval, within a finite timeframe, it is clear that the true behaviour of the continuous signal may not be captured properly [98]. That is because the large time step between consecutive measurements, compounded by an insufficient amount of data points will cause the true characteristics of the captured waveform, or, dynamic behaviours to be lost [144]. Furthermore, the characteristics of the smaller frequency component will become more difficult to be extracted. Consequently, the sampling errors are generated and can lead to inaccurate Prony solutions. Such phenomena can be explained and reflected by an increase in the condition number.

Suppose the measured data can be approximated by a summation of n damped exponential functions, namely $y(k)$:

$$y(k) = \sum_{i=1}^{n} A_i e^{(\sigma_i k T_{sample})} \cos(\omega_i k T_{sample} + \phi_i) \tag{4-10}$$

where A is the magnitude of the signal, σ is the damping factor, ω is the angular frequency and ϕ is the phase angle. Assume the sampling interval (T_{sample}) is based on the minimum Nyquist sampling rate, Equation (4-10) becomes:

$$y(k) = \sum_{i=1}^{n} A_i e^{(\sigma_i k T_{sample})} \cos(\frac{2\pi k f_i}{2 f_n} + \phi_i) = \sum_{i=1}^{n} A_i e^{(\sigma_i k T_{sample})} \cos(\frac{\pi k f_i}{f_n} + \phi_i) \tag{4-11}$$

where the magnitude of the oscillatory frequency is ranked as:

$$f_1 \le f_2 \le \cdots \le f_n \tag{4-12}$$

Substituting Equation (4-12) into Equation (4-11):

$$\begin{aligned} y(k) = {} & A_1 e^{(\sigma_1 k T_{sample})} \cos(\frac{\pi k f_1}{f_n} + \phi_1) + A_2 e^{(\sigma_2 k T_{sample})} \cos(\frac{\pi k f_2}{f_n} + \phi_2) + \cdots + \\ & A_n e^{(\sigma_n k T_{sample})} (-1)^{n+k} \cos(\phi_n) \end{aligned} \tag{4-13}$$

From Equation (4-13), it can be clearly noted that only the maximum and minimum points of f_n can be correctly identified using a small finite sample size. Smaller frequency components, such as, f_1 and f_2 cannot be mapped out with similar precision

to f_n. Consequently, in comparison, estimating their oscillatory parameters would be relatively more difficult. In addition, due to the nature of the data matrix of the Linear Prediction methods, the minimum oscillatory frequency f_1 is dependent on the spread of data. That can be explained in terms of determinants. According to the *Laplace Expansion of Determinant*, the determinant of the mxm data matrix can be simplified into calculating the determinants of many $2x2$ matrixes, which has the general form of:

$$\begin{bmatrix} a_k & a_{k-1} \\ a_{k+1} & a_k \end{bmatrix} \tag{4-14}$$

where the variable *a* represents the collected data and the determinant is defined as:

$$\det = a_k^{\,2} - a_{k+1}a_{k-1} \tag{4-15}$$

In typical power system networks, the frequency of generator oscillations usually ranges from, 0.1 Hz to 2 Hz, depending on the network structure. The inter-area oscillation is much smaller than the local modes. Therefore, under the worst case scenario, one can assume f_1 << f_n and Equation (4-15) could be expressed in terms of Equation (4-13) as:

$$\begin{aligned}
\det = &\left[A_1 e^{(\sigma_1 kT_{sample})} \cos(\frac{\pi k f_1}{f_n} + \phi_1) + \cdots + A_n e^{(\sigma_n kT_{sample})} (-1)^{n+k} \cos(\phi_n) \right]^2 \\
&- \left[A_1 e^{(\sigma_1 (k-1)T_{sample})} \cos(\frac{\pi (k-1) f_1}{f_n} + \phi_1) + \cdots + A_n e^{(\sigma_n (k-1)T_{sample})} (-1)^{n+k-1} \cos(\phi_n) \right] \\
&\square \left[A_1 e^{(\sigma_1 (k+1)T_{sample})} \cos(\frac{\pi (k+1) f_1}{f_n} + \phi_1) + \cdots + A_n e^{(\sigma_n (k+1)T_{sample})} (-1)^{n+k+1} \cos(\phi_n) \right] \qquad \text{(4-16)} \\
&\because f_1 << f_n \\
&\Rightarrow \frac{\pi (k-1) f_1}{f_n} \approx \frac{\pi (k+1) f_1}{f_n} \approx \frac{\pi k f_1}{f_n} \to 0
\end{aligned}$$

Consequently, the eigenvalue (λ_{min}) associated with f_1 becomes:

$$\begin{aligned} &\because \det(\mathbf{A}) \approx \det(f_2 f_3 \dots f_n) \\ &\Rightarrow \lambda_{\min} \to 0 \\ &\therefore \kappa(\mathbf{A}) = \frac{\lambda_{\max}}{\lambda_{\min}} \to \infty \end{aligned} \tag{4-17}$$

Note the eigenvalue refers to solutions of Linear Prediction data matrix. If the data matrix is over-determined, then the condition number is $\kappa(\mathbf{A}^H\mathbf{A})$ where the superscript H denotes the conjugate transpose of $\boldsymbol{A}$ [98, 158].

According to Equation (4-17), the slow sampling errors can be captured and reflected by a significant increase in the condition number. Similar effects will exist for other oscillating frequencies with similar magnitude to f_1. Therefore, the reconstruction of the signal using a small data size and sampling at the minimum rate is prone to errors.

4.3.1.2 Effects of Small Sampling Interval

Apart from the errors generated by using large sampling intervals, the observations made by Kulp [98] and Lee *et al.* [152] showed Prony Analysis also becomes less reliable at small sampling intervals. The reason is because; the accuracy of the Prony solutions relies heavily on the diversity of the elements in the constructed data matrix [154, 155]. Hence, when using a smaller sampling interval, the difference between the neighbouring measurements in the data matrix is relatively smaller. That can be shown mathematically as:

$$\begin{aligned} &\text{if } T_{sample} \to 0 \\ &\Rightarrow y(k) \approx y(k+1) \end{aligned} \tag{4-18}$$

Based on this behaviour, the *mxm* data matrix can be defined as:

$$\begin{aligned} &\mathbf{A} = \left[a_{ij} \right] \\ &\because a_{11} \approx a_{12} \approx \cdots \approx a_{ij} \\ &\Rightarrow a_{ij} \approx L \qquad \forall \text{ i,j} \in \square \end{aligned} \tag{4-19}$$

where, L represents a constant value. For simplicity, assume $\boldsymbol{A}$ to be a symmetrical matrix and the determinant of $\boldsymbol{A}$, referring to *Cramer's Rule*, can be expressed as:

$$\begin{aligned} &\det(\mathbf{A}) = a_{1j}c_{1j} + a_{2j}c_{2j} + \cdots + a_{mj}c_{mj} \quad or \quad \det(\mathbf{A}) = a_{i1}c_{i1} + a_{i2}c_{i2} + \cdots + a_{im}c_{im} \\ &\because a_{ij} \approx L \\ &\Rightarrow \det(\mathbf{A}) \approx Lc_{1j} + Lc_{2j} + \cdots + Lc_{mj} \quad or \quad \det(\mathbf{A}) \approx Lc_{1j} + Lc_{2j} + \cdots + Lc_{mj} \end{aligned} \tag{4-20}$$

The variable c_{ij} is known as the *cofactor* and is formulated as:

$$c_{ij} = (-1)^{i+j} M_{ij} \tag{4-21}$$

where M_{ij} is the regarded as the *minor* and it is the determinant of order $m\text{-}1$, namely, the determinant of the submatrix of $\boldsymbol{A}$. In other words, the minor is calculated by deleting the row and column entry of the data matrix. Therefore, $det(\boldsymbol{A})$ is decomposed into m number of determinants of order $m\text{-}1$, $m\text{-}2$ and so on; until the second order determinant. The first order determinant is a_{11}. According to [159], the summation of m eigenvalues of $\boldsymbol{A}$ can be defined as the sum of all the main diagonal entries of $\boldsymbol{A}$. This is known as the *trace* of the data matrix in linear algebra and can be formulated as:

$$tr(\mathbf{A}) = \sum_{i=1}^{m} a_{ii} = \sum_{l=1}^{m} \lambda_l \tag{4-22}$$

In addition, the product of the eigenvalues is expressed as:

$$\det(\mathbf{A}) = \lambda_1 \lambda_2 \ldots \lambda_m \tag{4-23}$$

and the eigenvalues could be ranked as follows:

$$\lambda_1 \geq \lambda_2 \geq \cdots \geq \lambda_m \tag{4-24}$$

Incorporating Equation (4-22) into this situation, the trace of $\boldsymbol{A}$ becomes:

$$\begin{aligned} &\because \sum_{i=1}^{m} a_{ij} \approx \sum_{i=1}^{m} L \approx mL \\ &tr(\mathbf{A}) \approx mL \approx \lambda_1 + \sum_{i=1}^{m-1} \lambda_i \end{aligned} \tag{4-25}$$

Here, the summation term of eigenvalues is close to zero because a matrix, whose elements are similar in magnitudes, results in near-zero determinants. Thus, the

maximum eigenvalue (λ_1) is approximately mL and minimum eigenvalue (λ_m) is close to zero. As a result, the condition number of a small sampling interval is:

$$\begin{aligned} &\kappa(\mathbf{A}) = \frac{mL}{\lambda_m} \\ &\because \lambda_m \to 0 \\ &\Rightarrow \kappa(\mathbf{A}) \to \infty \end{aligned} \tag{4-26}$$

Therefore, the errors resultant to using fast sampling rate can be again captured and reflected by a significant increase in the condition number.

From these mathematical derivations, the ideal sampling interval will exist in the range of $[1/2f_n, \infty]$. In addition, the optimal interval is dependent on the number and magnitude difference between oscillation frequencies [98]. That means different oscillations will result in different optimal sampling interval.

4.3.2 Potential Implementation Considerations

For online applications, parallel-processing is recommended for determining the sampling interval because it allows simultaneous multiple computations. Compared with sequential-processing, it can enhance the real-time capability of Prony Analysis. The trade off is the increasing computational complexity required. However, with the advances in computers, adopting parallel computation is considered to be a feasible option. That aspect is discussed in Chapter 6.

Apart from using the data for online calculations, the processed results can be archived for other offline applications. For example, slower Eigen analysis can be performed to double check every solution. Furthermore, the precision of the state space model can also be improved by using real-time information from the archived database.

In actual system operations, the sampling parameters would rarely vary after a few Prony iterations, as the frequencies of the inter/intra-area oscillations do not change abruptly. By applying that knowledge, it follows that a significant and an abrupt increase in the condition number would signify that a disturbance had occurred or, resolved. Therefore, only during those occurrences, would the proposed sampling scheme be activated to compensate for changes. On the other hand, a steady

increase in the condition number, following a passage of iterations, would indicate that oscillations are gradually being dampened. That is because, under a fixed system order when the well-decayed mode is unable to be tracked, the corresponding singular values of the data matrix would be replaced by non-oscillatory related values. Thus, the computed condition number begins to increase over time.

Note that the resultant condition number will increase when there are more poles that needs to be detected [157, 158]. That is because the columns of the data matrix will increase in size to accommodate the increasing system order. Hence, the condition number threshold should be set according to the number of the potential modes. Based on the experimental results and the observations made in [98] and [152], the threshold is recommended to be set as:

$$\kappa_{Acceptable} < 10^{n} \tag{4-27}$$

where, n refers to number of defined oscillatory modes in the extracted signal.

4.4 *Simulations and Evaluations*

In order to evaluate the Enhanced Prony Analysis, two different scenarios are adopted:

1) A synthetic signal containing two oscillatory modes
2) Kundur's Two-Area Network

The objective of the first scenario is to verify if the proposed condition number is able to reflect the estimation inaccuracies caused by using inappropriate sampling intervals. The effectiveness of the condition number is also verified with the relative error approach. Meanwhile, the adequacy of the sampling interval is examined using a fixed data size. Hence, the error detection performance of both techniques under different monitoring/sampling windows can also be assessed.

The second scenario evaluates the actual sampling operation of the Enhanced Prony Analysis in a more realistic and widely published test case environment. The aim is to compare the proposed sampling method against the traditional fixed sampling approach.

4.4.1 Test Case 1: Evaluating the Performance of the Condition Number and Relative Error Techniques

A modified version of the example used by Xiao *et al.* in [151], is chosen as the test bench for this study. The parameters of the two oscillatory modes within the signal are listed in Table 4-1 and its corresponding time-domain characteristics are illustrated in Figure 4-3. A white noise with a SNR of 40 dB was applied. The system order and the reduced SVD order were assumed to be 20, and 4 respectively.

Since the oscillatory parameters are known and referring to Nyquist-Shannon criterion, the maximum sampling interval (T_{sample}) can be determined as:

$$T_{sample} = \frac{\pi}{\omega_{\max}} = \frac{1}{2 f_{\max}} \tag{4-28}$$

where $\omega_{\max}$ represents the maximum angular speed and $f_{\max}$ is the highest oscillatory frequency. In this case, the sampling interval should be less than or equal to 0.3268 second. For this example, a total of 10 different sampling intervals, ranging from [0.1*0.3268] to [1.0*0.3268] were implemented. The modal parameters were computed at each interval, along with, the associated relative error and the condition number. A fixed data size containing 50 measurements was used for all simulated scenarios.

The outcomes of the simulations are summarized in Table 4-2 and Table 4-3. Note that σ and f represents the damping factor and the oscillatory frequency respectively. According to Table 4-2, it is obvious that using an inadequate sampling interval such as [0.1*0.3268] and [1.0*0.3268], generates inaccurate Prony solutions. It would cause the status of the actual system to be misinterpreted. Conversely, the sampling intervals within the range of [0.4*0.3268] and [0.9*0.3268] were identified to be adequate for conducting Prony analysis. Specifically; the intervals, like [0.6*0.3268] and [0.7*0.3268] were the most suitable. Those observations were also captured by the relative errors and the condition numbers listed in Table 4-3. Larger values of those techniques indicated that the corresponding sampling intervals were less suitable.

Table 4-1 Modal Contents of the Synthetic Signal from [151]

Mode	Amplitude	Damping Factor	Frequency (Hz)	Phase (rad)
1	160.74	0.15	0.46	1.32
2	173.38	0.45	1.53	0.86

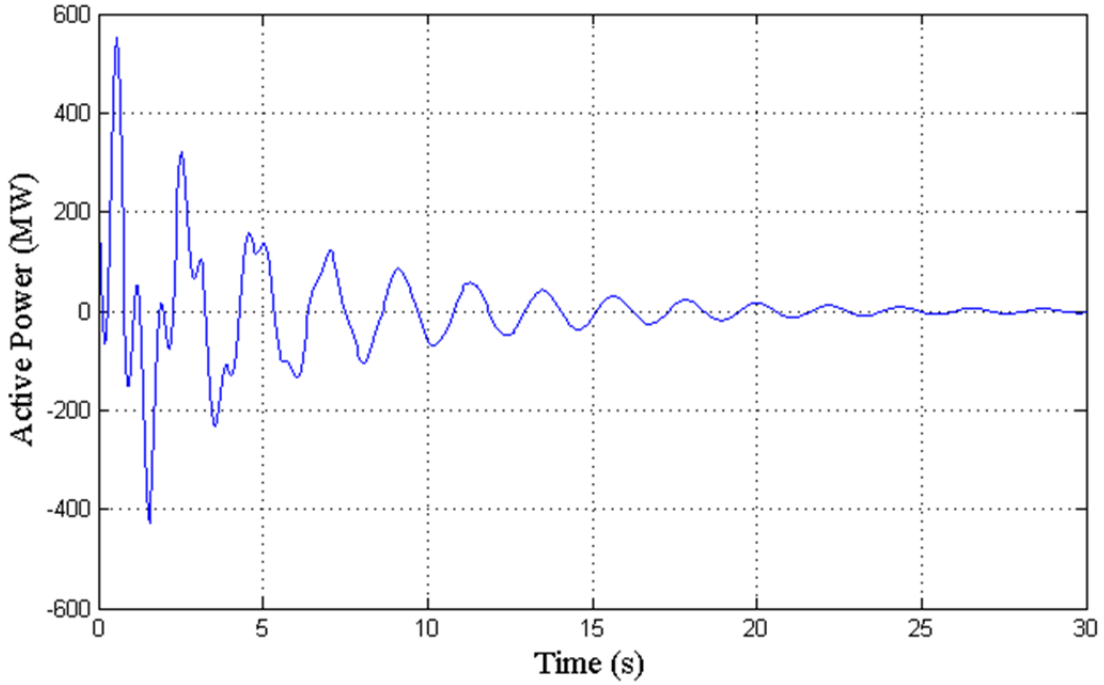

Figure 4-3 The dynamics of the simulated signal

The use of the condition number for examining the adequacy of the sampling interval has been demonstrated to be a feasible alternative for the relative error approach. According to Figure 4-4 and Figure 4-5, the values obtained by the proposed condition number approach correlate with those of the relative error technique. Furthermore, compared with the relative error in terms of the calculated magnitude, the condition number is able to provide a more distinct boundary line between the appropriate and inappropriate intervals. Hence, the desired sampling intervals can be more easily identified when using the condition number as a quality control indicator.

For this study, any intervals with a condition number less than 100 were considered to be suitable for conducting Prony estimation. However, the performance using the [0.4*0.3268] and [0.9*0.3268] raised an interesting point. Despite both computed condition numbers being slightly above the tolerable boundary; they were still able to approximate each modal parameter with less than 5% error. To understand the nature of that phenomenon, the simulated environment was changed for further investigations.

The original SNR level of 40 dB was dropped to 20 dB. The resultant solutions are outlined in Table 4-4. Compared with Table 4-2, both [0.4*0.3268] and [0.9*0.3268] were no longer able to achieve similar detection accuracies. That means that those intervals marginal, or, slightly above the defined threshold are more sensitive to changes in the surrounding environment. Consequently, the appropriateness of the sampling interval would need to be regularly monitored. That would add unnecessary computational stress and complexity to the system.

Table 4-2 Estimated Modal Parameters at Various Sampling Intervals

Sampling Interval (s)	Mode 1		Mode 2	
	σ	f (Hz)	σ	f (Hz)
[0.1 * 0.3268]	0.074	0.622	0.481	1.464
[0.2 * 0.3268]	0.050	0.458	0.425	1.524
[0.3 * 0.3268]	0.166	0.456	0.428	1.526
[0.4 * 0.3268]	0.155	0.459	0.444	1.530
[0.5 * 0.3268]	0.149	0.460	0.446	1.530
[0.6 * 0.3268]	0.148	0.460	0.448	1.530
[0.7 * 0.3268]	0.150	0.460	0.450	1.530
[0.8 * 0.3268]	0.152	0.460	0.454	1.532
[0.9 * 0.3268]	0.149	0.460	0.460	1.529
[1.0 * 0.3268]	0.152	0.460	0.028	1.530

Table 4-3 The Computed Condition Number and Relative Error at Various Sampling Intervals

Sampling Interval (s)	Relative Error	Condition Number
[0.1 * 0.3268]	8.1×10^{-1}	1.6×10^{6}
[0.2 * 0.3268]	7.9×10^{-2}	3.2×10^{3}
[0.3 * 0.3268]	2.7×10^{-2}	1.3×10^{3}
[0.4 * 0.3268]	4.5×10^{-3}	4.0×10^{2}
[0.5 * 0.3268]	2.1×10^{-3}	9.3×10^{1}
[0.6 * 0.3268]	1.7×10^{-3}	6.1×10^{1}
[0.7 * 0.3268]	1.6×10^{-3}	4.7×10^{1}
[0.8 * 0.3268]	3.3×10^{-3}	5.5×10^{1}
[0.9 * 0.3268]	5.6×10^{-2}	3.1×10^{2}
[1.0 * 0.3268]	4.2×10^{0}	1.3×10^{4}

In contrast, from Table 4-4, the more adequate intervals, such as, [0.6*0.3268] and [0.7*0.3268] were still able to track the oscillatory parameters with reasonable precision despite changes in the signal characteristics. Therefore, choosing the sampling interval with a smaller condition number would increase the reliability of the calculated Prony solutions. Although the determined appropriate sampling intervals only refer to one particular scenario, they still provide a wider operational diversity than choosing those with larger condition numbers. As a result, the frequencies of searching for new sampling intervals can be minimized.

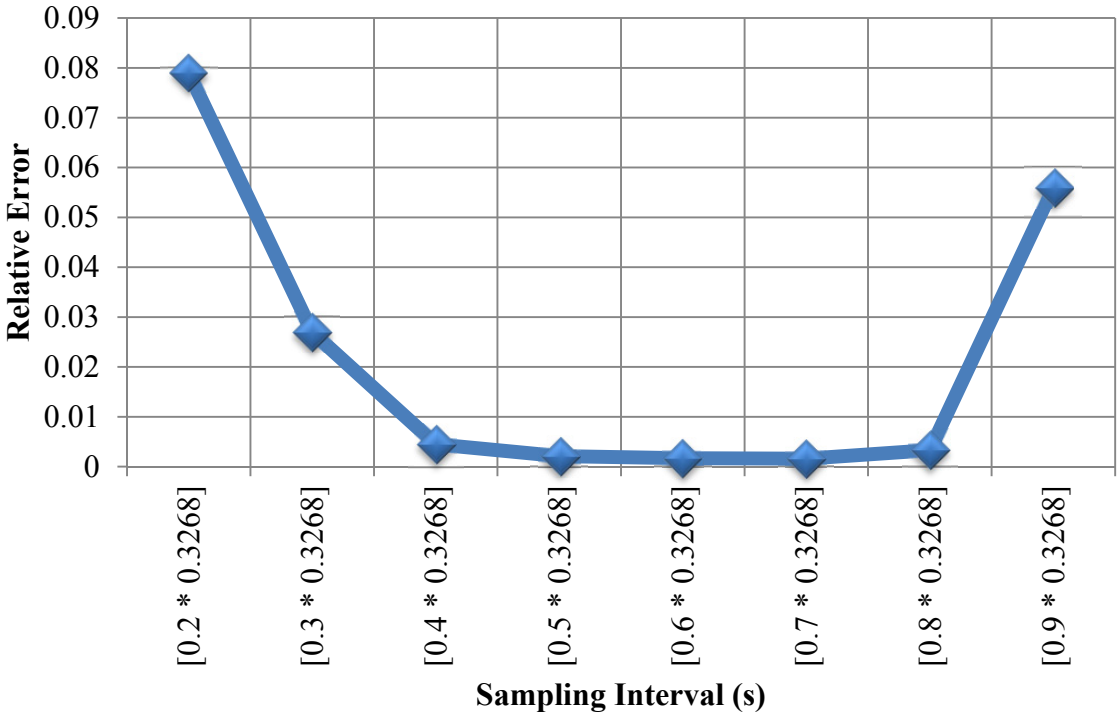

Figure 4-4 Calculated relative error at various sampling intervals

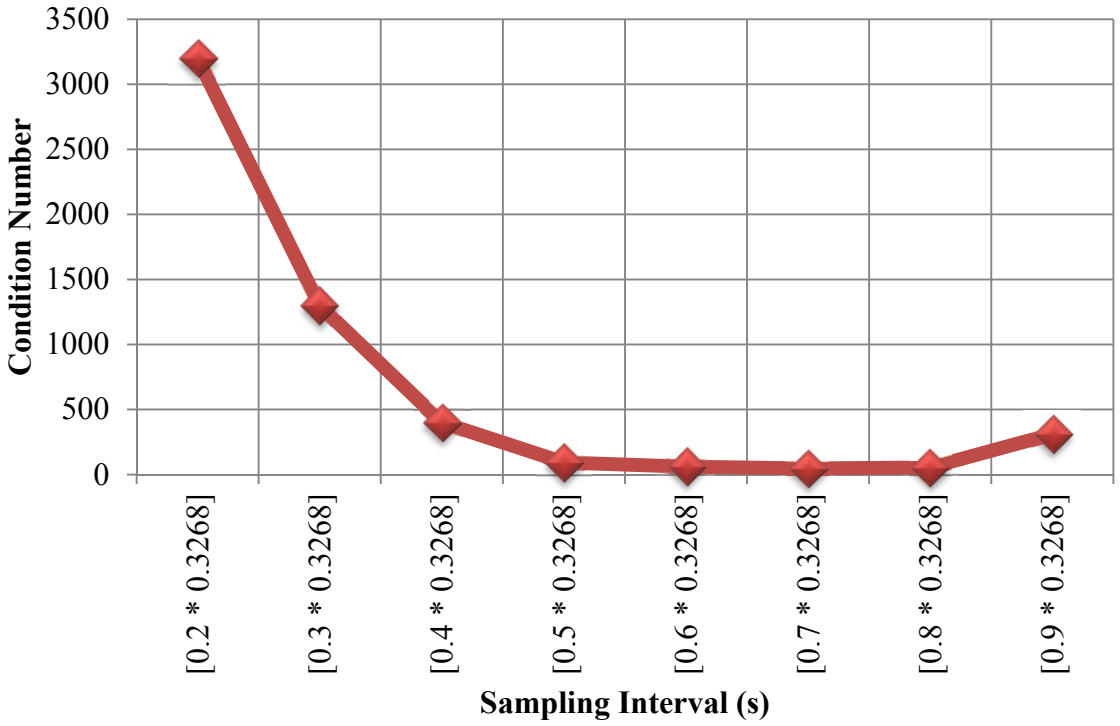

Figure 4-5 Computed condition number at various sampling intervals

Table 4-4 Parameter Estimations at Different Noise Level

Sampling Interval (s)	Mode 1		Mode 2	
	σ	f (Hz)	σ	f (Hz)
[0.4 * 0.3268]	0.127	0.451	0.562	1.541
[0.6 * 0.3268]	0.135	0.459	0.456	1.534
[0.7 * 0.3268]	0.153	0.459	0.442	1.532
[0.9 * 0.3268]	0.142	0.461	0.880	1.581

Although the proposed sampling scheme provides a range of suitable sampling intervals for the users to select from, it is recommended that they choose the one with the smallest condition number. Any intervals with their condition number close to the defined threshold should be avoided. In this study, the use of the condition number as a quality index for assessing the appropriateness of the sampling interval was successfully demonstrated.

4.4.2 Test Case 2: Examining the Sampling Performance of the Enhanced Prony Analysis

In a power grid, the number of oscillations and their modal parameters are often unknown. Therefore, the next step is to verify the performance of the proposed sampling scheme using the data collected from Kundur's Two-Area network [1]. Referring to Figure 4-6, the simulated power grid can be subdivided into two regions, each area consists of two generators and a load. For this network, the system exhibits three electromechanical modes:

1) A lightly damped inter-area mode with a frequency around 0.58 Hz. Both generators in Area 1 oscillate against the other generators in Area 2.
2) A local oscillation of 1.17 Hz in Area 1. G1 oscillates against G2.
3) A local oscillation mode of 1.14 Hz in Area 2. G3 oscillates against G4.

Note: those oscillatory frequencies vary depending on the experienced disturbances, and the operating conditions. In addition, all simulations were conducted using

DigSILENT Power Factory ver. 13.2.333 (Professional). The network settings are provided in Appendix C.

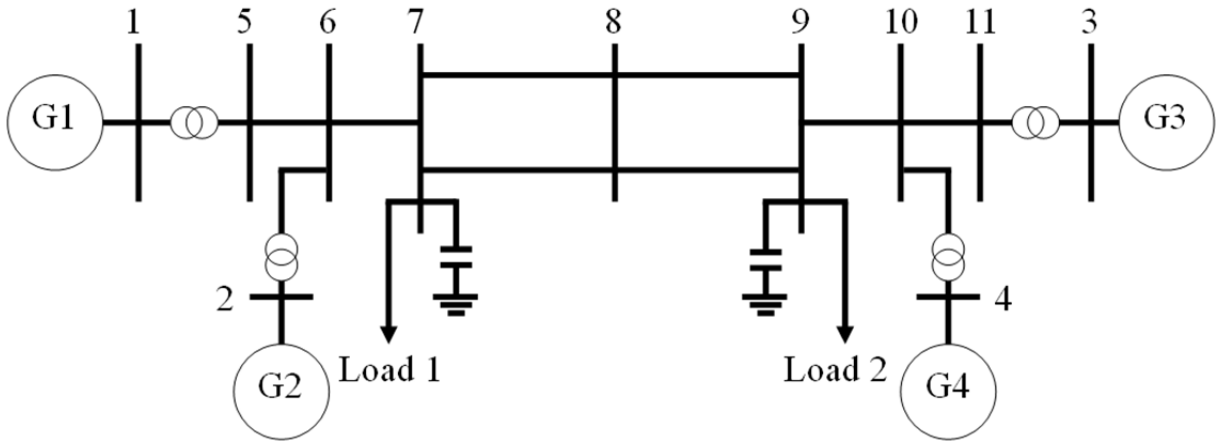

Figure 4-6 Outline of the simulated Two-Area network

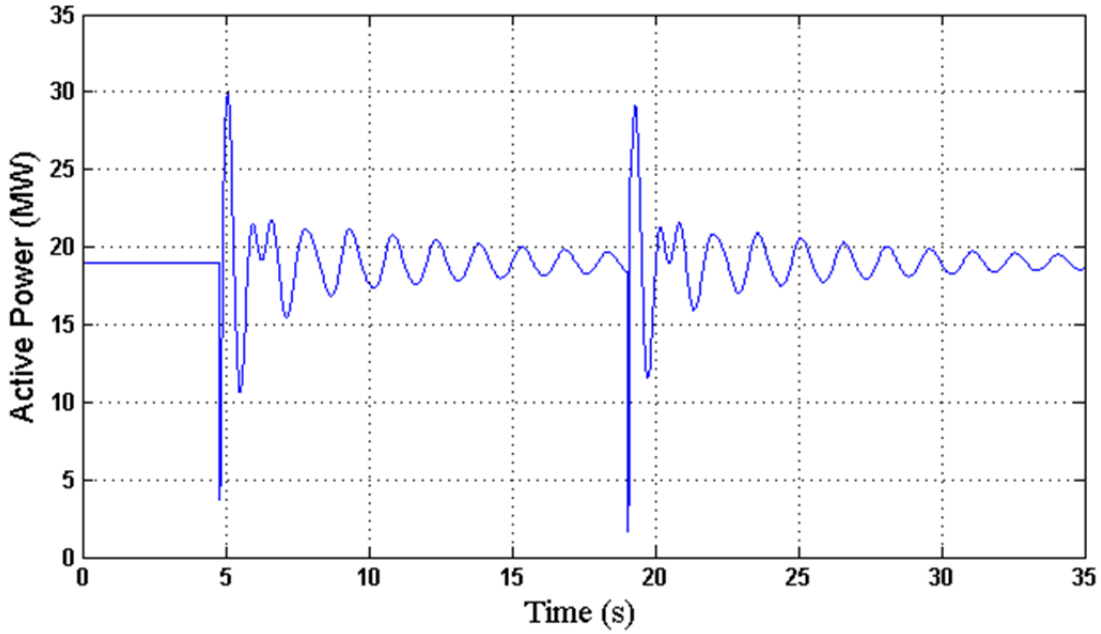

Figure 4-7 Captured power behaviour between Gen 1 and Gen 2 due to multiple line outages

Table 4-5 Modal Parameters after each Line Outage Event

Condition	Mode	Damping Factor	Frequency (Hz)
Line 8-9 Outage at 5s	Inter-Area	0.12	0.63
	Local	0.94	1.14
Line 7-8 Outage at 20s	Inter-Area	0.11	0.63
	Local	0.96	1.14

In this study, the electromechanical oscillations were excited by two line outage events. Their characteristics are summarized in Table 4-5 and Figure 4-7. The power measurements collected at Gen 1 and Gen 2 are utilized for modal approximations. Since, the first 5 seconds contained only the steady-state dynamics, they were not included in the analysis. The system order and the reduced SVD orders were set as 20, and 8 respectively.

Compared with Test Case 1, more realistic values were chosen as the sampling intervals. Suppose the PMU sampled at 50 Hz (or 0.02 second period), a total of 10 down-sampled intervals were adopted, ranging between, 0.02 second to 0.2 second. The developed sampling scheme assessed and then selected the appropriate interval to conduct Prony Analysis. In contrast, the sampling interval of the conventional fixed sampling approach is chosen to be 0.1 second. Furthermore, a monitoring window with duration of 10 second was applied. In order to capture the changing oscillatory behaviours, each window was overlapped by 5 seconds of the previous one. In this study, the developed sampling algorithm was activated in the first monitoring window and it identified 0.16 second to be the most adequate interval for this operating scenario. Since the preset tolerance threshold was not breached in all monitoring timeframes, the selected interval was kept throughout the entire simulation.

According to the results outlined in Figure 4-8 and Figure 4-9, the proposed sampling scheme provided more accurate detection than the fixed interval approach. Although the estimated damping factor of the inter-area oscillation by the proposed method was slightly less accurate during the 20 to 30 second window, the overall modal estimation accuracy was still better than the fixed interval option for that timeframe. Given that the local oscillation decayed rapidly after each line outage, Prony Analysis was only able to track it in certain monitoring timeframes; as shown in Figure 4-9. The solutions of the 15-25 second window were not included in the final results. Prony failed to detect the modal parameters using both sampling methods. The reason is that the time-invariant Prony Analysis was unable to capture the changing modal behaviour caused by the line outage at 20 second period.

Next, by processing the computed results, the magnitude of the improved estimation error percentages of each monitoring window are summarized in Figure 4-10. These values were computed by finding the error differences of the sum of modal parameters (damping factor + oscillatory frequency) between the proposed and the fixed sampling schemes. As discussed in Subsection 4.2, that bar graph shows that the adequacy of the sampling interval is dependent on the number of the oscillatory frequencies. Thus, the proposed sampling scheme is able to outperform the fixed sampling approach in the presence of the local mode (i.e. 5-15 and 20-30 windows). Nevertheless, the performance of both sampling options can be regarded the same when there is only one oscillation in the extracted signal.

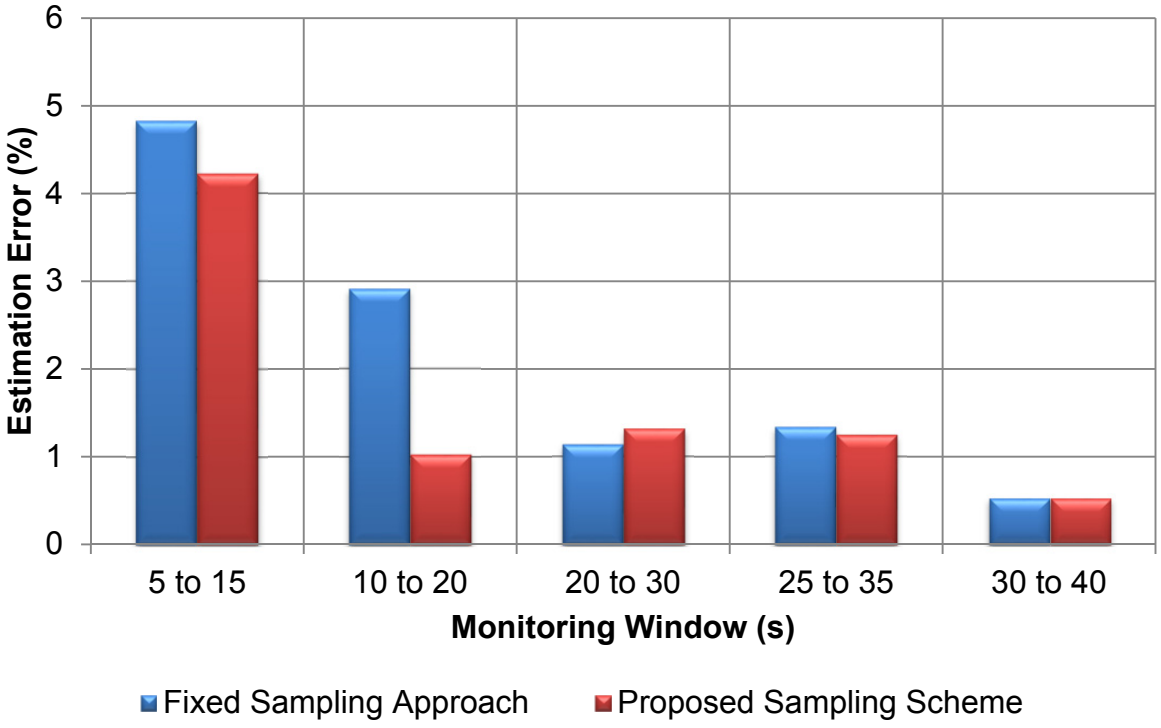

(a)

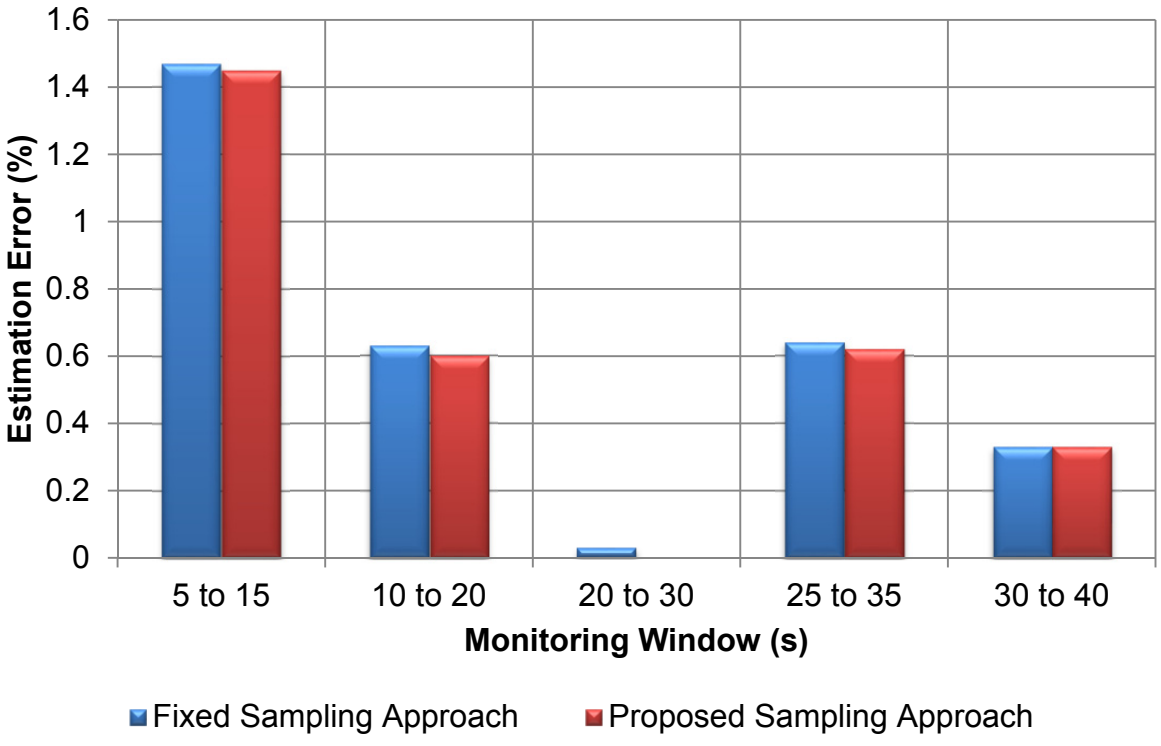

(b)

Figure 4-8 Tracking the inter-area mode using the fixed and the proposed sampling schemes: (a) damping factor and (b) the oscillatory frequency

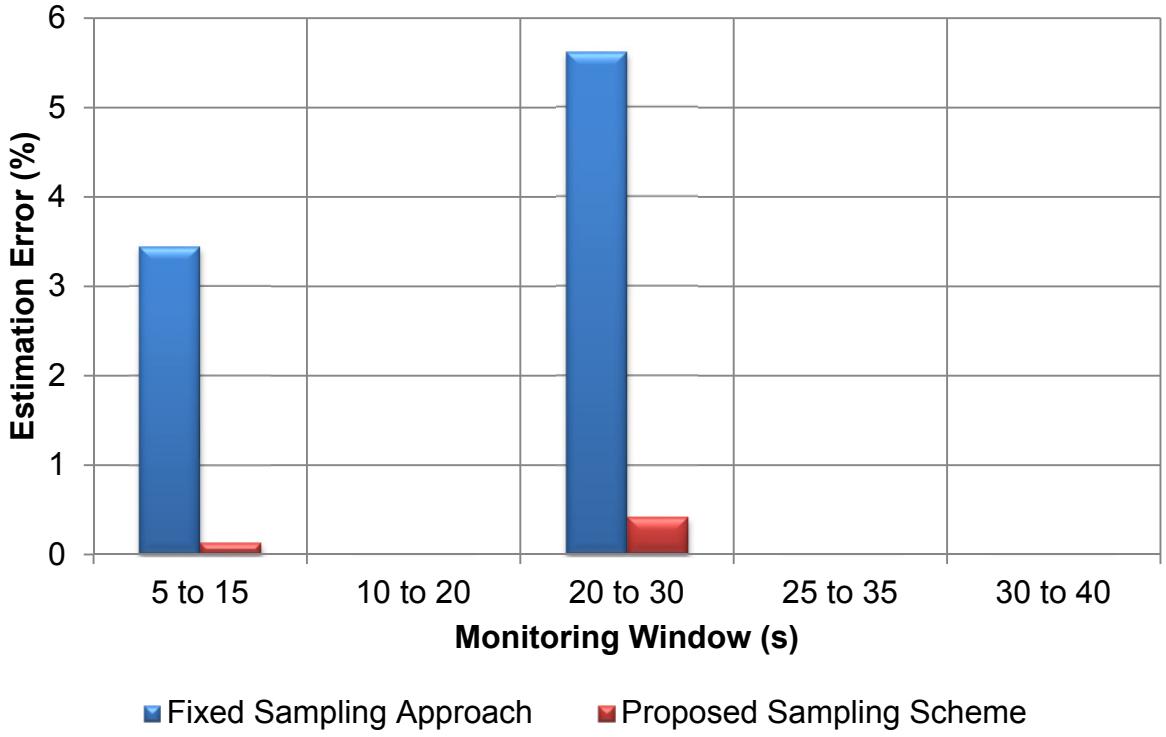

(a)

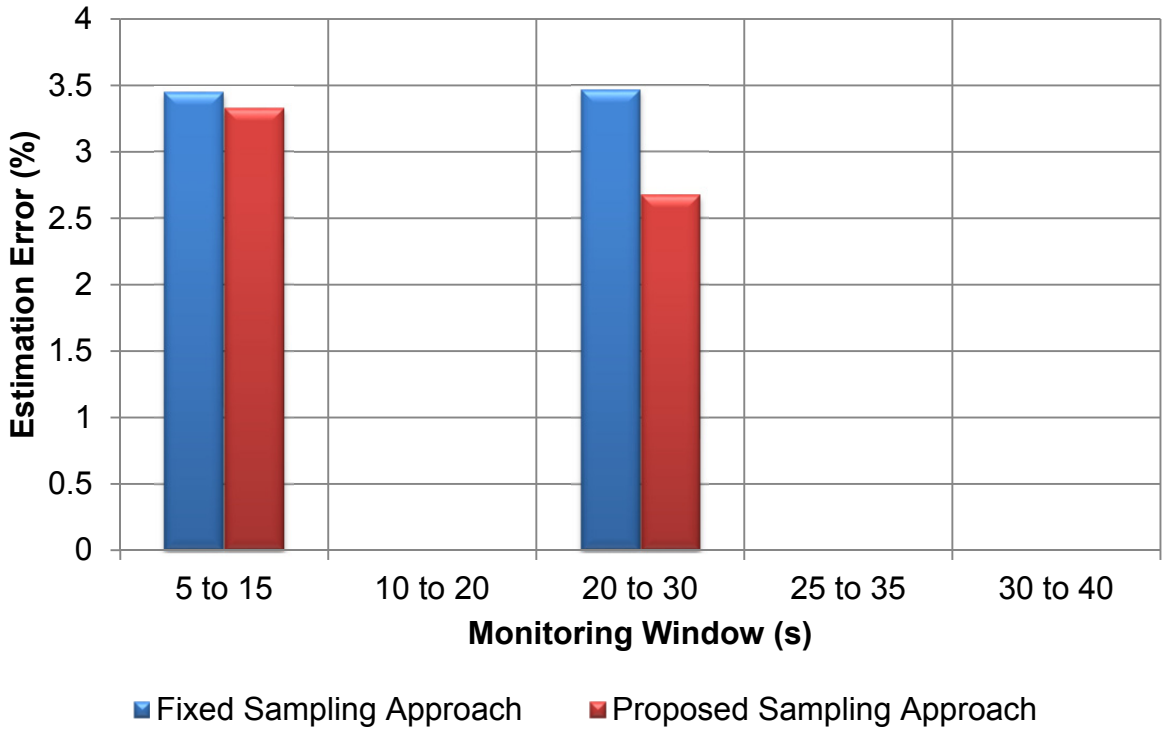

(b)

Figure 4-9 Tracking the local mode using the fixed and the proposed sampling schemes: (a) damping factor and (b) the oscillatory frequency

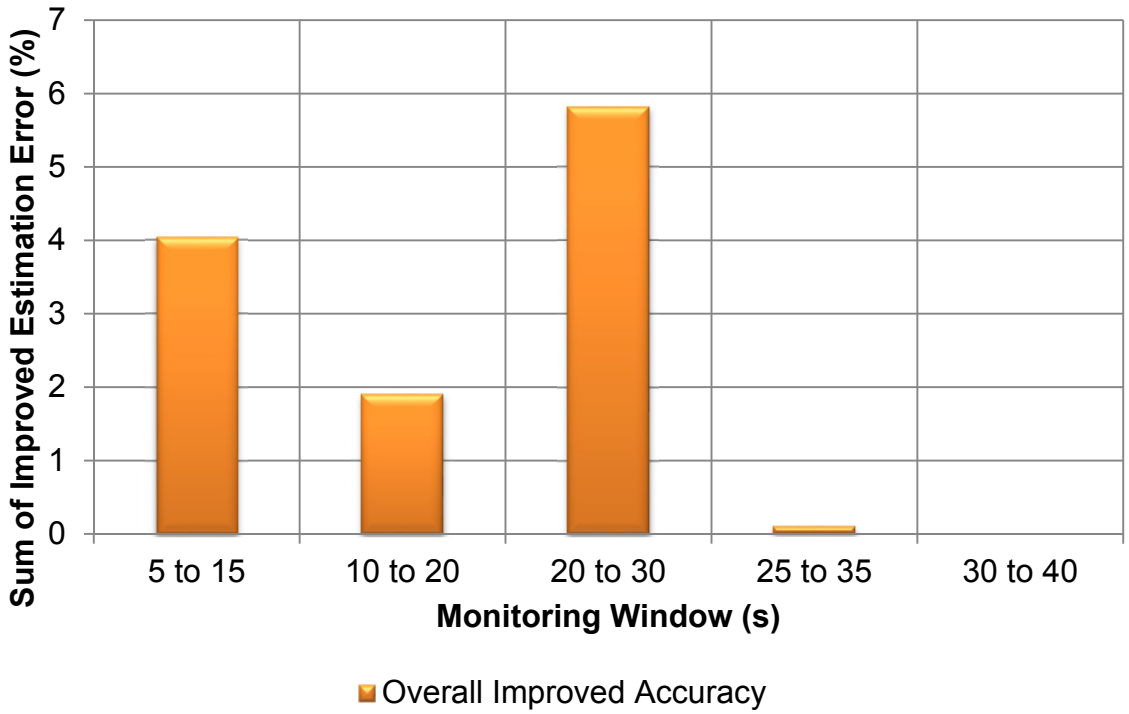

Figure 4-10 Summary of the improved estimation error percentages when using the proposed sampling scheme

4.5 *Discussion*

From the simulation results, the proposed sampling scheme has been shown to be able to minimize the impact of inappropriate sampling within the computed modal solutions. Note: the main objective of the method was to provide a range of sampling intervals for users to choose from. Subsequently, the system operators are able to select their desired oscillatory update/refresh rate; knowing, that the calculated Prony results are trustworthy.

Since the proposed scheme is designed to minimize the relative errors incurred in AR coefficients, it does not interfere with solving the characteristic equation. Hence, the fundamental time-invariant nature of Prony Analysis is not changed. Overall, the proposed sampling scheme should be treated as a step towards improving approximation accuracy in an ill-posed digital environment.

4.6 *Remarks*

In this chapter, the Enhanced Prony Analysis was developed. The key feature was the integration of a sampling scheme to examine the appropriateness of the selected sampling interval for a particular operating situation. Since the condition number was mathematically proven to be able to capture the sampling errors, it was integrated into the scheme as a quality index. That is further verified from the simulation results; the condition number is able to achieve similar effectiveness to the existing relative error technique. In general, compared with traditional fixed sampling approach, the proposed sampling scheme was demonstrated as enhancing the accuracy of the computed Prony solutions. In conclusions: the Enhanced Prony Analysis, embedded with the developed sampling scheme, is capable of providing more reliable modal estimations. It is suitable to be implemented into systems like the New Zealand grid, which can experience multiple oscillations simultaneously.

5 The Enhanced Kalman Filter

5.1 *Introduction*

Referring to Chapter 1, New Zealand's grid is subjected to several electromechanical oscillations, and is known to experience two inter-area oscillations simultaneously. Thus, tracking multiple oscillations is a necessary requirement for ensuring reliable system operations. Two mature methods, Prony and Kalman Filter, were identified as suitable monitoring candidates. The merits of both methods were addressed in Chapter 3. Subsequently, in Chapter 4, the estimation confidence of Prony solutions was enhanced by introducing a quality assessing index. The motivation of this chapter was to customize Kalman Filter, proposed by Korba in [129], to track multiple oscillatory modes. Hence, it may be applied to stressed systems such as the New Zealand grid.

As observed from the test cases conducted in Chapter 3, the performance of Kalman Filter is limited to detecting the dominant mode. Meanwhile, it is dependent on the adequacy of the initial variable settings. Inadequate selection of the initial state variables for Kalman Filter can produce biased results and affect the convergence performance. Nevertheless, such concerns can be minimized if the modal parameters are approximated in advance. Since the operating conditions are constantly changing, the need to identify system parameters prior to running Kalman Filter is desirable for prevention of misleading results.

Apart from the initialization factor, the main characteristic difference between the methods is that Prony was formulated to track multiple modes, while, Kalman Filter was originally designed to monitor the dominant mode. That was a reasonable approach because not all power grids experience simultaneous multiple oscillations. Yet, as seen from the observations outlined in Chapter 3, equipping Kalman Filter with the capability to detect multiple oscillations is potentially possible.

The primary objectives of this chapter are to provide a multiple oscillatory detection capability, and to enhance Kalman Filter's recursive operation. Those aims are realized by:

1. Redefining state representation,
2. Enhancing initialization procedures,
3. Providing nonlinear tracking capability,

Firstly, defining the state variables is a crucial stage. It dictates what to detect. The simplest path is to equip Kalman Filter to monitor multiple modes by modifying the existing state variables. Presently, the states of Kalman Filter represent the autoregressive (AR) coefficients used to formulate the characteristics equation seen in Prony Analysis. As shown in Figure 5-1, the oscillatory parameters are computed by rooting the polynomial equation in the continuous domain. That can be considered as an indirect modal estimation approach. Therefore, to avoid excess intermediate calculations, the proposed alternative is to redefine the states to directly represent the eigenvalues of the oscillatory modes in the discrete domain. As a result, Tustin approximation and the polynomial rooting procedures, implemented by Korba in [129], can be omitted.

Secondly, the approximated modal solutions are dependent on the convergence accuracy. That is influenced by the reliability of the initialized state variables. In order to provide trustworthy initial values, estimating the system parameters prior to conducting Kalman Filter is more favourable than using predefined offline settings. Therefore, Hankel Singular Value Decomposition (HSVD) was applied to set the values of the initialized state variables. It is a fitting technique and provides modal estimates in a similar manner to Prony Analysis.

Thirdly, since the network dynamics are not linear, the use of a linearized recursive engine as seen in the original Kalman Filter, can introduce steady-state convergence errors. The use of Extended Kalman Filter is recommended. By combining those additional traits, the modified Kalman Filter is proposed and subsequently known as Extended Complex Kalman Filter (ECKF). Unlike the original Kalman Filter, ECKF is designed to operate in a non-linear non-predetermined operational environment.

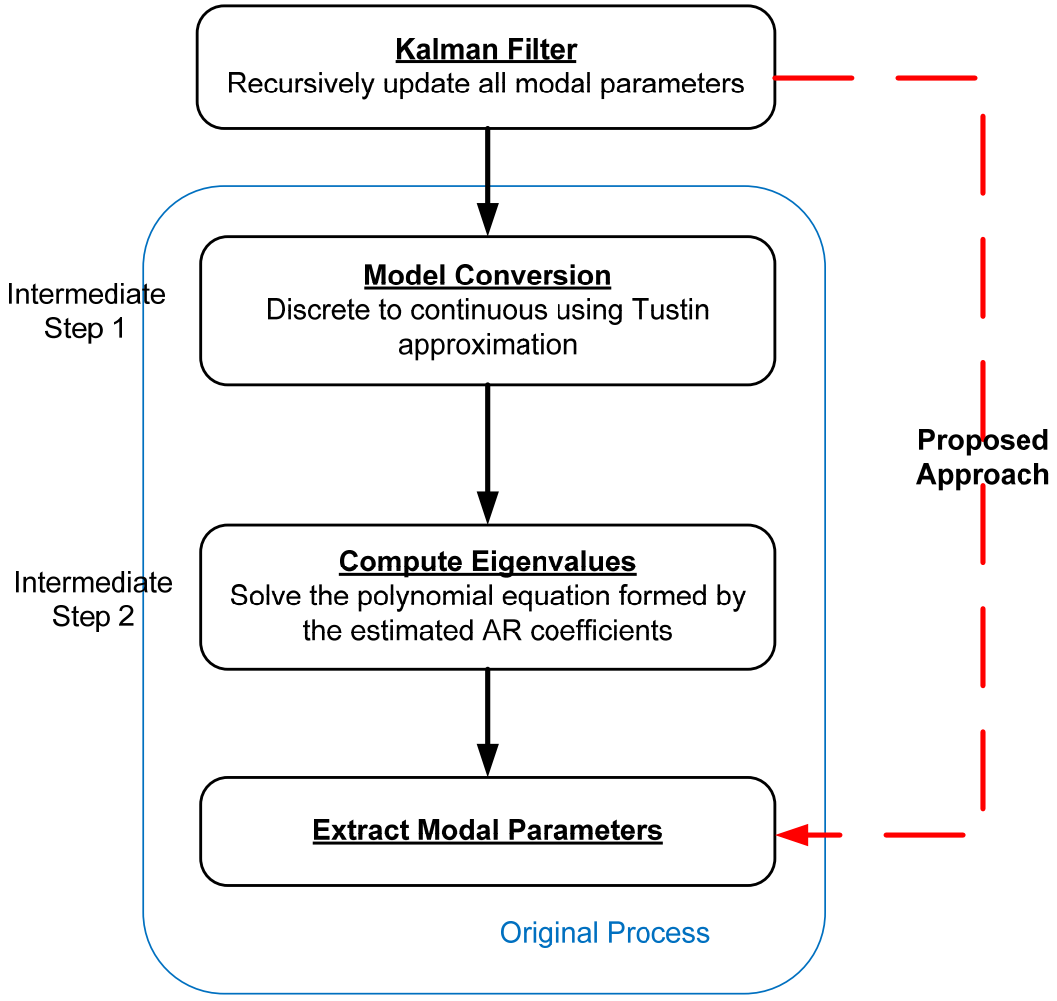

Figure 5-1 The original and proposed modal extraction process

5.2 *Outline of the proposed Extended Complex Kalman Filter Method*

5.2.1 Signal Model Formulation

As documented in [85], [121] and [129], the electromechanical oscillations can be represented as a sum of m exponentially damped sinusoidal waveforms with additive white noise v_k. Therefore, an observation signal y_k at time k can be modelled as:

$$y_k = \sum_{i=1}^{m} a_i e^{\lambda_i k T_s} + v_k, \ \ for\ k = 1, 2, \ldots, N \tag{5-1}$$

where T_s is the sampling interval and a_i represents the complex amplitude of the i^{th} eigenvalue λ_i of the signal. By decomposing λ_i into its rectangular complex form, the signal becomes:

$$y_k = \sum_{i=1}^{m} a_i e^{(-\sigma_i + j2\pi f_i) k T_s} + v_k, \ \ for\ k = 1, 2, \ldots, N \tag{5-2}$$

Here, σ and f are the damping factor and the oscillatory frequency respectively.

5.2.2 State Formulation

In order to implement Extended Complex Kalman Filter, the observation signal y_k needs to be transformed into the state-space representation. Unlike Kalman Filter in [129], the general state transition and the observation models of ECKF are defined as:

$$x_{k+1} = f(x_k) \tag{5-3}$$

$$y_k = H x_k + v_k \tag{5-4}$$

Here, the i^{th} eigenvalue at k^{th} instance is represented by two states denoted as $x_k(i)$ and $x_k(i+1)$ and expressed as:

$$\begin{aligned} x_k(i) &= e^{(-\sigma_i + j2\pi f_i) T_s} \\ x_k(i+1) &= a_i e^{(-\sigma_i + j2\pi f_i) k T_s} \end{aligned} \tag{5-5}$$

Therefore, a signal consisting of m number of eigenvalues is modelled by $2m$ states [101, 160]. Subsequently, the state transition and the observation models from Equations (5-3) and (5-4) become:

$$\begin{bmatrix} x(1) \\ x(2) \\ x(3) \\ x(4) \\ \vdots \\ x(2m-1) \\ x(2m) \end{bmatrix}_{k+1} = \begin{bmatrix} x(1) \\ x(1)x(2) \\ x(3) \\ x(3)x(4) \\ \vdots \\ x(2m-1) \\ x(2m-1)x(2m) \end{bmatrix}_{k} \tag{5-6}$$

$$y_k = x_k(2) + x_k(4) + \ldots + x_k(2m) + v_k \tag{5-7}$$

and the measurement/observation matrix H is defined as:

$$H_{1x2m} = \begin{bmatrix} 0 & 1 & 0 & 1 & \ldots & 0 & 1 \end{bmatrix}^T \tag{5-8}$$

Compared with the original Kalman Filter [129], the formulated state representation estimates the oscillatory parameters in a simpler and more direct manner. As a result, the risk of introducing additional process errors during the domain transformation and the polynomial rooting procedures were prevented.

5.2.3 Summary of Recursive Estimation of Modal Parameters

A summary of ECKF operation is outlined below:

$$\hat{x}_{k|k} = \hat{x}_{k|k-1} + K_k(y_k - H\hat{x}_{k|k-1}) \tag{5-9}$$

$$\hat{x}_{k+1|k} = f(\hat{x}_{k|k}) \tag{5-10}$$

$$K_k = \hat{P}_{k|k-1}H^H\left[H\hat{P}_{k|k-1}H^H + R_k\right]^{-1} \tag{5-11}$$

$$\hat{P}_{k|k} = \hat{P}_{k|k-1} - K_k H\hat{P}_{k|k-1} \tag{5-12}$$

$$\hat{P}_{k+1|k} = F_k\hat{P}_{k|k}F_k^H + Q_k \tag{5-13}$$

where,

$$
\begin{aligned}
F_k &= \left.\frac{\partial f(x_k)}{\partial x_k}\right|_{x_k=\hat{x}_{k|k}} \\
\hat{P}_{k|k} &= \hat{\Sigma}_{k|k}/\sigma_v^2 \\
\hat{P}_{k+1|k} &= \hat{\Sigma}_{k+1|k}/\sigma_v^2 \\
\hat{\Sigma}_{k|k} &= E\left\{\left(x_k-\hat{x}_{k|k}\right)\left(x_k-\hat{x}_{k|k}\right)^H\right\} \\
\hat{\Sigma}_{k+1|k} &= E\left\{\left(x_{k+1}-\hat{x}_{k+1|k}\right)\left(x_{k+1}-\hat{x}_{k+1|k}\right)^H\right\} \\
\hat{x}_{1|0} &= \overline{x}_1 \\
\hat{P}_{1|0} &= \hat{\Sigma}_{1|0}/\sigma_v^2 \\
\hat{\Sigma}_{1|0} &= \Sigma_{x_1} \\
\Sigma_{x_1} &= E\left\{\left(x_1-\overline{x}_1\right)\left(x_1-\overline{x}_1\right)^H\right\}
\end{aligned}
\tag{5-14}
$$

Here, K is the filter gain, $\hat{x}$ is the state vector, P is the covariance matrix, R is the correlation factor of the measurement noise and Q is the correlation matrix of the process noise. Note: the superscript symbol H denotes the complex conjugate transpose operator. As a result, the damping factor and oscillatory frequency of the i^{th} mode can be computed from the estimated state vector x_k by the following equations:

$$\sigma_i = -\frac{\ln(|\,x_k(2i-1)\,|)}{T_s} \tag{5-15}$$

$$f_i = \frac{\tan^{-1}\dfrac{\mathrm{Im}\{x_k(2i-1)\}}{\mathrm{Re}\{x_k(2i-1)\}}}{2\pi T_s} \tag{5-16}$$

Subsequently, the damping ratio (ζ) of i^{th} mode can be extracted as:

$$\zeta_i = \frac{-\sigma_i}{\sqrt{\sigma_i^2+(2\pi f)^2}}\,x100\% \tag{5-17}$$

Note that the non-linear tracking ability of the proposed ECKF (F_k) is only effective towards weakly non-linear system dynamics, i.e. tracking fast transient event like capacitor switching is not possible [101, 161].

5.2.4 Enhancing the Initialization Process with Hankel Singular Value Decomposition

Similar to Kalman Filter, the effectiveness of Extended Complex Kalman Filter is dependent on the knowledge of the initial conditions of the states. Since the exact network operating point at a particular instant is often unknown, the accuracy and the speed of ECKF to converge and monitor the true modal information cannot be guaranteed.

In order to resolve this issue, Linear Prediction (LP) technique is integrated into ECKF. It is capable of providing reliable modal estimates without prior knowledge of the network behaviour. From existing oscillation monitoring methods, three suitable candidates of the LP family were selected: Prony Analysis, Matrix Pencil and Hankel Singular Value Decomposition (HSVD). Referring to Liu *et al.* [126], comparative evaluations of all three methods were completed. They concluded that HSVD and Prony Analysis were less sensitive towards noise than Matrix Pencil. In terms of the computation time, HSVD was relatively faster than the others. It is an improved version of Singular Value Decomposition (SVD) used in Prony Analysis and is based on Kung's state-space base approach, [162]. Thus, HSVD was selected for computing the initial conditions of ECKF. Note: the purpose of HSVD is to point ECKF to converging in the right direction. It does not act as a reference for validating the accuracy of estimated solutions. Therefore, compared to standard Prony Analysis, a significantly smaller batch of measurements is required for computation. Outlines of HSVD operation are stated as follow:

1. Construct an overdetermined Hankel data matrix with a dimension of DxE, where D and E are both greater than the system order m. The matrix is expressed as:

$$H_{HSVD} = \begin{bmatrix} y_1 & y_2 & \cdots & y_E \\ y_2 & y_3 & \cdots & y_{E+1} \\ \vdots & \vdots & \ddots & \vdots \\ y_D & y_{D+1} & \cdots & y_{D+E-1} \end{bmatrix} \tag{5-18}$$

2. Apply SVD to the data matrix in order to extract the left and right eigenvectors, which are represented by U and V matrices respectively. Singular values δ_i are contained in the diagonal entries of the S matrix and are ranked in terms of their magnitudes from largest to smallest i.e. $\delta_1 > \delta_2 > \ldots > \delta_E$ .Thus, the data matrix can be decomposed into:

$$H_{HSVD} = U_{DxD} S_{DxE} V^H_{ExE} \tag{5-19}$$

3. Next, truncate the Hankel data matrix to a rank F matrix by retaining the first F columns. The rest are discarded as their associated singular values are too small and therefore, can be assumed to be perturbed by noise. The modified data matrix becomes:

$$H'_{HSVD} = U_{DxF} S_{FxF} V^H_{ExF} \tag{5-20}$$

4. By using least square approach, the eigenvalues of the data matrix can be computed by solving the following equation:

$$\underline{U}_{DxF} Z = \overline{U}_{DxF} \tag{5-21}$$

where Z contains the estimated eigenvalues λ of the measured signal. The variables $\underline{U}$ and $\overline{U}$ are derived from U_{DxF} by omitting its first and last row respectively. The extracted damping factors and the oscillatory frequencies from the obtained Eigenvalues are then used for the initialization process.

5.2.5 Tuning Considerations for ECKF

Like other modal approximation techniques, the performance of the proposed ECKF is dependent on the adequacy of the selected order of the estimated model. In this case, the system order represented the number of oscillatory modes in the captured signal. If the order was set less than the actual value, a highly smoothed spectrum would be obtained. Consequently, inaccurate dynamic information of the network is generated. Alternatively, if the order chosen was too large, then, overfitting the model to the noise component would occur. Since the number of oscillations occurring in the power system at any instance is unknown, estimating the actual model is not

practical. A good engineering practice is to allow overfitting instead of underfitting. When a larger order is used, spurious noise modes are introduced from overfitting. However, those modes usually contain frequencies much higher than the generator oscillations. They can be subsequently filtered out by using techniques like Welch's periodogram [125]. Furthermore, since the total number of potential oscillations in a network is usually known, the upper limit of the estimated order can be defined.

Similar to Kalman Filter, ECKF requires tuning of its measurement and process noise correlation factors, namely; R and Q respectively [140]. Inadequate calibrations could yield biased estimations, and affect the sensitivity of the monitoring procedure towards noise. Referring to the guidelines set by Korba [129], a good design approach is to assume that the process correlation factor is constant, and experimentally identify the noise correlation value in order to achieve the desired estimation accuracy. From conducted experimental observations, selecting the elements of *Q* to around 0.01 and *R* to 0.9 has been found to be a suitable starting point at which to conduct ECKF over a wide range of monitoring scenarios. Note: the objective is not to find the optimal settings, but to determine the ratio that best suits the requirements of the network.

Refresh time defines how often the modal parameters are updated. Present oscillation detection techniques, like Prony Analysis, conduct modal estimations around once every 10 seconds [29]. The design objective is to minimize the demand for more data storage, and computational power. Unlike block-processing Prony Analysis, ECKF requires a smaller data pool. Frequent updates would have minimal demand on its data storage. In practice, the refresh rates can be increased when the power grid is subjected to a disturbance, and reduced during its normal operation. The refresh time should be determined by the needs of the transmission system operator.

5.3 *Implementations and Evaluations*

The objective is to verify if the modified Kalman Filter is adequate for the intended new application. That is, the ability to detect and identify multiple time-varying modal parameters. Kalman Filter, Prony Analysis and Robust RLS are also included to provide additional comparisons.

In total, three network test cases were used: 1) a synthetic signal, 2) Kundur's Two-Area Network and 3) the New Zealand Phasor data. Four test cases were subsequently formulated. Simulation results are presented in the upcoming subsections. Note: the results are averaged over 100 Monte Carlo trials.

5.3.1 Test Case 1: Synthetic Signal

To distinctly highlight the fundamental nature of ECKF, a well-controlled environment is needed. Hence, a synthetic signal contaminated by white noise was applied with the modal parameters listed in Table 5-1. According to the table, 0.5 Hz mode contained the highest modal energy. That made it the dominant mode, followed by 1.5 Hz and 0.9 Hz modes respectively. In order to evaluate the monitoring accuracy, the signal was corrupted by three different SNR levels: 20dB, 30 dB and 40 dB. A sampling interval of 0.1 second (10Hz) was used and the parameter estimations were conducted over a 10 second sampling window. The computed results were compared with those of Kalman Filter and Prony Analysis. The recursive Kalman Filter, and ECKF calculated their modal parameters by averaging the solutions of each time window. Hence, comparisons with the block-processing Prony Analysis could be drawn. The approximation results are listed in Table 5-2. Note: the values in the bracket are the standard deviations.

Table 5-1 Modal Parameters of the Simulated Synthetic Signal

Mode	Amplitude	Damping Factor	Frequency (Hz)
1	1.5	0.1	0.5
2	0.5	0.3	0.9
3	0.7	0.5	1.5

Table 5-2 Monitoring Results of ECKF, Kalman Filter and Prony Analysis

SNR (dB)	Method	Mode 1		Mode2		Mode 3	
		Damping Factor	Frequency (Hz)	Damping Factor	Frequency (Hz)	Damping Factor	Frequency (Hz)
20	ECKF	0.099 (2.6×10^{-3})	0.500 (1.4×10^{-3})	0.301 (2.0×10^{-2})	0.900 (5.4×10^{-3})	0.500 (3.2×10^{-2})	1.50 (1.4×10^{-2})
	Kalman Filter	0.104 (3.2×10^{-3})	0.499 (3.7×10^{-4})	0.360 (2.5×10^{-2})	0.927 (3.0×10^{-3})	0.529 (3.2×10^{-2})	1.50 (4.4×10^{-3})
	Prony	0.100 (2.1×10^{-3})	0.500 (3.2×10^{-4})	0.307 (2.0×10^{-2})	0.901 (2.7×10^{-3})	0.504 (2.6×10^{-2})	1.50 (4.1×10^{-3})
30	ECKF	0.100 (1.5×10^{-3})	0.500 (2.4×10^{-3})	0.300 (7.9×10^{-3})	0.900 (5.0×10^{-3})	0.500 (1.4×10^{-2})	1.50 (1.2×10^{-2})
	Kalman Filter	0.102 (1.0×10^{-3})	0.499 (1.1×10^{-4})	0.356 (8.7×10^{-3})	0.925 (1.1×10^{-3})	0.527 (1.0×10^{-2})	1.50 (1.4×10^{-3})
	Prony	0.100 (6.5×10^{-4})	0.500 (9.5×10^{-5})	0.301 (6.6×10^{-3})	0.900 (8.9×10^{-4})	0.501 (9.0×10^{-3})	1.50 (1.3×10^{-3})
40	ECKF	0.100 (1.4×10^{-3})	0.500 (2.2×10^{-3})	0.300 (4.3×10^{-3})	0.900 (4.8×10^{-3})	0.500 (1.0×10^{-2})	1.50 (1.3×10^{-2})
	Kalman Filter	0.101 (3.2×10^{-4})	0.499 (3.6×10^{-5})	0.359 (2.3×10^{-3})	0.925 (3.5×10^{-4})	0.527 (3.3×10^{-3})	1.50 (4.2×10^{-4})
	Prony	0.100 (2.1×10^{-4})	0.500 (3.0×10^{-5})	0.300 (2.0×10^{-3})	0.900 (2.8×10^{-4})	0.500 (2.8×10^{-3})	1.50 (4.0×10^{-4})

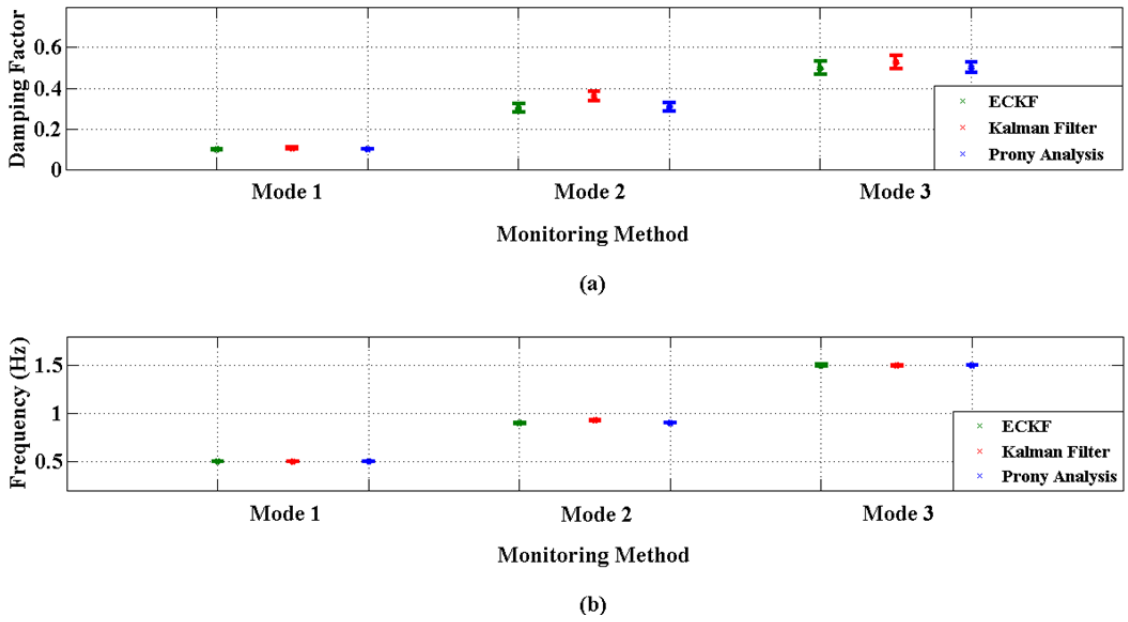

Figure 5-2 Standard deviations of estimated modal parameters under 20 dB noise: a) damping factor and b) oscillatory frequency

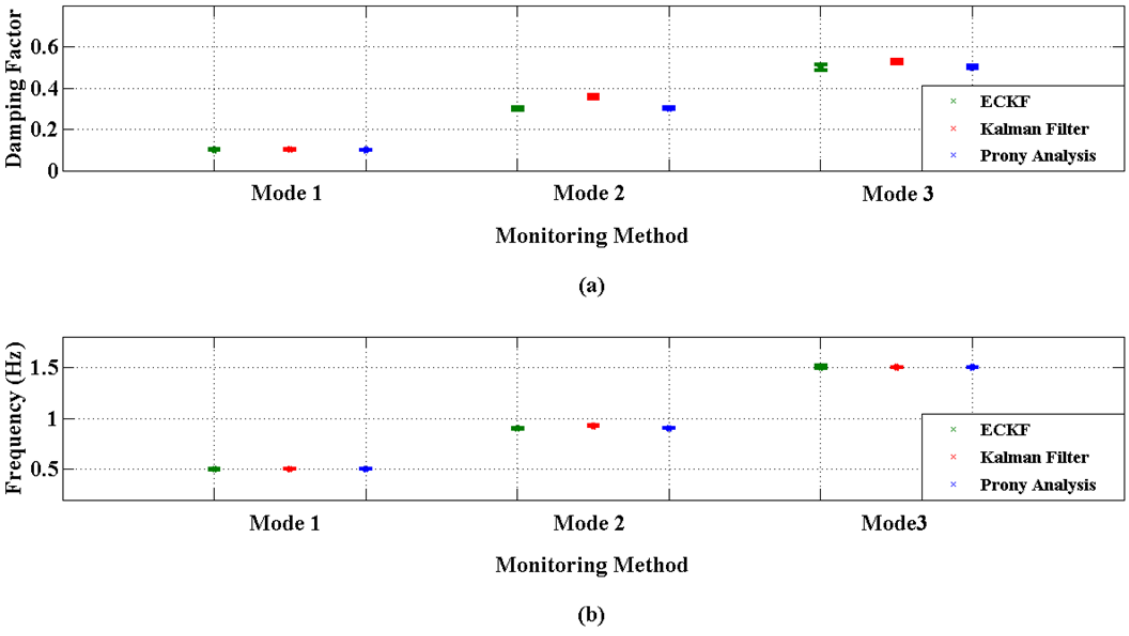

Figure 5-3 Standard deviations of estimated modal parameters under 30 dB noise: a) damping factor and b) oscillatory frequency

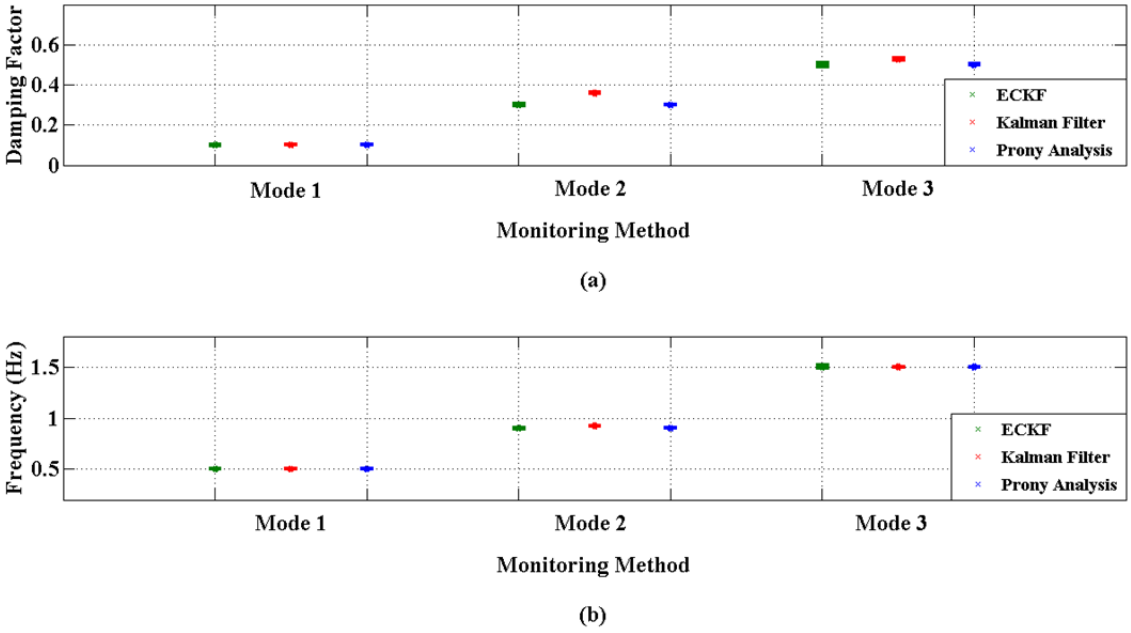

Figure 5-4 Standard deviations of estimated modal parameters under 40 dB noise: a) damping factor and b) oscillatory frequency

Referring to Table 5-2 and Figure 5-2 to Figure 5-4, ECKF was able to detect the dominant Mode 1 with a similar accuracy to Kalman Filter and Prony Analysis. Meanwhile, the proposed method extended Kalman Filter's functionality by monitoring Mode 2 and 3 with similar precision to Prony Analysis. Under various SNR levels, ECKF and Prony Analysis tracked all modal contents with less than 5% error. Conversely, as expected, Kalman Filter was unable to provide similar precision to the other techniques for tracking the two less dominant oscillations. Nevertheless, it was still able to detect their damping factors with an estimation error of less than 20%. Moreover, as seen in Chapter 3, Kalman Filter was able to detect the associated frequencies with acceptable precision. That demonstrated that the recursive engine of Kalman Filter is sound. By expressing the states in a different manner, the resultant ECKF method was able to broaden Kalman Filter's application to monitor multiple oscillations.

Owing to the use of HSVD, the enhanced initialization process allowed the monitoring effectiveness of ECKF to be less affected by the noise component than Kalman Filter. That can be observed in the corresponding standard deviations. For ECKF and

Prony Analysis, the calculated standard deviations of each mode, have similar values under all simulated noise conditions. In contrast, the standard deviations obtained by Kalman Filter tended to increase when operating at lower SNR levels. From the iterations within the defined sampling window, both Kalman Filter and ECKF calculate the modal parameters by averaging their approximated solutions. Since each iterative result contained the errors perturbed by the random noise factor, the overall average contained the sum of those inaccuracies. Consequently, the obtained Monte Caro results of both recursive techniques have a more diverse population. In the contrary, the block-processing Prony Analysis only extracted the modal contents once every sampling window. Therefore, noise incurred errors would be relatively less than with the other two methods.

Apart from tracking multiple modes, the ability to detect oscillations with nearby frequency components was also assessed. Such situation does not exist in the New Zealand grid, but it may occur in other systems. Mode 2 was now changed to a frequency of 0.6 Hz, and the corresponding oscillatory dynamics are shown in Figure 5-5.

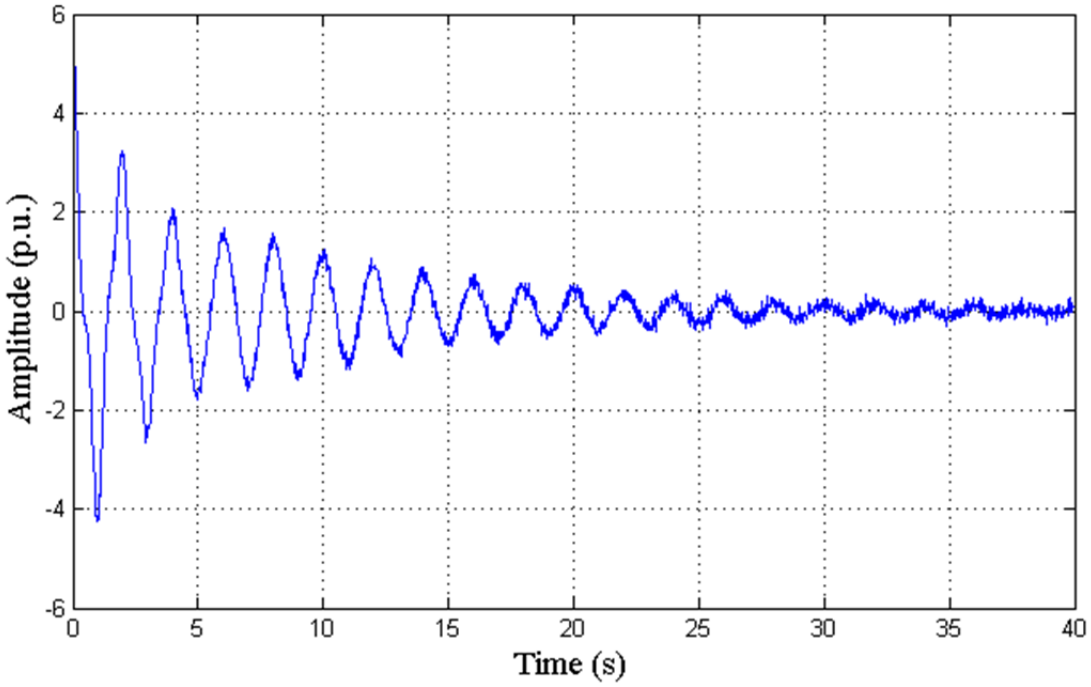

Figure 5-5 Synthetic signal with nearby frequency components and is corrupted by 20 dB noise

The corresponding results are summarized in Table 5-3 and Figure 5-6 to Figure 5-8. In the case of Kalman Filter, the presence of nearby Mode 2 has made it more challenging to extract the dominant modal parameters. Hence, it was unable to estimate Mode 1's damping factor as accurately as in the original study. The rise in estimation errors was mainly because Kalman Filter treated Modes 1 and 2 as one oscillatory mode.

Table 5-3 Results of Three Methods When Tracking Oscillatory Parameters with Nearby Frequency Components

SNR (dB)	Method	Mode 1		Mode2		Mode 3	
		Damping Factor	Frequency (Hz)	Damping Factor	Frequency (Hz)	Damping Factor	Frequency (Hz)
20	ECKF	0.101 (9.6×10^{-3})	0.500 (4.2×10^{-3})	0.303 (3.6×10^{-2})	0.603 (2.2×10^{-2})	0.500 (3.2×10^{-2})	1.50 (1.3×10^{-2})
	Kalman Filter	0.124 (3.6×10^{-3})	0.496 (3.9×10^{-4})	-	-	0.51 (3.2×10^{-2})	1.50 (4.9×10^{-3})
	Prony	0.100 (3.5×10^{-3})	0.500 (5.7×10^{-4})	0.308 (2.9×10^{-2})	0.602 (6.8×10^{-3})	0.500 (3.9×10^{-2})	1.50 (1.0×10^{-2})
30	ECKF	0.100 (6.3×10^{-3})	0.500 (1.9×10^{-3})	0.301 (3.0×10^{-2})	0.600 (7.8×10^{-3})	0.500 (1.5×10^{-2})	1.50 (1.2×10^{-2})
	Kalman Filter	0.122 (1.1×10^{-3})	0.496 (1.1×10^{-4})	-	-	0.501 (9.6×10^{-3})	1.50 (1.5×10^{-3})
	Prony	0.100 (1.2×10^{-3})	0.500 (1.9×10^{-4})	0.302 (1.3×10^{-3})	0.600 (2.0×10^{-3})	0.500 (1.6×10^{-2})	1.50 (9.1×10^{-3})
40	ECKF	0.100 (2.2×10^{-3})	0.500 (2.1×10^{-3})	0.300 (1.3×10^{-2})	0.600 (4.1×10^{-3})	0.500 (8.3×10^{-3})	1.50 (1.2×10^{-2})
	Kalman Filter	0.121 (3.5×10^{-4})	0.496 (3.5×10^{-5})	-	-	0.501 (2.9×10^{-3})	1.50 (4.6×10^{-4})
	Prony	0.100 (3.8×10^{-4})	0.500 (5.5×10^{-5})	0.300 (4.3×10^{-3})	0.600 (6.2×10^{-4})	0.500 (7.1×10^{-3})	1.50 (9.7×10^{-3})

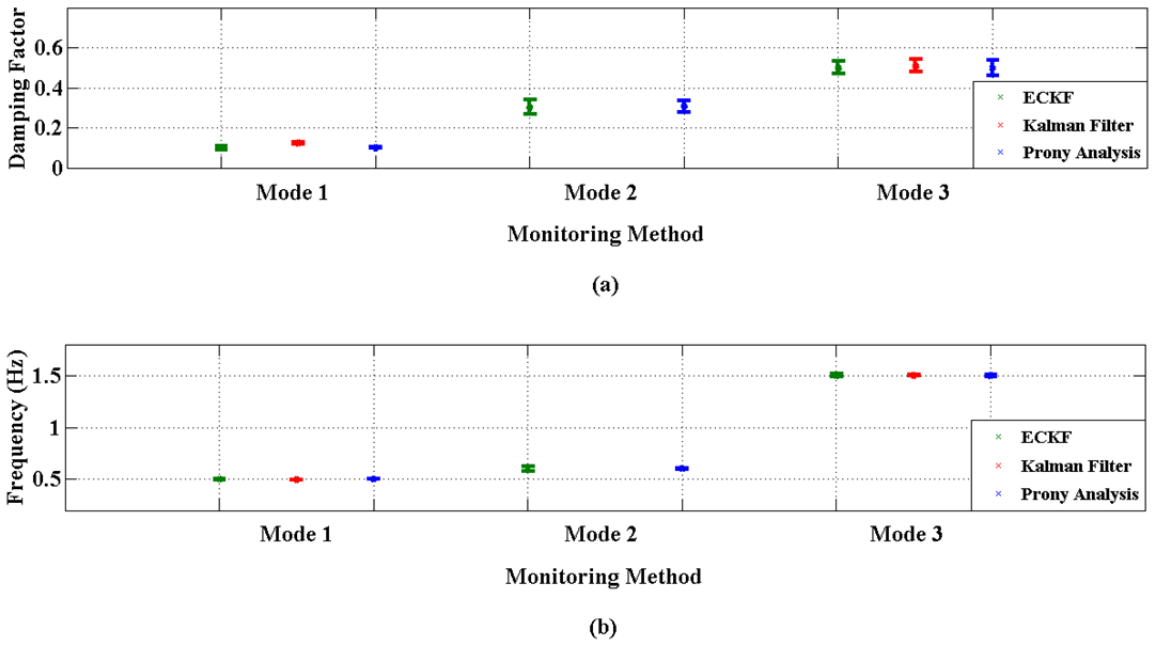

Figure 5-6 Standard deviations of tracking modal parameters with nearby frequencies under 20 dB noise: a) damping factor and b) oscillatory frequency

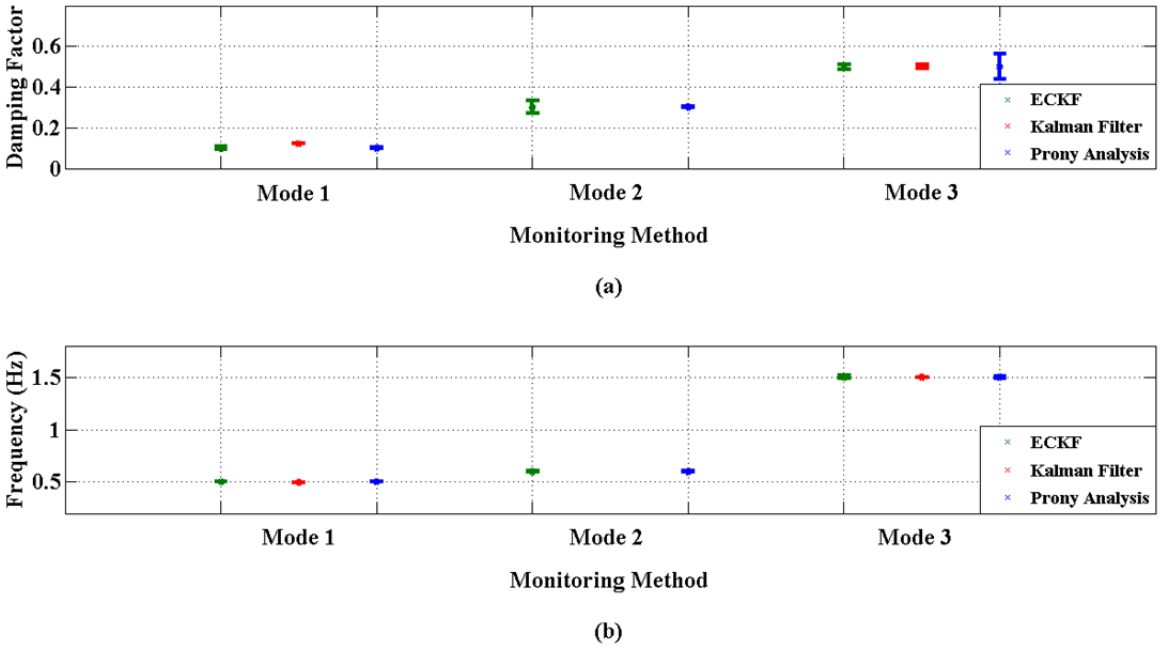

Figure 5-7 Standard deviations of tracking modal parameters with nearby frequencies under 30 dB noise: a) damping factor and b) oscillatory frequency

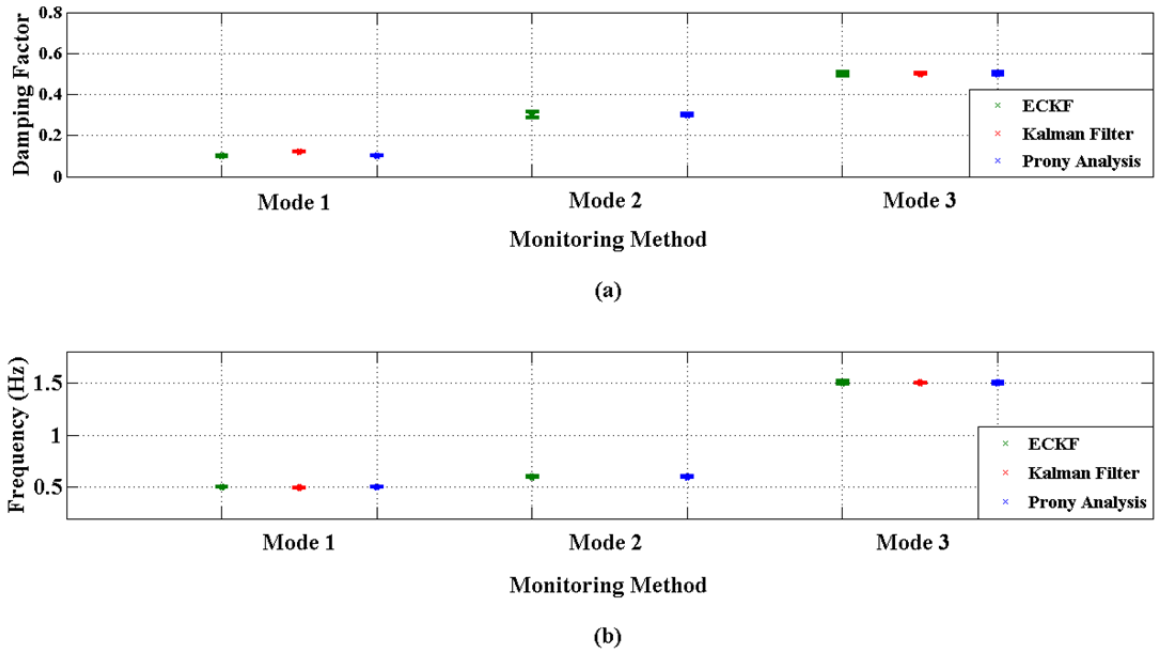

Figure 5-8 Standard deviations of tracking modal parameters with nearby frequencies under 40 dB noise: a) damping factor and b) oscillatory frequency

In contrast, ECKF was able to track all three modes with a similar precision to Prony Analysis. The use of HSVD and the nonlinear recursive engine allowed ECKF to decouple those modes with nearby frequencies and thus, be able to provide better detection accuracy than its predecessor, Kalman Filter. That was especially true at lower SNR levels. Nevertheless, detecting oscillations with nearby frequencies was still a demanding task. That was reflected by a rise in the standard deviation of the approximated modal contents for all three methods. Due to the limited amount of the available measurements, isolating the modal contents between two nearby oscillations and from the noise component was more challenging for the recursive ECKF than Prony Analysis. Consequently, the observed increase in the standard deviation of ECKF solutions was generally higher than the corresponding Prony results. Nevertheless, such issues could be resolved if more data were provided to ECKF. According to the noted observations, Kalman Filter and ECKF may be less attractive than Prony for monitoring nearby oscillations.

5.3.2 Test Case 2: Single Line Outage Scenario

In this study, the performance of the proposed ECKF was examined in a more realistic environment. The main objective was to assess the capability of ECKF to track two oscillations after a line outage contingency. The scenario was similar to that carried out by Quintero in [111]. Line 8-9 was opened after 4 seconds into the simulation for a duration of 0.1 second. Voltage and current phasor measurements are extracted at Generators 1 and 2 for modal estimations. Unlike Test Case 1, ECKF was only compared with Prony Analysis. That was because Prony was known to be the most mature and most widely adopted technique for tracking time-invariant behaviour.

The simulations were conducted over a period of 20 seconds. The steady-state data prior to the disturbance were not used. Based on the modal analysis conducted in DIgSILENT, two oscillatory modes were present in Area 1. Their associated damping factor and frequency values are listed in Table 5-4. The resultant time-domain dynamics due to the line outage are shown in Figure 5-9. Note: a white noise with a SNR level of 20 dB was applied to the extracted signal.

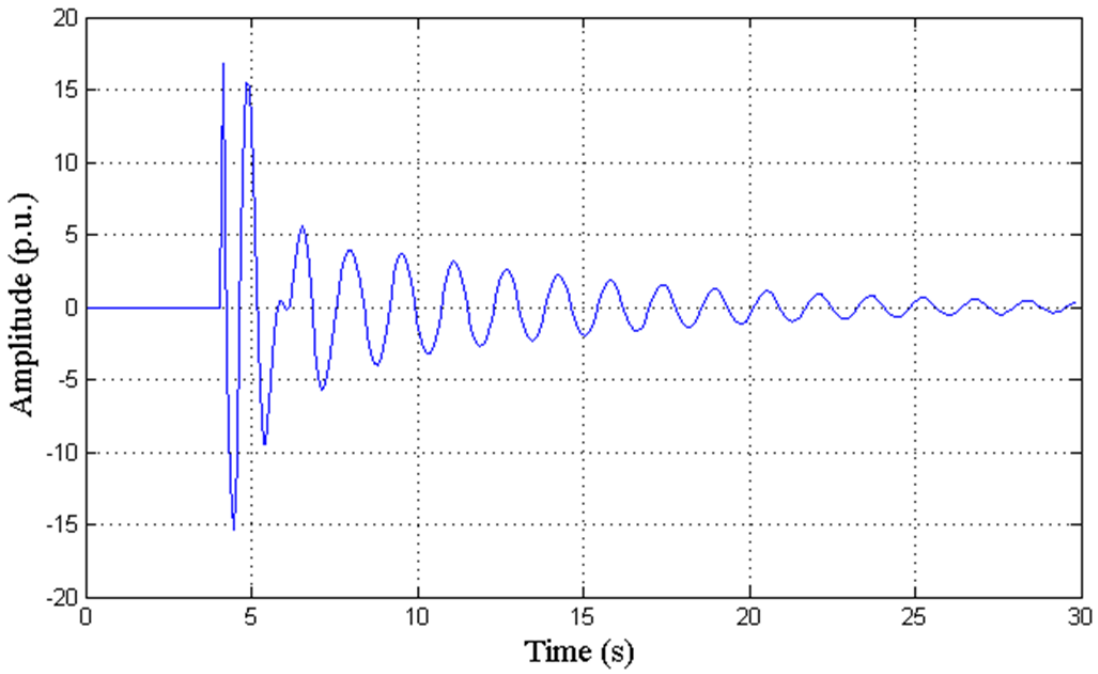

Figure 5-9 Recorded power dynamics between Gen 1 and Gen 2 due to a line outage event

Table 5-4 Oscillatory Parameters after a Single Line Outage Event

Mode	Damping Factor	Frequency (Hz)
Inter-Area	0.11	0.64
Local	0.94	1.14

Table 5-5 Tracking Performance of ECKF and Prony Analysis

Window (s)	Method	Mode 1		Mode2	
		Damping Factor	Frequency (Hz)	Damping Factor	Frequency (Hz)
4-20	ECKF	0.105 (1.4×10^{-3})	0.637 (6.5×10^{-4})	0.941 (4.5×10^{-2})	1.15 (6.2×10^{-3})
	Prony	0.108 (7.8×10^{-4})	0.637 (1.3×10^{-4})	0.998 (7.6×10^{-3})	1.15 (1.5×10^{-3})

Table 5-5 suggests that both methods were able to track the modal parameters with reasonable accuracies. However, as seen in Figure 5-10 and Figure 5-11, the ECKF solutions (blue) had a larger population spread than the Prony estimations (green) for the less dominant Mode 2. Its solutions are much closer to the true value (represented by the red + sign in Figure 5-10 and Figure 5-11) than those approximated by Prony Analysis. That was also reflected by the mean value of Mode 2, listed in Table 5-5. Prony had a slightly higher error than ECKF.

The observations made through these simulations demonstrated that the proposed ECKF detection were able to extend the original Kalman Filter to track multiple oscillations. The integration of HSVD allows ECKF able to provide a similar accuracy to Prony Analysis while retaining Kalman's recursive nature.

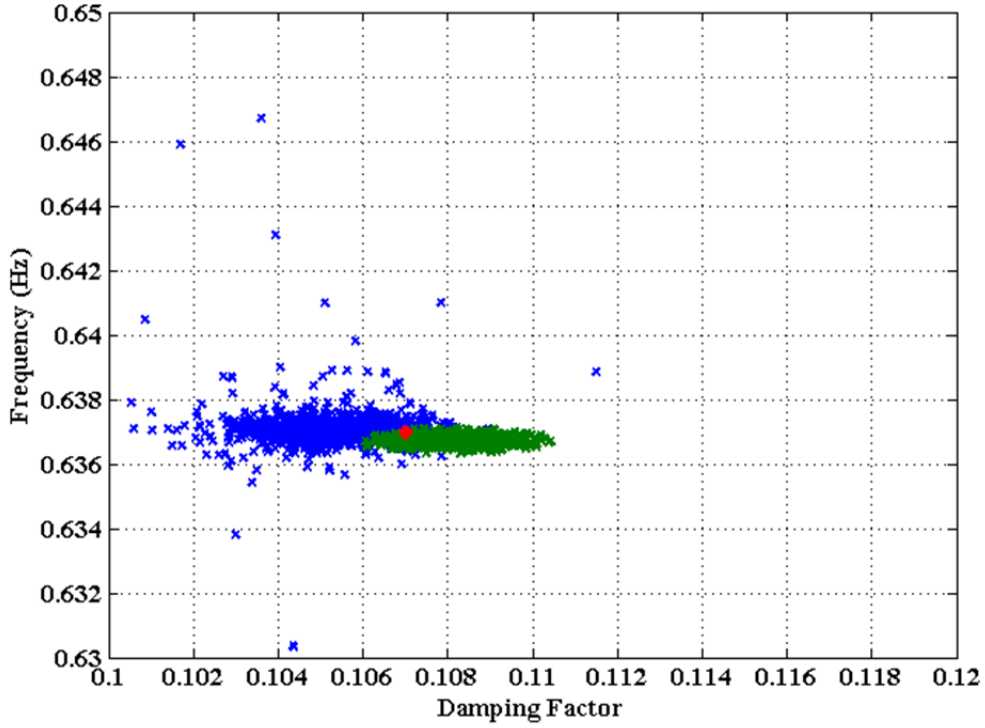

Figure 5-10 Root-Locus plot showing the estimated Mode 1 solutions obtained from 1000 Monte Carlo simulations

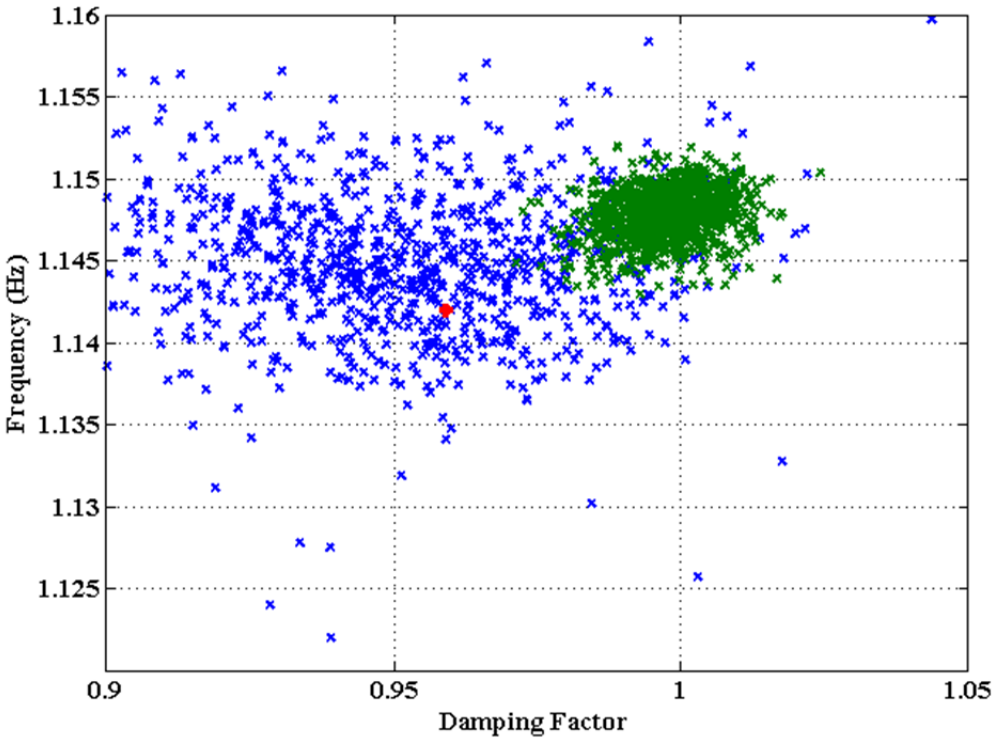

Figure 5-11 Root-Locus plot showing the estimated Mode 2 solutions obtained from 1000 Monte Carlo simulations

5.3.3 Test Case 3: Multiple Load Variation Disturbances

In this study, the ability of ECKF to track changing oscillatory parameters was analyzed. The Two-Area network, as used in *Test Case 2* was implemented. During the simulation, the power demand of *Load 2* was increased by 10% at 5 and 20 second intervals. The ringdown phasor data obtained from generators 3 and 4 were used for the modal estimations. Two distinct electromechanical modes were identified. The oscillatory parameters after each load variation are listed in Table 5-6 and the overall time-domain behaviour is illustrated in Figure 5-12. The extracted signal was subjected to a noise level of 20 dB. Since this study focused on assessing time-varying tracking capability, Robust RLS method proposed by Zhou *et al.* [146], was selected as the referencing candidate. As stated by its authors, the ambient tracking technique is also capable of detecting ringdown behaviours. Prony was not applied because it is a time-invariant technique.

Referring to the results shown in Table 5-7, both methods achieved similar approximation accuracies over the 40 second timeframe. Furthermore, in the first few windows, the proposed ECKF was able to estimate the averaged modal parameters more accurately than Robust RLS. However, as the time progressed, Robust RLS was able to provide similar or even, slightly more accurate modal approximations than ECKF. That was especially evident in the last two windows. That was also observed by the increase in the standard deviation of Mode 2's damping factor in ECKF solutions. The reason was because the well damped Mode 2 was becoming more difficult to be tracked by the ringdown oriented ECKF. Robust RLS was originally built for ambient tracking and therefore, the decreasing oscillatory amplitudes were less of a problem for it. Nevertheless, ECKF was able to achieve a similar time-varying tracking performance as Robust RLS. Modifying the proposed ECKF to operate under the ambient condition is potentially feasible, but it is outside the scope of this PhD research.

Table 5-6 Oscillatory Parameters after Each Load Variation

Condition	Mode	Damping Factor	Frequency (Hz)
After First Load Event	Inter-Area	0.097	0.62
	Local	0.89	1.14
After Second Load Event	Inter-Area	0.085	0.59
	Local	0.79	1.14

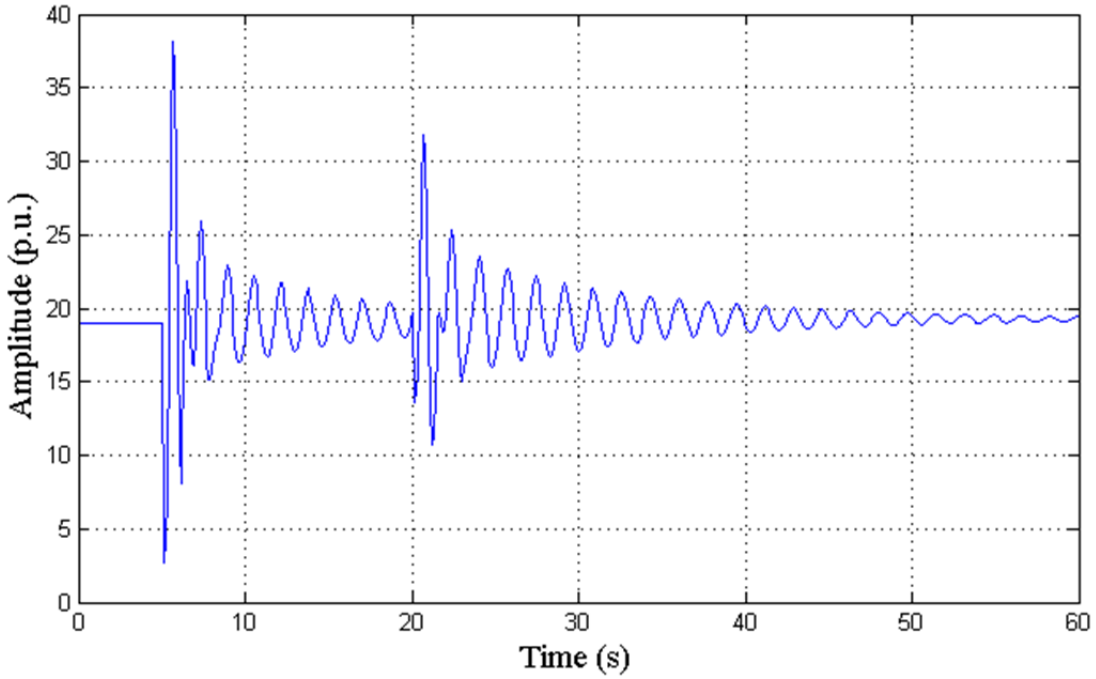

Figure 5-12 Recorded power dynamics between Gen 3 and Gen 4 due to multiple load variations

Table 5-7 Performance of ECKF and Robust RLS When Monitoring Multiple Load Variations

Window (s)	Method	Mode 1		Mode2	
		Damping Factor	Frequency (Hz)	Damping Factor	Frequency (Hz)
5-15	ECKF	0.095 (3.8×10^{-3})	0.61 (3.7×10^{-3})	0.88 (8.0×10^{-2})	1.17 (2.0×10^{-2})
	Robust RLS	0.090 (2.0×10^{-3})	0.60 (3.6×10^{-3})	0.82 (2.5×10^{-2})	1.16 (8.1×10^{-3})
10-20	ECKF	0.091 (4.1×10^{-3})	0.61 (2.3×10^{-3})	0.86 (9.8×10^{-2})	1.16 (3.0×10^{-2})
	Robust RLS	0.094 (3.4×10^{-3})	0.59 (6.8×10^{-3})	0.85 (6.9×10^{-2})	1.17 (1.0×10^{-2})
15-25	ECKF	0.091 (4.4×10^{-3})	0.60 (4.2×10^{-3})	0.88 (9.8×10^{-2})	1.16 (3.3×10^{-2})
	Robust RLS	0.090 (4.0×10^{-3})	0.59 (8.3×10^{-3})	0.89 (6.1×10^{-2})	1.15 (1.2×10^{-2})
20-30	ECKF	0.085 (1.3×10^{-2})	0.58 (7.7×10^{-3})	0.78 (5.6×10^{-2})	1.17 (1.9×10^{-2})
	Robust RLS	0.088 (1.2×10^{-2})	0.58 (7.3×10^{-3})	0.77 (4.4×10^{-2})	1.15 (2.4×10^{-2})
25-35	ECKF	0.087 (2.3×10^{-3})	0.58 (1.2×10^{-3})	0.78 (1.0×10^{-1})	1.18 (2.4×10^{-2})
	Robust RLS	0.088 (1.3×10^{-3})	0.58 (1.1×10^{-3})	0.77 (3.3×10^{-2})	1.15 (2.2×10^{-2})
35-40	ECKF	0.086 (2.6×10^{-3})	0.58 (2.5×10^{-3})	0.79 (1.4×10^{-1})	1.18 (3.2×10^{-2})
	Robust RLS	0.087 (9.8×10^{-4})	0.58 (1.2×10^{-3})	0.78 (4.9×10^{-2})	1.15 (2.4×10^{-3})

5.3.4 Test Case 4: Tracking Oscillations in New Zealand Network

The New Zealand network is a longitudinal power grid with the major load centres and the generation sources located at its physical extremities. It is prone to electromechanical oscillations, similar to those experienced by WSCC. Currently, the New Zealand grid transfers around a peak power of 1,000 MW over a distant of more than 1,000 km from the central South Island to the upper North Island. That has resulted in the occurrence of one local, and two Inter-Area oscillations. They are:

- A 1.6 Hz local mode: in the main generation reserve situated in the middle of the North Island.
- A 1.1 Hz inter-area mode: present in the middle of the South Island. The inter-area is speculated to involve the hydro generations in the middle of South Island with the generation reserves in the North Island.
- A 0.7 Hz inter-area mode: in the south of the South Island. The oscillation exists in the two double circuit tie-lines which supply the aluminium smelter plant at Tiwai Point.

Unlike North American or European power grids, the frequency range of New Zealand's electromechanical oscillations is widely apart. Although the power grid was able to tolerate those oscillations in the past, their presence can no longer be ignored because the peak transmission capacity and the demand of the load centres shows continuous recent growth.

Therefore, the main purpose of this simulation was to verify if the detecting capability of the proposed ECKF was suitable for New Zealand grid. This is a preliminary investigation that assessed the performance of the developed ECKF using actual synchrophasor measurements. More extensive field testing is needed in the future before deploying the monitoring algorithm into operation. In this study, the opening of a 220 kV bus coupler circuit breaker, at Benmore substation, on 28 November 2007, was chosen as the test bench. A snapshot capturing that ringdown event is shown in Figure 5-13. Based on the recorded PMU data collected from Twizel substation in the South Island, two distinct, well-damped oscillations were identified by Transpower New Zealand Limited [43]. They were around 1.05 Hz and 1.40 Hz with the latter one, the dominant mode. All results were updated every 5 seconds. The PMU sampling

rate was defaulted at 50 Hz and the monitoring operation was carried out at a down sampled interval of 0.1 second (10 Hz) instead. In this study, the monitoring performances were conducted using the raw Twizel data captured between the times: 15:51:00, and 15:51:10. The obtained ECKF solutions were subsequently compared with those obtained by Prony, Kalman Filter and Robust RLS methods. Note that the ambient noise in this study is not white noise.

Referring to Table 5-8; ECKF, Prony Analysis and Robust RLS methods were able to monitor both modes with reasonable precision in the first time window. Because the first window was more ringdown dominated, the monitoring accuracy of the ECKF and Prony Analysis were slightly better than Robust RLS method. As designed, Kalman Filter was able to track the dominant Mode 2 accurately.

However, in the second window, the block-processing Prony Analysis was unable to achieve a similar performance to the other three recursive-based techniques. That was because the modes had decayed significantly and therefore, Prony was no longer able to detect the damping factors with an adequate accuracy. Furthermore, being an ambient detection scheme, Robust RLS was able to achieve slightly more accurate modal approximations than the proposed ECKF. Similar to Prony Analysis, the proposed ECKF, found it more challenging to track well-decayed modes. Thus, the associated estimation errors rose, compared with those obtained in the first window. A similar trend was also seen by Kalman Filter. The overall estimation errors were relatively higher than ECKF.

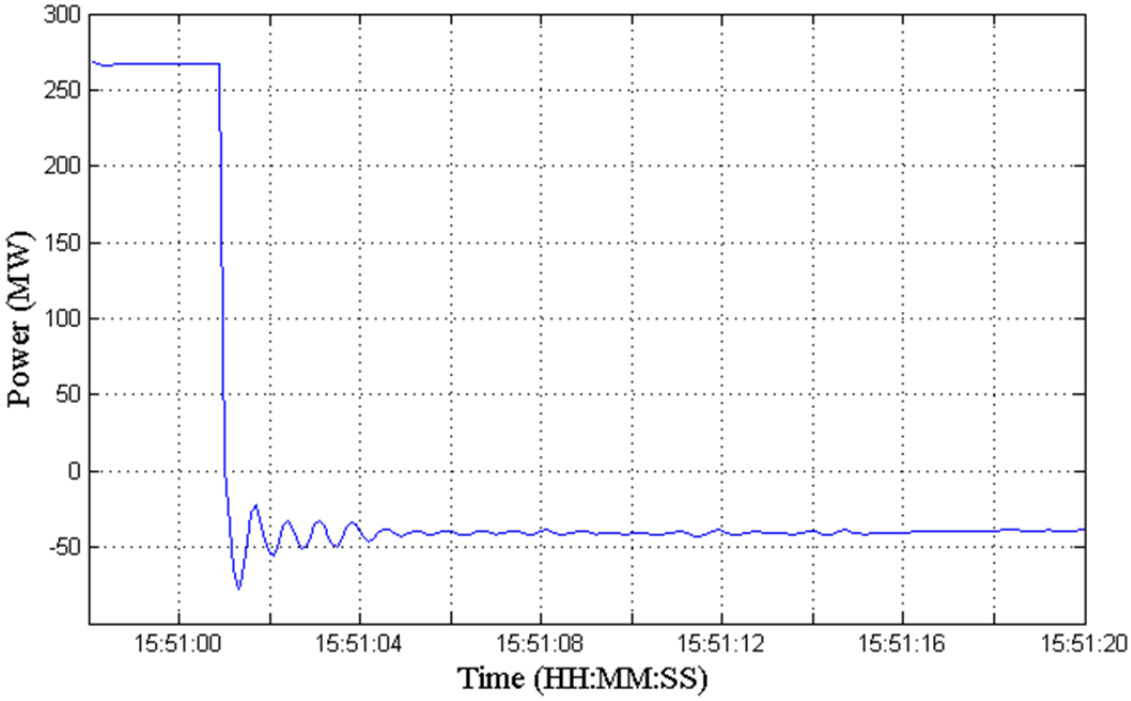

Figure 5-13 Captured ringdown behaviour on 27 November 2007

Table 5-8 Monitoring Performance of all Four Methods Based on New Zealand PMU Data

Time (s)	Mode	ECKF		Kalman Filter		Prony Analysis		Robust RLS	
		σ	f (Hz)	σ	f (Hz)	σ	f (Hz)	σ	f (Hz)
15:51:00 – 15:51:05	1	0.44	1.04	0.93	1.03	0.45	1.04	0.48	1.04
	2	0.66	1.40	0.68	1.38	0.65	1.39	0.66	1.41
15:51:05 – 15:51:10	1	0.55	1.03	0.78	1.08	-	1.02	0.54	1.04
	2	0.61	1.40	0.62	1.37	-	1.40	0.65	1.41

5.4 *Discussion*

As previously noted, Kalman Filter is currently operating in many nations. Its present function is to monitor the dominant mode. The formulated ECKF is able to provide Kalman Filter with a different role which extends its ability to tracking multiple oscillations. Instead of AR coefficients seen in the original Kalman Filter, the state variables are redefined to directly model the oscillatory eigenvalues. Thus, the process errors now avoided were those introduced by converting into the continuous domain using Tustin approximation and subsequently solving the AR characteristic equation. Overall, the proposed ECKF is capable of achieving similar detection accuracy to Prony Analysis for tracking multiple ringdown oscillations. It also provides a similar performance to Robust RLS when monitoring multiple time-varying oscillatory parameters.

Meanwhile, stressed grids with large power transfers over long distances may experience multiple electromechanical oscillations simultaneously. Therefore, being able to monitoring multiple oscillations is essential for ensuring the reliability of the system operation for networks such as the New Zealand grid. Hence, the developed ECKF is a recommended potential candidate for the task. However, further testing using real synchrophasor measurements is required to understand the operating characteristics of the enhanced Kalman Filter in the New Zealand network. Although Robust RLS and other detection methods are all suitable candidates for monitoring power oscillations, the main merit of ECKF is its ability to be easily integrated into Kalman Filter. Instead of introducing a totally different monitoring technique into an existing system that uses Kalman Filter, the more appropriate and simpler option is to upgrade from Kalman Filter into ECKF.

5.5 *Remarks*

An Extended Complex Kalman Filter was formulated to extend the existing role of Kalman Filter to detect multiple electromechanical oscillations. Furthermore, the integration of Hankel Singular Value Decomposition (HSVD) technique into ECKF has improved the accuracy of the initialization process. Based on the exhaustive Monte Carlo simulations, the proposed ECKF technique was shown to provide

estimation accuracy at par with Prony Analysis while retaining Kalman's recursive nature of implementation. Hence, ECKF is considered to be more attractive for the New Zealand grid than the enhanced Prony Analysis discussed in Chapter 4. The effectiveness of ECKF was also compared with Robust RLS procedure. The test cases used to demonstrate the enhanced Kalman Filter method included synthetic data generated in the Two-Area system, and the practical New Zealand grid disturbance.

6 Potential of Parallel-Processing

6.1 *The Needs for Parallel-Processing*

Referring to Chapters 4 and 5: the developed Enhanced Prony Analysis, and Kalman Filter mainly focused on their theoretical formulation. The scope of this chapter is toward implementation issues. Since the ultimate goal is to establish an online oscillatory monitoring system suited for New Zealand system, computing speed is identified as a crucial factor to consider in the implementation procedure. This chapter explores the potential benefits of applying parallel-processing to reduce the computing time of the proposed methods.

In general, the efficiency of monitoring the dynamics of the grid is based on the refresh rate. That is dependent on the computational speed of the installed hardware. Faster updates allow operators more time to react and provide any necessary remedial actions to the grid. However, calculations often involve manipulating many large matrices, or solving large sets of algebraic equations simultaneously [1, 163]. Analysis such as power flow, and stability assessment requires solving a large set of non-linear algebraic equations to approximate each node in the network. Stability analysis demands more computational power as it needs to solve both algebraic and differential equations to correlate the dynamics at each bus with the rest of the connected network. Therefore, in order to maintain a reliable and secure network operation, faster and more powerful computing devices are required.

Since the monitoring and the control strategies can be decomposed into independent subroutines and executed concurrently, computing devices with parallel-processing capability are desirable. However, in the past, such functionality was predominately seen in supercomputers rather than those from the mainstream market. Consequently, most power system operations are generally conducted sequentially off-line.

Feasible solutions to improving the calculation time in power systems are modifying the implemented algorithms, or utilizing better single-core processors. In terms of algorithm modification, minimizing the complexity of the applied analysis has been observed to reduce the calculation time [163]. The most common technique is to linearize the network around an operating point, and thus generate a sparse state-space matrix. The improvement in computing speed is limited [164]. In the 1990s, a multi-processor configuration was proposed in many publications [163-166]. However, establishing adequate interconnections between each CPU has traditionally been difficult to realize [165]. Alternatively, faster processing speed can be obtained by using processors with higher clock frequency [167]. Unfortunately, limitations in Integrated Circuit fabrication have resulted in a slow-down in the rapid increases in clock speed. Hence, manufacturers increase the number of available CPU cores, as opposed to the clock speed [167]. Unlike supercomputers or the 1990s proposed multi-CPU systems, the cores are integrated into one unit. That reduces the interconnection difficulties between processors. As a result, the concept of adopting parallel-processing, using mainstream computers is now feasible and economical.

Furthermore, the demand to provide closer to real-time monitoring, and global visibility of the network dynamics, have inspired operators to develop new operating architectures and control strategies. As a result, Wide Area Monitoring Systems (WAMS) based on the newly installed Phasor Measurement Units (PMUs) have been proposed and implemented in many nations [9]. Subsequently, applications such as: real-time monitoring of voltage stability, lightly-damped oscillations, frequency stability and dynamic load behaviours can be implemented.

Since WAMS implementation is still in its infancy, existing publications mainly focus on exploring potential PMU applications [9, 12, 18, 23, 29]. Consequently, enhancing the existing WAMS operations in terms of optimizing the implementation procedures has been less researched. The optimization and subdivision of computational tasks are not regarded as necessary. However, many proposed real-time applications require powerful computers to simultaneously analyze the multiple incoming Phasor

data. As a result, adopting parallel-processing for the developed oscillatory monitoring methods is a logical and practical solution.

6.2 *The Present Development of Parallel Computing for Oscillations Monitoring*

Like all network monitoring algorithms, the ability to provide early oscillatory warnings and to provide additional reaction time depends on the data analysis speed. WAMS-based oscillation detection strategies, like those published in [85, 101, 121, 127, 129, 168], are primarily based on sequential programming. Optimization and subdivision of computational tasks are not regarded as necessary. Publications such as [29, 100, 143], have recommended the use of parallel computing techniques to enhance operational speed and system performance. Evaluations with respect to the sequential algorithms have not been found in any existing work. Monitoring the oscillations is usually conducted online and in a real-time environment. Therefore, using sequential-processing may lead to a sub-optimal operation for detecting dynamic network behaviours. Consequently, unstable oscillations may, potentially, not be detected in time. They could subsequently lead to angular instabilities of generators across the grid. Details regarding the implementation of parallel-processing for oscillatory monitoring are outlined in the following subsections.

6.2.1 Background and Selection of Parallel Architecture

In order to achieve faster execution times, one must consider the architecture of the target platform. Modern computers tend to be equipped with multiple CPU cores which can be leveraged by an algorithm capable of being decomposed into concurrent subroutines [169]. There are three main parallel computing architectures: *Single-Instruction Multiple-Data*, *Multiple-Instruction Single-Data*, and *Multiple-Instruction Multiple Data*.

Single-Instruction Multiple-Data (SIMD) is useful for algorithms which require repetitive execution of the same function on different objects. This means, instead of queuing up to wait for the same task to be carried out sequentially, the same instruction is issued to all variables at the same time over *N* number of identical processors. As a result, the speedup of adopting SIMD can be theoretically defined

as *N* times faster than a single processor. It is commonly used in applications such as: image processing, matrix manipulation and sorting [170]. Vector processors are an example of a SIMD implementation.

The basic principle of *Multiple-Instruction Single-Data* (MISD) is: to subdivide the monitoring operation into a set of subroutines, where, the output of one subroutine becomes the input of the next. This is also known as the pipeline approach. Each stage of the pipeline can be executed in parallel. Unlike SIMD, MISD operation is mostly seen only in sorting applications [171].

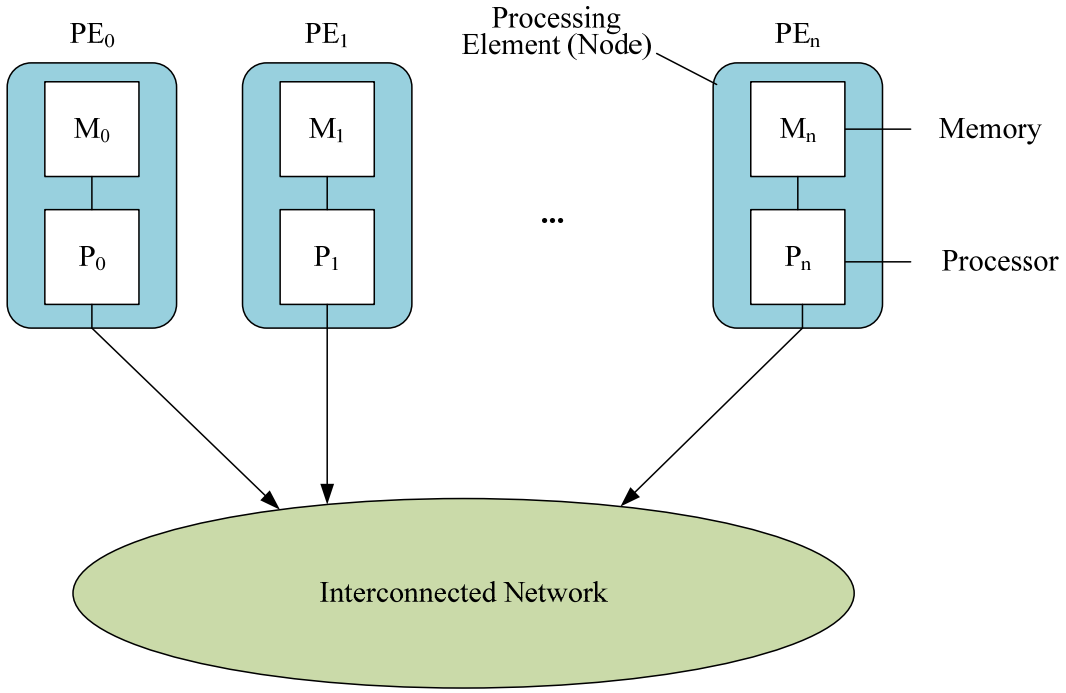

Figure 6-1 Overview of the MIMD Framework

In this chapter, a *Multiple-Instruction Multiple-Data* (MIMD) framework, as shown in Figure 6-1, is used. Compared with MISD, MIMD is an improvement which is capable of processing multiple data streams concurrently by storing independent instructions on each available processor. However, that causes MIMD to demand more computational resources than its SIMD counterpart. Although the performance of MIMD, may be weaker than SIMD, it is a more popular option among architecture designers. That is related to its better economy, robust design constraints, and

application flexibility [170, 171]. Furthermore, SIMD's demand for specialized hardware such as vector processors makes it more difficult to implement. MIMD has been adopted in this chapter because; the modern power industry uses conventional desktop machines built on this architecture.

6.3 *Implementations and Evaluations*

Two test cases were formulated to evaluate the merits of parallel-processing as applied to the Enhanced Prony Analysis, and the derived ECKF monitoring method. Their main objective was to identify ways of improving computing speed. The first study examined the performance of concurrently processing decomposed ECKF subroutines. The second experiment evaluated the potential of simultaneously running multiple Prony analyses to determine an appropriate sampling interval.

The goal was to examine the impact of implementing parallel-processing. The use of a synthetic signal was considered adequate in that context. In addition, the performance issues, associated with the mathematical formulation of the algorithms, are of lesser importance. Details regarding the algorithm development of the ECKF and Enhanced Prony Analysis can be referred to in Chapters 4 and 5 respectively. Although the estimated oscillatory parameters are not listed in the results, a maximum error of 5%, was tolerated in all simulations.

The choice of programming language also plays an important role. Presently, Transpower Limited, the grid operator for New Zealand, uses MATLAB to conduct off-line verifications of the oscillatory parameters extracted by Psymetrix software [43, 47]. However, adopting MATLAB for online monitoring applications has been observed to compromise the update speed [102]. Therefore, this chapter implemented all monitoring methods in C++ and parallelism was introduced using the Intel OpenMP toolbox. Apart from assessing the software implementation, the effect of the utilized hardware was also assessed. The main purpose was to examine the percentage increase of calculating speed when the number of cores was increased.

6.3.1 Test Case 1: Assessing the Performance of the Parallelized ECKF Subroutines

In order to apply MIMD, the proposed ECKF algorithm needed to be decomposed into several subtasks. Firstly, the dependency of the variables, outlined in Equations (5-9) to Equation (5-13) was identified. A visual illustration of the breakdown of ECKF operation was provided in Figure 6-2. From that diagram, it can be seen that the filter gain must be calculated first. Subsequently, the remainder of the algorithm can be decomposed into two concurrent subroutines: 1) updating the covariance matrix $\hat{P}$, and 2) computing the state vector $\hat{x}$.

Table 6-1 Hardware Specifications used in Test Case 1

Hardware	CPU Type	Memory Size
1	Intel T5600 (2 Cores rated 1.83 GHz)	1.5 GB DDR2 (800 MHz)
2	Intel Q9550 (4 Cores rated 3.81 GHz)	4 GB DDR2 (1066 MHz)

Table 6-2 Performance of ECKF under Sequential and Parallel Implementation

Hardware	Architecture	Computational Time (ms)			
		N = 100	N = 200	N = 400	N = 800
1	Sequential	21.8	80.2	170.8	279
	Parallel	15.0	46.8	102.6	217.6
2	Sequential	16	42	109	116.2
	Parallel	15	31	94	100

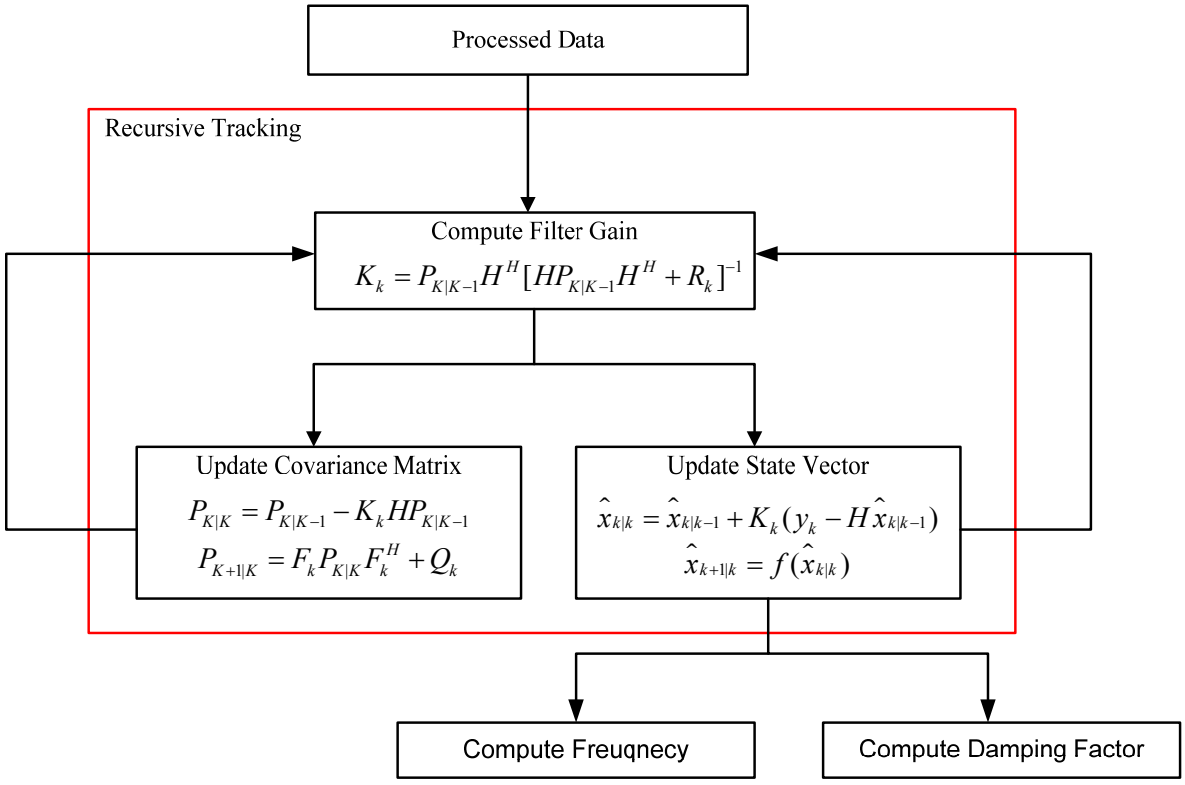

Figure 6-2 Outline of the parallelized ECKF Subroutines

In this study, the software assessment was conducted by comparing the calculation speed of both the sequential and the parallel structures when handling different data sizes. Furthermore, simulations were conducted using two hardware configurations, as outlined in Table 6-1. In total, four different sample sizes with a sampling rate of 10 Hz were used. Processing speeds were computed by averaging ten independent trials. They are listed in Table 6-2.

According to Table 6-2, parallel-processing was capable of providing faster computing speeds than the sequential approach under both hardware specifications. However, it can be seen that the superiority of the parallel architecture deteriorated as the sample size increased. The phenomenon is captured in Figure 6-3. The primary cause was; the parallelism of the ECKF method. As stated above, the monitoring method was decomposed into two independent subroutines: the covariance matrix, and state vector. The covariance matrix calculation requires the multiplication of multiple large matrices, which uses BLAS [172] library in C++. Since

BLAS adopts Strassen's algorithm [173], the operation has a completion time of $O(n^{2.807})$. That was much greater than the vector multiplication used to calculate the state vector completed in $O(n)$ time [172, 173]. Hence, the computational intensity of the subroutines was not balanced. OpenMP toolbox conducts parallelization in a static distribution manner. In other words, every parallel event is allocated with the same CPU power regardless of their computational power demand. Hence, those limitations lead to a reduced speed-up factor.

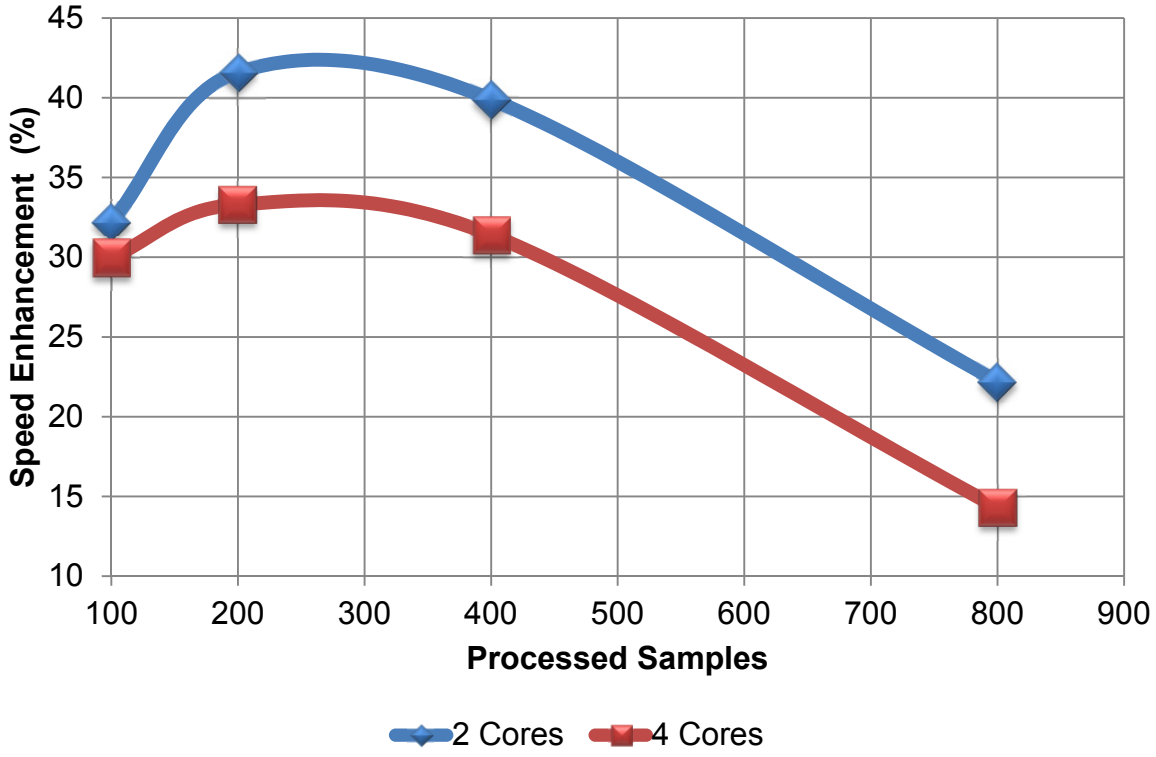

Figure 6-3 Speed improvement of parallel-processing compared with sequential computing

6.3.2 Test Case 2: Evaluating the Effectiveness of the Parallelized Enhanced Prony Analysis

The primary goal of this study was to evaluate the potential benefits of parallelizing the proposed sampling scheme as outlined in Chapter 4. Related to Figure 4-2, the traditional implementation procedure would be to sequentially run Prony Analysis, *X* number of times. That then would incur delays to the status update rate. Therefore, referring to Figure 6-4, a MIMD structure was implemented where each Prony Analysis was allocated to compute one set of measurements. As a result, a faster calculation time was achieved.

In this simulation, the assessments were conducted by examining the calculation time characteristics when dealing with multiple data sets of equal sizes. Here, 10 data pools were adopted, with each containing measurements extracted at different down-sampled intervals. Unlike Test Case 1, the assessments were carried out using different hardware specifications which are shown in Table 6-3.

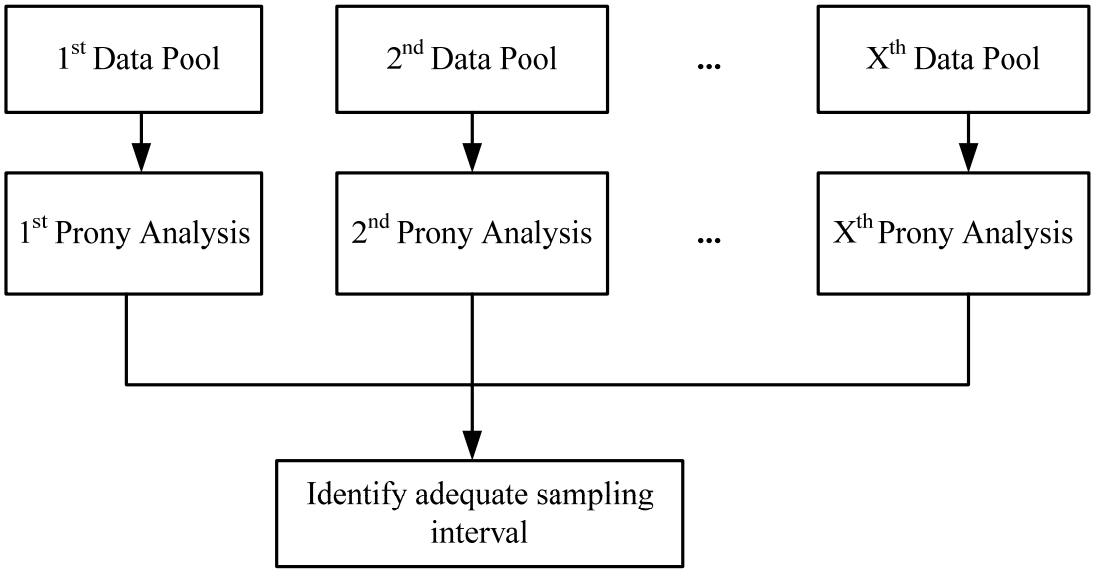

Figure 6-4 Overview of the parallelized sampling method for the Enhanced Prony Analysis

Table 6-3 Hardware Specifications used in Test Case 2

Hardware	CPU Type	Memory Size
1	Intel T5600 (2 Cores rated 1.83 GHz)	1.5 GB DDR2 (800 MHz)
2	Intel Xeon W3520 (8 Cores rated 2.67 GHz)	12 GB DDR2 (1066 MHz)

Table 6-4 Performance of Multiple Prony Analysis at N Number of Sampling Intervals

Hardware	Type	Computational Time (ms)									
		N=1	N=2	N=3	N=4	N=5	N=6	N=7	N=8	N=9	N=10
1	Sequential	91	160	225	291	361	428	495	560	630	680
	Parallel	91	102	173	180	250	260	325	360	397	430
2	Sequential	47	78	125	156	175	203	235	281	297	328
	Parallel	47	62	78	94	110	120	125	140	156	172

The performance results of sequential and parallel-processing are listed in Table 6-4. Note: the symbol *N* represents the number of data pools used to identify the appropriate sampling interval. Overall, parallel-processing was able to reduce the computing time by about 30%. Furthermore, as observed in Table 6-4, the computing speed was proportional to the number of Prony being carried out simultaneously. Therefore, the actual reduction in processing time became more significant as more candidates were used for selecting the desired sampling interval. Parallel-processing is an ideal option for implementing the Enhanced Prony Analysis in the New Zealand grid. It ensured the oscillations are still able to be monitored in a real-time environment despite the additional attached enhancements. Similar to the first test case, using CPUs with more cores did not provide a significant speed-up improvement.

6.4 *Discussion*

Overall, parallel-processing has been demonstrated to be a promising approach for replacing the sequential computing option. That assists in realizing the proposed enhanced oscillation detection methods, as outlined in Chapters 4 and 5. Observations made in the two test cases suggested that the impact of the hardware configuration was a key factor in enhancing computing speed. However, one should note that the relative percentage of speed enhancement, as shown in Figure 6-3, does not increase when more than two cores were used. Thus, it is proposed that a dual-core configuration is sufficient for present online monitoring applications. However, the use of alternative hardware architectures such as vector processors may provide increased benefits.

6.5 *Remarks*

The wide-spread availability of multi-core processors in recent years has allowed parallel-processing to become a feasible alternative for many computing applications. The objective of Wide Area Monitoring Systems is to provide a real-time network detection. Therefore, adopting parallelization as an implementation procedure is considered as an adequate approach.

In this chapter, the use of parallel-processing for monitoring power oscillations in a smart grid framework has been presented. The Extended Complex Kalman Filter (ECKF), proposed in Chapter 5 and the Enhanced Prony Analysis, from Chapter 4, were selected as candidates for parallelism. ECKF demonstrated the potential of computing parallel decomposed subroutines, while the Enhanced Prony Analysis showed the possibility of running multiple algorithms simultaneously. Both examples adopted a Multiple-Instruction Multiple-Data (MIMD) architecture. According to a comparative analysis of each algorithm, with its sequential counterpart, the parallelized ECKF and the Enhanced Prony Analysis were able to achieve faster computing times. The magnitude of the speed improvement of parallelism depended on the hardware configuration. In general, a dual-core configuration was considered sufficient for online oscillatory monitoring in New Zealand's power systems.

7 The Effects of Load Characteristics on WACS-Based PSS

7.1 *Introduction*

As the dependency on digital devices increases, the associated operational philosophies based on continuous analogue concepts must also be subsequently modified. As noted in Chapter 1, the purpose of monitoring the electromechanical oscillations is to allow the operators to have more time to react to unstable modal behaviours. Subsequently, appropriate damping strategies can be applied to remediate any resultant network instabilities.

The focus of this dissertation has been related to monitoring the electromechanical oscillations. As with those monitoring operations, the performance of the damping controllers can also be enhanced by using synchrophasor data. Therefore, this chapter explores the effects of using PMU measurements for damping the inter-area oscillations under various load characteristics.

In order to ensure that all electromechanical oscillations are sufficiently damped, Power System Stabilizers (PSS) are installed in most thermal generators to provide damping controls to the oscillatory modes [174]. That is accomplished through the excitation system. PSS compensates the phase difference between the electric torques and the rotor speed deviations of the generator [108, 175-177].

In general, the conventional PSS are usually single-loop controllers, which utilize the local input signals. By combining robust control theories like, H_2 or H_∞ methods, with Linear Matrix Inequality (LMI) framework, the conventional PSSs are able to damp the inter-area oscillations. Nevertheless, they lack global observability. Since the inter-area oscillation is a global dynamic phenomenon, under certain operating conditions, it may be observable in one region and controllable in another [105, 178, 179]. Consequently, the traditional PSS controllers may not be able to provide

sufficient modal damping. They may even amplify the degrading process of a lightly damped inter-area oscillation [1, 109, 180, 181]. To achieve a near maximum observability of the swing modes, a combination of the remote, and the local signals are needed. Such a requirement can be satisfied by utilizing the data from the increasingly available Phasor Measurement Units (PMU). As a result, signals such as a distant generator's rotor speed, or the tie-lines power readings, can be sent to the local PSS [110, 111, 113, 182, 183]. In this chapter, this type of design is defined as Wide Area Control System (WACS) based controllers. Their inputs consist of both local and remote PMU data.

An inter-area mode cannot be solely explained in terms of the rotor behaviour of a particular group of generators. Instead, the phenomenon involves additional factors like the interconnecting transmission network, and system loading. Although many recent studies have been conducted on designing and analyzing the performance of WACS-based PSS, most of them are simulated under the assumption of a constant linear impedance [108, 110, 111, 113, 182]. That is not sufficient to simulate all the potential dynamics encountered in a real power network. In an actual system operation, the load characteristics often exhibit other traits, and are not always purely impedance based [180, 181]. In addition, several past publications have demonstrated that the damping performance of PSS towards inter-area oscillations was significantly influenced by the load characteristics [104, 114, 184]. Hence, the impact of different load characteristics on the operation of WACS-based PSS needs to be looked into.

For this research, a simple WACS-based PSS, similar to the one formulated by Chow *et al.* [105], was adopted for examining the impact of the load attributes. The network stress was simulated by varying the power transfers between the tie-lines. The investigation was designed to evaluate the capability of a WACS-based PSS to maintain adequate damping compared with a conventional PSS that used local signals. Since investigating the damping control is beyond the scope of this thesis, these assessments are conducted at a preliminary level. Nevertheless, the aim was to provide fundamental observations which established a foundation for any future research in this area.

7.2 *Outline of the Study System*

7.2.1 Review of the Two-Area Network

All simulations are conducted using the Two-Area power network, discussed in Chapter 4. The power grid was subdivided into two regions. Each area consisted of two generators and a load. Every generator was equipped with a fast static exciter (*EXAC4*) and a governor (*IEEEG1*). In addition, *G3* was set as the angular reference. The system data used are presented in Appendix C. For that network, the system exhibited the three electromechanical modes:

1) A lightly damped inter-area mode with a frequency of 0.65 Hz
2) A local oscillation of 1.15 Hz in *Area 1*
3) A local oscillation mode of 1.20 Hz in *Area 2*

Note: those oscillatory frequencies varied slightly depending on the PSS model, the power transfer quantity, the load characteristics, and the load magnitudes.

7.2.2 Outline of the Conventional and the WACS-Based PSS Designs

A block diagram outlining a conventional PSS operation is shown in Figure 7-1. Here, E_t is the machine terminal voltage, V_{ref} is the exciter reference voltage, ΔT_e is the rotor electric torque, ΔT_m is the rotor mechanical torque, $\Delta\omega$ is the deviation of the rotor speed, and $\Delta\delta$ is the rotor angle deviation. The conventional PSS was effective in damping local oscillations. It was effective to a limited degree, if coordinated, or tuned carefully to damping the inter-area mode. However, depending on the load characteristics and the load magnitudes, the observability of the inter-area oscillation may not always be available from the local signals received by PSS. Consequently, poor damping may occur and subsequently, force the operators to conservatively restrain the allowable power transfer limit. In this work, the classic speed stabilizing model (*STAB1*), shown in Figure 7-2 was used to represent the conventional PSS.

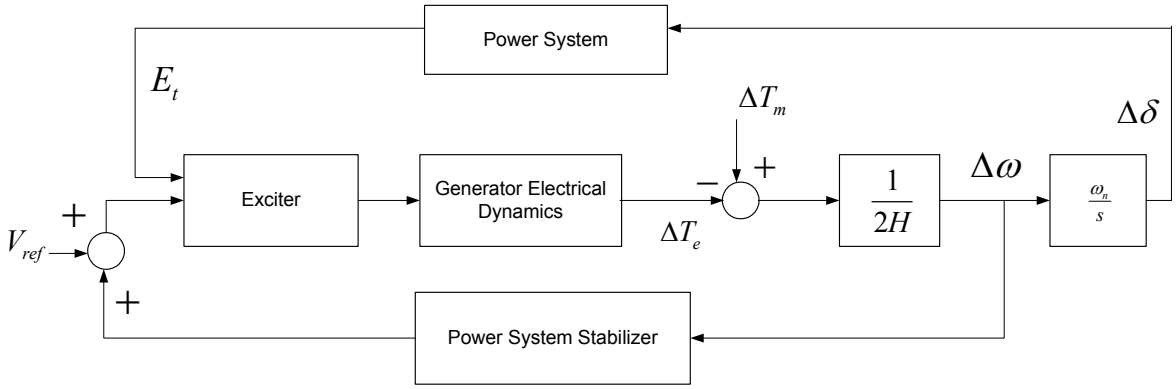

Figure 7-1 Block diagram outlining PSS action

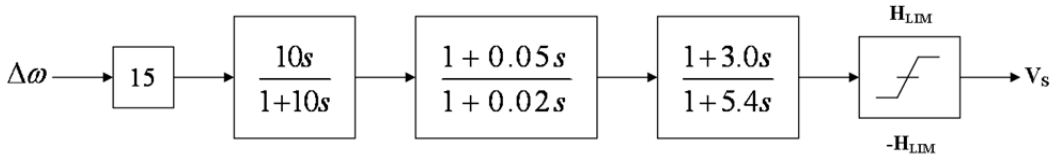

Figure 7-2 Control block diagram of the conventional PSS

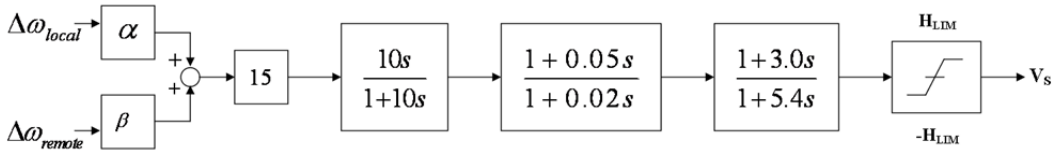

Figure 7-3 Control block diagram of the proposed WACS-based PSS

There is no standardized WACS-based PSS model at present because *Wide Area Control System* is still an emerging architecture. To facilitate an unbiased performance comparison with the conventional PSS in this paper, the WACS-based design should possess a similar structure. Therefore, in this study a modified *STAB1* model, shown in Figure 7-3 was developed. The main modification was the addition of an input channel used to receive the rotor speed data from the remote generator. Furthermore, based on the coherency concept from [105], the weighting factors (*α* and *β*), were added to both inputs of WACS-based PSS. Hence, the combined data received by PSS contained rich information about the lightly damped inter-area mode, while maintaining sufficient sensitivity to provide an adequate damping for the local mode.

7.2.3 PSS Allocations in the Two-Areas Power Network

One generator in each region was equipped with PSS. According to modal analysis, placing PSS at *G1* and *G3* was the most suitable. They had the highest participation factors in their areas, related to damping the inter-area mode. In order to distinctly capture the operational differences between both kinds of PSS, two types of network configurations were considered; *Conventional* and *Wide Area*. The *Conventional* approach adopted traditional designs for both PSS units in the power grid. The main objective of the *Conventional* setup was to act as a reference for assessment of the *Wide Area* structure.

In this chapter, *Wide Area* PSS arrangement refers to implementing a combination of conventional and WACS-based design. That is a realistic and practical approach. The reason; extra communication channels and PMU instalments are required to upgrade all conventional PSSs to WACS-based configuration. Since the number of inter-area oscillations is generally less than local ones, demands for WACS-based PSSs are only required at strategic locations. Therefore, in this work, only one WACS-based PSS was installed at *G1* and its remote signal was provided by *G3*. The second, conventional PSS is located at *G3*.

7.2.4 Load Modelling: Basic Concepts

The non-linear load model used in the simulation software, *DigSILENT Power Factory ver. 13.2.333 (Professional),* is composed of a parallel combination of static and dynamic components. The static load is a voltage dependant exponential model governed by the following two equations:

$$P = P_0 \left(\frac{V}{V_0} \right)^{Kpu} \tag{7-1}$$

$$Q = Q_0 \left(\frac{V}{V_0} \right)^{Kqu} \tag{7-2}$$

The subscript 0 denotes the initial operating conditions of the system. Constant power, current and impedance are achieved by setting the values of Kpu to 0, 1 and 2 respectively. In contrast, Kqu is set at a constant value of 1 for all three cases. In addition, the dynamic load is based on the motor-load and the general outline of the

modelled non-linear dynamic load is shown in Figure 7-4. The dynamic and static load characteristics were set to 80% and 20% accordingly with a time constant (T_1) of 0.5 seconds. The voltage limits ($udmax$ and $udmin$) were 1.2 and 0.8 p.u. respectively. Further details regarding to this model can be obtained from [185].

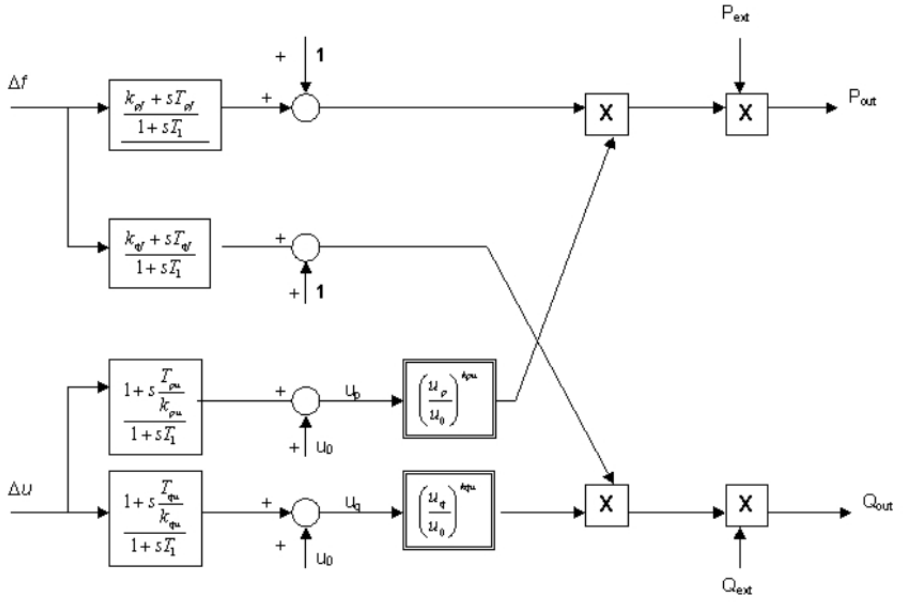

Figure 7-4 DIgSILENT load model used to approximate the behaviour of the non-linear dynamic load [185]

7.3 *Simulations and Evaluations*

Three different test cases were formulated to compare the damping performance of *Conventional* and *Wide Area* network configurations. Each case was based on one of the three load characteristics of interest; constant impedance, power, and current. For each load characteristic, three different operating conditions, associated with the specified power transfer quantities, were considered; 200 MVA, 300MVA, and 400 MVA. The load magnitudes under these power transfers are defined as follows:

- Load 1 = 1166 MW; Load 2 = 1568 MW for 200 MW scenario
- Load 1 = 1066 MW; Load 2 = 1668 MW for 300 MW scenario
- Load 1 = 967 MW; Load 2 = 1767 MW for 400 MW scenario

Their main purpose was to simulate different stress levels experienced by the network. That was achieved by setting the reactive power demand of each load to 100 MVar under all conditions.

Exhaustive simulations, using different disturbance scenarios, were conducted to investigate the effectiveness of PSS operation. *G2* experienced a small-signal disturbance, created by, an additional 0.05 p.u. torque after 1 second of simulation. Calculations of the damping factors, the oscillatory frequencies, and the damping ratios were computed after a timeframe of 20 seconds. Damping assessments of conventional and WACS-based PSS were carried out by examining the operational performance of *Conventional* and *Wide Area* arrangements. Comparisons were related to evaluating the adequacy of damping ratio associated with the inter-area mode. Only damping ratios over 5% were considered to be significant [108]. Based on this requirement, the weighting factors α and β were set 1.7 0.3 respectively for all simulations. In addition, plots of *G1*'s active power were used to capture the damping performance in the time-domain.

7.3.1 Test Case 1: Constant Impedance

The motivation of this test case was to demonstrate and verify the capability of WACS-based PSS damping for inter-area oscillation. Referring to Table 7-1, results from all the simulated power transfer scenarios showed that *Wide Area* achieved a higher inter-area damping ratio than a *Conventional* setup. Furthermore, under *Wide Area* configuration, smaller peak oscillatory amplitudes were observed from plots in Figure 7-5 to Figure 7-7. Note: the red lines represent the *Conventional* setup and the blue lines are the *Wide Area* configuration. Thus, WACS-based PSS demonstrated its potential to enhance the stability of inter-area oscillation by providing an adequate damping over a more diverse operating range. In terms of local modes, both arrangements were able to provide adequate damping. For *Wide Area* setups, the 20% damping of the local mode in *Area 1* was mainly due to the improved performance from the WACS-based PSS installed at *G1*.

Table 7-1 Damping Performance of the Traditional and WACS-Based PSS under Constant Impedance

Power Transfer	Conventional			Wide Area		
	Damping Factor	Frequency (Hz)	Damping Ratio (%)	Damping Factor	Frequency (Hz)	Damping Ratio (%)
200MW	1.54	1.20	20.0	1.59	1.20	20.4
	1.07	1.19	14.2	1.07	1.19	14.1
	0.28	0.67	6.76	0.31	0.67	7.39
300MW	1.56	1.20	20.4	1.59	1.20	20.7
	1.10	1.18	14.6	1.09	1.19	14.6
	0.26	0.65	6.41	0.29	0.66	7.05
400MW	1.57	1.19	20.5	1.12	-1.19	20.8
	1.12	1.18	14.9	1.59	-1.18	14.9
	0.22	0.63	5.54	0.25	-0.64	6.23

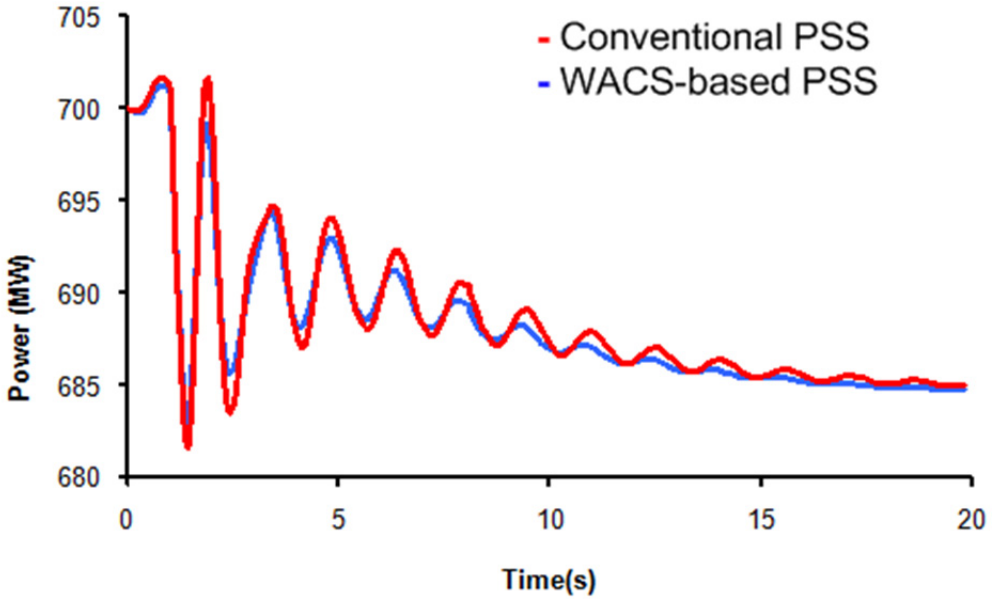

Figure 7-5 Damping performance under constant impedance with 200 MW power transfer

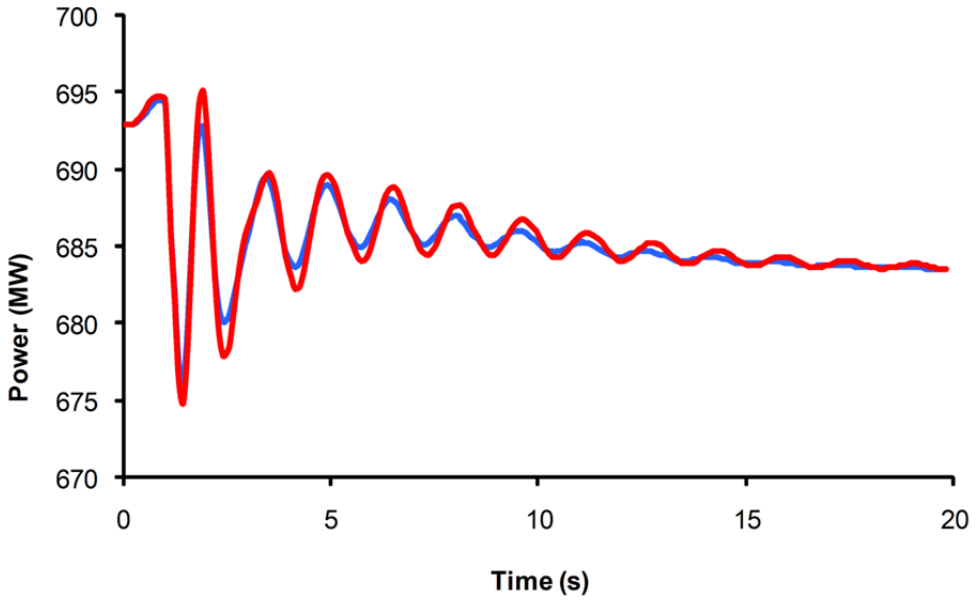

Figure 7-6 Damping performance under constant impedance with 300 MW power transfer

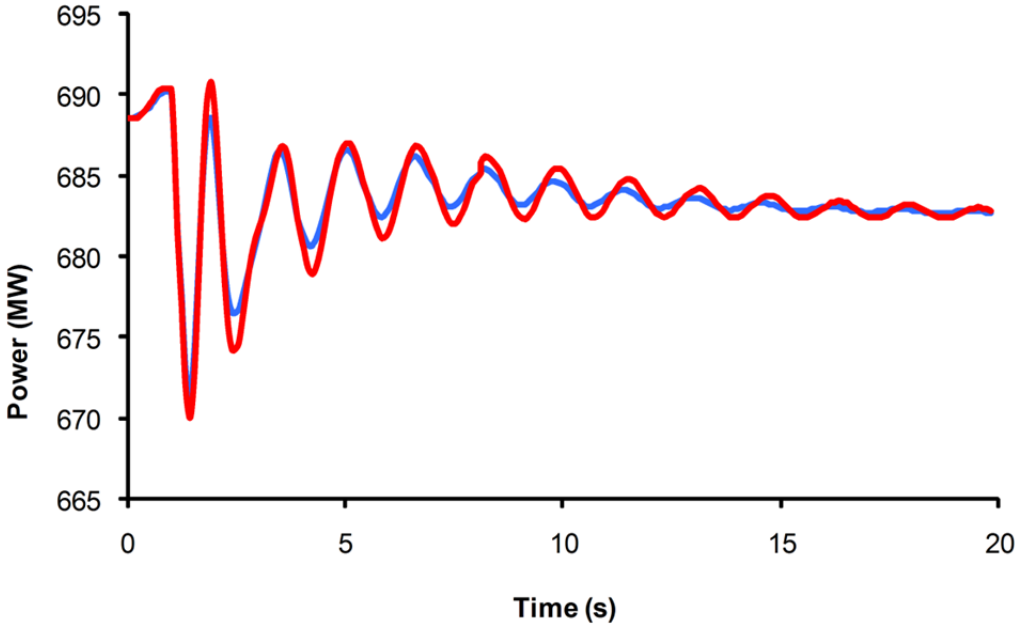

Figure 7-7 Damping performance under constant impedance with 400 MW power transfer

7.3.2 Test Case 2: Constant Power

The objective of this study was to simulate a realistic situation which could be experienced during a power system operation. Results from Table 7-2 show that the damping capability of both arrangements was worse than the constant impedance situation. That trend can also be observed from Figure 7-8 to Figure 7-10. Clear increases in oscillatory overshoots and slower rate of decay compared with constant impedance scenarios were seen from those plots. Nevertheless, the *Wide Area* configuration was still able to achieve an adequate inter-area stability for up to 400 MVA of power transfer. In contrast, the damping performance of the *Conventional* arrangement was unable to meet the tolerable limits under all three operating conditions. Despite the significant decline in damping performance, both setups were able to provide sufficient damping for local oscillations.

Table 7-2 Damping Performance of the Traditional and WACS-Based PSS under Constant Power

Power Transfer	Conventional			Wide Area		
	Damping Factor	Frequency (Hz)	Damping Ratio (%)	Damping Factor	Frequency (Hz)	Damping Ratio (%)
200MW	1.22	1.20	15.9	1.33	1.20	17.3
	0.88	1.19	11.7	0.86	1.19	11.4
	0.18	0.66	4.45	0.22	0.66	5.18
300MW	1.17	1.20	12.5	1.28	1.20	16.7
	0.84	1.19	11.2	0.84	1.19	11.1
	0.17	0.63	4.22	0.21	0.64	5.22
400MW	1.08	1.20	14.2	1.21	1.20	16.0
	0.84	1.19	11.2	0.87	1.19	11.6
	0.14	0.59	3.87	0.19	0.60	5.03

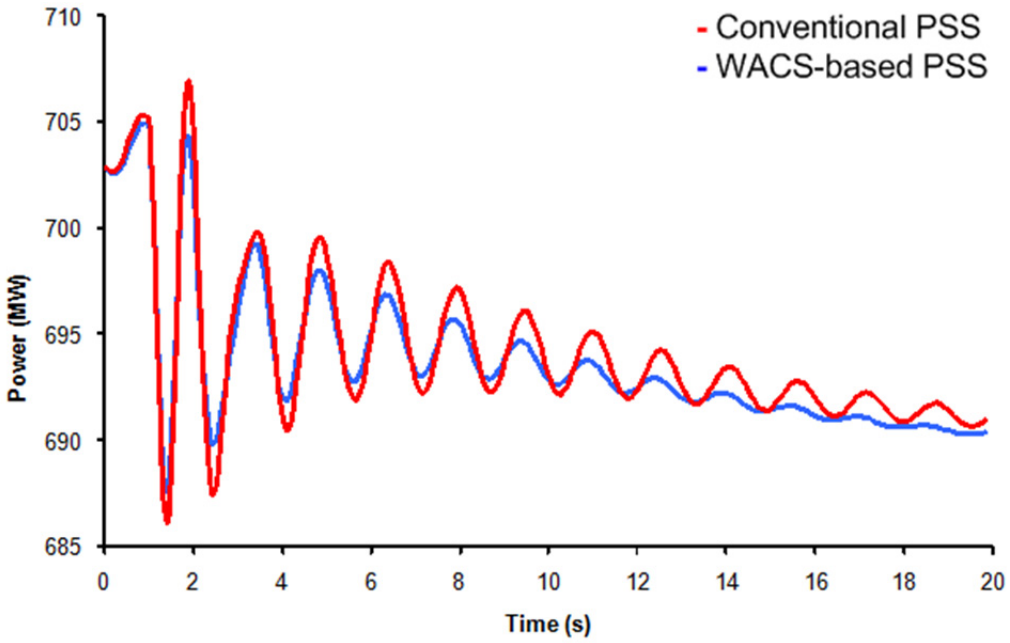

Figure 7-8 Damping performance under constant power with 200 MW power transfer

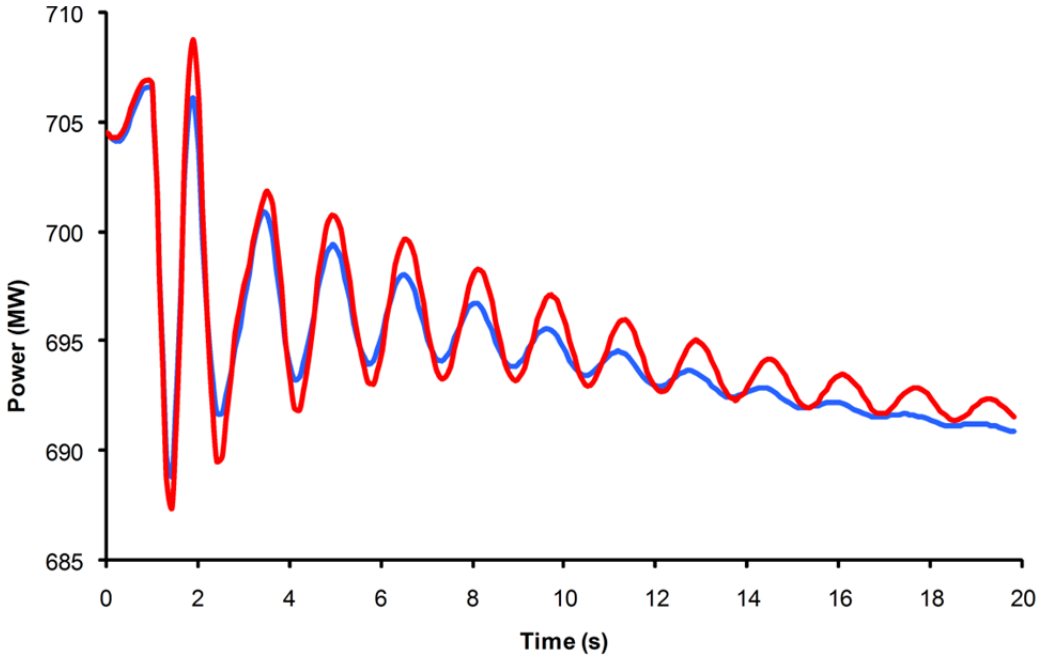

Figure 7-9 Damping performance under constant power with 300 MW power transfer

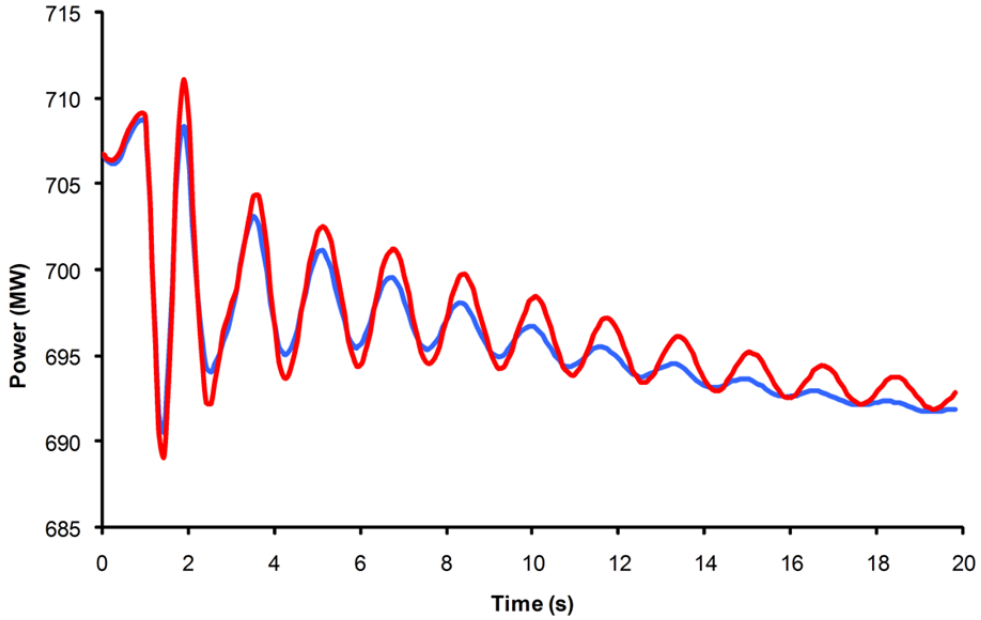

Figure 7-10 Damping performance under constant power with 400 MW power transfer

7.3.3 Test Case 3: Constant Current

Although, in practice, the loads are seldom modelled as constant current, that type of load characteristic was also evaluated in these investigations. Its performance was compared with the other, two types, of load models. According to the results observed and displayed in Table 7-3, and Figure 7-11 to Figure 7-13, it can be seen that the effectiveness of damping inter-area mode for both configurations was between the, constant impedance, and constant power load models. The percentage dropped in damping ratio of the *Wide Area* arrangement, was distinctively less than, the *Traditional* arrangement. In contrast, local oscillations were still well damped.

Table 7-3 Damping Performance of Traditional and Wide Area Configurations under Constant Current

Power Transfer	Conventional			Wide Area		
	Damping Factor	Frequency (Hz)	Damping Ratio (%)	Damping Factor	Frequency (Hz)	Damping Ratio (%)
200MW	1.49	1.20	19.4	1.54	1.20	19.9
	1.04	1.19	13.8	1.03	1.19	13.7
	0.25	0.66	6.01	0.28	0.67	6.66
300MW	1.52	1.20	20.7	1.55	1.20	20.2
	1.07	1.18	14.2	1.06	1.19	14.1
	0.24	0.65	5.80	0.27	0.65	6.49
400MW	1.50	1.20	19.6	1.54	1.20	20.0
	1.06	1.18	14.2	1.06	1.18	14.1
	0.20	0.63	5.18	0.24	0.63	5.94

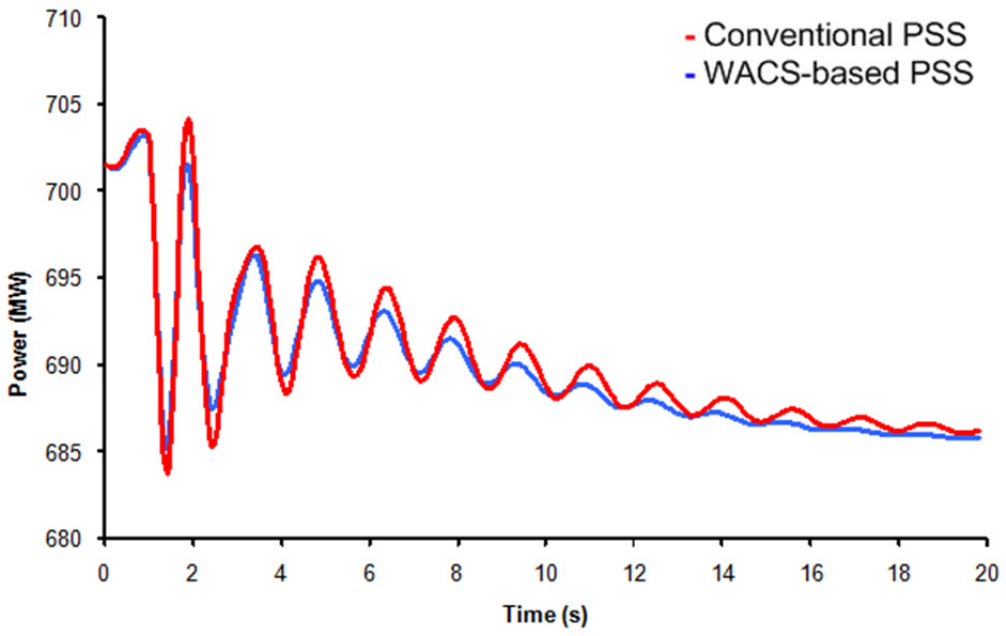

Figure 7-11 Damping performance under constant current with 200 MW power transfer

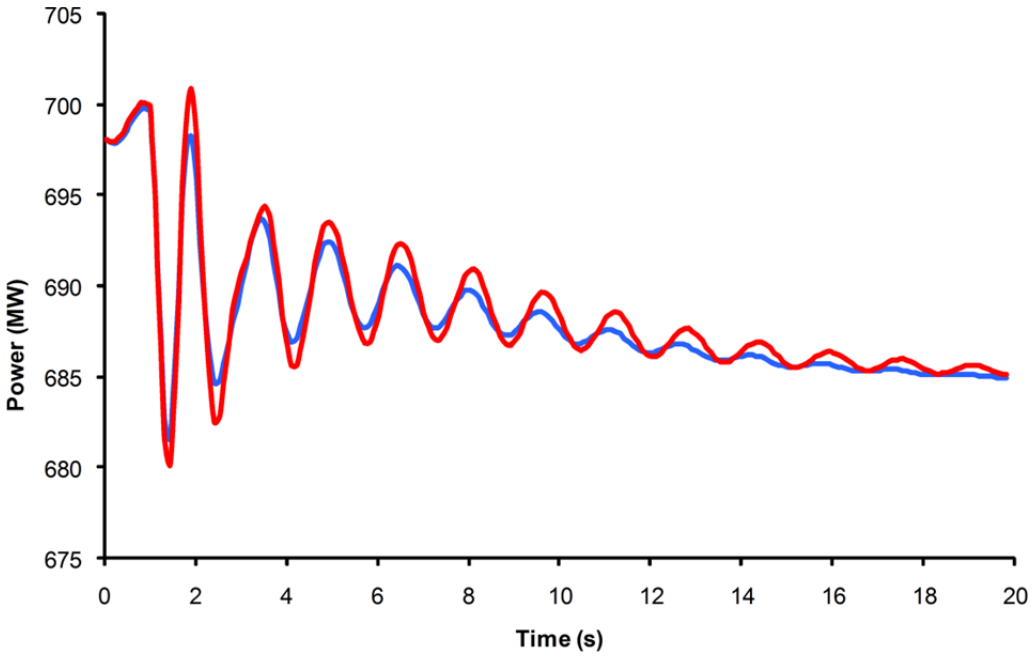

Figure 7-12 Damping performance under constant current with 300 MW power transfer

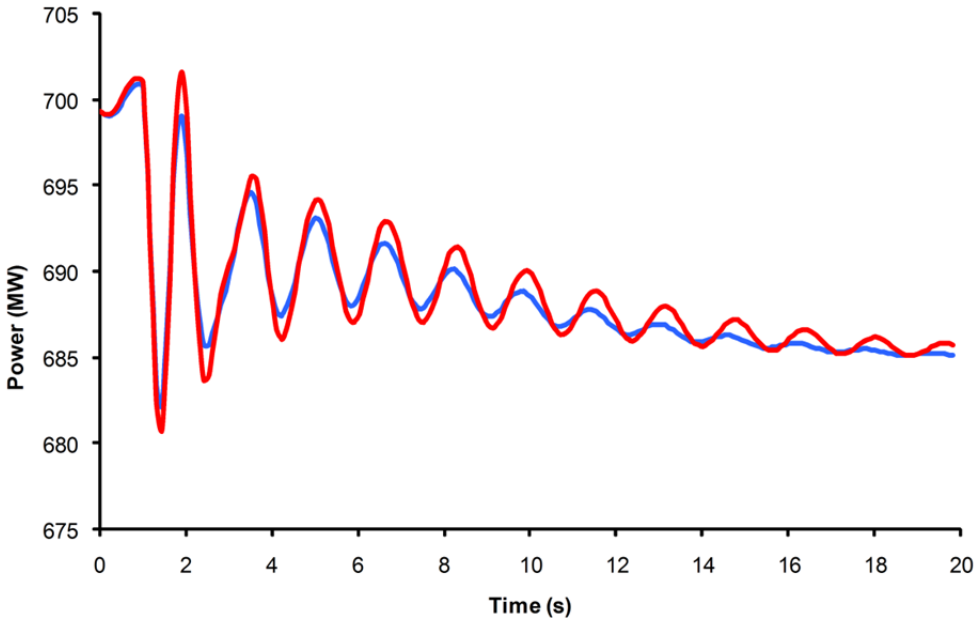

Figure 7-13 Damping performance under constant current with 400 MW power transfer

7.4 *Discussion*

From the observations presented in the previous section, it can be seen that the damping operation of the inter-area and the local oscillations are affected by the load characteristics. Although both types of PSS are dependent on load behaviours, WACS-based PSS, was less sensitive related to, its enhanced network observability. Nevertheless, appropriate load models need to be considered when designing WACS-based PSS, in order to increase the stability of inter-area modes.

Since resolving unstable inter-area oscillation is a global problem, the stress experienced by the power grid, can, have an effect towards its damping efficiency. The results from Table 7-1 to Table 7-3 generally capture the reduction of inter-area damping ratio as the power transfer quantity increased. However, by installing WACS-based PSS into the network, the rate of this decline was reduced. On the contrary, the damping operation of PSS towards local modes was less sensitive to network stress. That may be due to, the local oscillation being nearby, or, within a power plant. As a result, influences of transmission stress experienced by tie-lines, are generally less significant than the behaviour of the generator.

Note that in the actual damping operation, there will be time delays. Firstly, the response delay is dependent on the refresh/update rate of the early warning system, which is primarily based on the data acquisition time. This may range between 10 to 20 seconds depending on the predefined monitoring window for gathering field measurements. Secondly, the communication delay to transmit the remote signal to the intended controller. This is dependent on the geographical location of the collected data and the communication infrastructure. In a worst case scenario, such time delay can be around 0.1 second [113].

7.5 *Remarks*

In this chapter, the effects of the load characteristics on the operation of Wide Area Control System–based, Power System Stabilizer was evaluated. From simulation results, the inter-area damping performed by the WACS-based PSS was observed to be impacted with different load characteristics. From the assessments, it was found that both the conventional and WACS-based PSS performed best under constant

impedance. They were comparatively less effective when dealing with the constant power loads. Despite the decrease in the operational efficiency, towards the different load behaviours, WACS-based PSS performed better when compared with the conventional design. In summary; based on the preliminary findings, the use of WACS-based PSS in a power network can be beneficial to the enhancement of the stability of inter-area oscillations under the constant impedance, the constant power, and the constant current load characteristics.

8 Conclusions and Future Works

8.1 *Conclusions*

The work presented in this dissertation focuses on developing the oscillation monitoring algorithms to meet the needs of the New Zealand power grid and those with similar operational characteristics. In particular, referring to Chapter 1, the motivation is related to tracking multiple ringdown oscillations.

In Chapter 2, the nature of the electromechanical oscillations was defined. Aging grids with lack of infrastructure upgrades are prone to inter-area oscillations because of an increasing network stress to meeting power demands. The oscillations are caused by the remote generators oscillating against each other, and they are difficult to detect. Many time-domain based monitoring methods utilizing data collected from Phasor Measurement Units (PMUs) have been formulated to monitor unstable oscillatory build-ups.

From the existing literature, Kalman Filter and Prony Analysis were identified as attractive candidates for the New Zealand operation. Subsequently, in Chapter 3, detailed evaluations of both techniques were conducted, and the merits of each method have been outlined. In general, Kalman Filter is identified as an algorithm that is capable of monitoring the time-varying behaviour of the dominant oscillatory mode. In contrast, Prony Analysis is credited for its ability to accurately detect multiple modes under unknown parameters. In addition, according to the experimental observations, several enhancements for each technique were proposed and assessed.

In general, the estimation accuracy of Prony Analysis was observed to be dependent on the sampling interval. The sampling interval selected for one scenario may not be suitable for all situations due to constantly changing network operating conditions. Therefore, in Chapter 4, the Enhanced Prony Analysis was formulated. The key aspect was the integration of the proposed sampling scheme to examine the

appropriateness of the selected sampling interval for a particular operating situation. That was achieved by using the condition number evaluation index to assess the adequacy of the constructed data matrix. As a result, the Enhanced Prony Analysis is not limited to operating at a fixed sampling interval. Overall, the Enhanced Prony Analysis is capable of providing more reliable modal estimations than the original version.

The estimation accuracy of Kalman Filter was shown to be dependent on its initialization process. Consequently, inadequate initial settings could produce biased solutions, or, lead to divergence. Kalman Filter was formerly developed to track the dominant mode, and therefore, tracking multiple oscillations can be challenging. Hence, in Chapter 5, an Extended Complex Kalman Filter (ECKF) was proposed to extend the existing role of Kalman Filter to enable the detection of multiple electromechanical oscillations. In addition, the integration of Hankel Singular Value Decomposition technique into ECKF improved the accuracy of the initialization process. The proposed ECKF technique was shown to provide an estimation accuracy at par with Prony Analysis, while retaining Kalman's recursive nature of implementation. Based on this attribute, ECKF is considered to be a more attractive option for the grid operation than, the Enhanced Prony Analysis. Meanwhile, preliminary evaluations using actual synchrophasor measurements collected from the New Zealand network demonstrated the proposed ECKF to be a suitable candidate for the New Zealand grid operation.

In Chapter 6, the potential benefits of utilizing parallel-processing to improve the computing speed were explored. The proposed ECKF and the Enhanced Prony Analysis were selected as candidates for parallelism. ECKF demonstrated the potential of computing parallel decomposed subroutines, while, the Enhanced Prony Analysis showed the possibility of running multiple algorithms simultaneously. Both examples adopted a Multiple-Instruction Multiple-Data (MIMD) architecture. According to the comparative analysis of each algorithm, with its sequential counterpart, the parallelized ECKF and Enhanced Prony Analysis were able to achieve faster computing times.

The effects of the load characteristics, related to the operation of Wide Area Control System (WACS) based Power System Stabilizer, were evaluated in Chapter 7. The inter-area damping performed by WACS-based PSS was observed to be impacted with the different load characteristics. Overall, WACS-based PSS performed best under the constant impedance. It was comparatively less effective when dealing with the constant power loads. Nevertheless, enhanced the damping performance, compared with, the conventional local signal based PSS designs.

8.2 *Publications*

Two journals and thirteen conferences, of which three are invited papers, have been published as a direct result of the work carried out for this thesis. Apart from two of the invited panel papers, all publications are available at the IEEE database. A complete list, based on their published dates, is shown below:

Journals:

1) “Enhancing Kalman Filter for tracking ringdown electromechanical oscillations,” *IEEE Transactions on Power Systems*, in Press. Digital Object Identifier: 10.1109/TPWRS.2011.2169284
2) “Adaptive sampling scheme for monitoring oscillations using Prony Analysis," *IET Generation, Transmission & Distribution,* vol. 3, pp. 1052-1060, 2009.

Invited Panel Papers:

1) "Synchrophasors and supporting infrastructure in New Zealand transmission grid," presented at *IEEE Power and Energy Society General Meeting,* 2011.
2) "Synchrophasors in the New Zealand grid," in *North American SynchroPhasor Initiative Work Group Meeting*, 2010.
3) "Monitoring electromechanical oscillations in New Zealand grid using Phasor measurement units," in *The Asia-Oceania Top University League on Engineering, Postgraduate Student Conference*, 2009.

Conference Proceedings:

1) "Sampling effects in monitoring power system low frequency oscillations using Prony Analysis and Kalman Filter," *Australasian Universities Power Engineering Conference*, 2011.
2) "Exploring parallel processing for wide area measurement data applications," *IEEE Power and Energy Society General Meeting*, 2011.
3) "Phasor measurement network and its applications in the New Zealand grid: overview and experiences," *IEEE Power and Energy Society General Meeting,* 2011.
4) "Parallel computing for smart power oscillation monitoring using Synchrophasor measurements," *IEEE Region 10 Conference,* 2010.
5) "Adaptive power system stabilizer tuning technique for damping inter-area oscillations," *IEEE Power and Energy Society General Meeting*, 2010.
6) "Incorporating instrument transformer measurement errors to voltage stability assessment," *Australasian Universities Power Engineering Conference*, 2010.
7) "Detection of lightly damped inter-area power oscillations using extended complex Kalman Filter," *IEEE Region 10 Conference,* 2009.
8) "Effects of load characteristics on the damping performance of power system stabilizers for inter-area oscillations," *Australasian Universities Power Engineering Conference*, 2009.
9) "Comparative assessment of Kalman Filter and Prony methods for power system oscillation monitoring," *IEEE Power & Energy Society General Meeting*, 2009.
10) "Effects of sampling in monitoring power system oscillations using on-line Prony Analysis," *Australasian Universities Power Engineering Conference*, 2008.

8.3 *Future Work*

This work has comprehensively assessed two oscillation detection techniques for the New Zealand transmission grid. From this work, three research directions have been identified. Some are currently being pursued by PhD students at the Power Systems Research Group, University of Auckland. They are: 1) ambient detection, 2) monitoring implementation and 3) damping control. Details related to each aspect are discussed in the following subsections.

8.3.1 Ambient Detection

Unlike the ringdown behaviour, the ambient oscillations refer to the oscillations generated during the normal operations. They have much smaller magnitudes than their ringdown counterparts and are more difficult to monitor. Nevertheless, based on the results obtained in Chapter 5, the proposed ECKF can be potentially modified to track ambient oscillations. Hence, extending the functionality of ECKF can be explored in the future. Robust RLS and Hilbert-Huang Transform methods are feasible candidates.

8.3.2 Monitoring Implementation

The next step is to explore the possibility of decomposing a monitoring application into several independent subroutines that can be reused for other online purposes. Instead of specific operations, the aim would be to treat the subroutines as *function blocks* for multi-purpose applications. That should lead to a minimization of the computational resources needed and an optimization of the monitoring infrastructure, when more than a single WAMS application is implemented. In addition, implementing state-of-the-art vector processors such as Nvidia's GPU to conduct parallel-processing can be investigated. In general, with the growing availability of multi-core processors in the market, the adoption of parallel-processing can be considered as a trend for the future.

Apart from hardware implementations, evaluating the detection capability using real synchrophasor measurements are also required. Following which, the developed methods can be calibrated to the specific transmission network.

8.3.3 Damping Control

According to the observations made in Chapter 7, establishing a wide area damping control infrastructure is an attractive option for the New Zealand network. The ultimate goal will be to utilize a monitoring system to achieve near, real-time controls. To accomplish that vision, designing a suitable WACS-based PSS, for the New Zealand operation, needs to be explored. The potential benefits of adopting either, a centralized, or, a decentralized control structure should also be researched.

Appendix A. Overview of SCADA System

A.1. *Supervisory Control Data Acquisition Systems*

In the 1960s, Supervisory Control Data Acquisition (SCADA) system was introduced into power systems worldwide. Its role is to provide a quasi, steady-state/static view of the overall grid performance. Any breaches in the operating margins are subsequently addressed through a user-friendly interface to minimize confusions. Subsequently, adequate actions are taken and the operating parameters are updated.

SCADA can be summarized as: a collection of equipments that will assist the operators at a remote location, with sufficient information, to conduct adequate monitoring and control supervision. To be precise, SCADA can be grouped into two categories:

1) Data acquisition
2) Network supervision

A.2. *SCADA Framework*

The main components of SCADA consist of a central host, (the national control centre); the data acquisition and control units (the remote terminal units, RTUs); the communication systems, and a software platform for monitoring and controlling the RTUs. Initially, the positive sequence measurements are collected by the remote terminal units installed at the local substations, or, power plants. The analogue transformer measurements are stored, and digitalized, prior to transmitting to a control centre. Those measurements are obtained, without a common reference time, by sequentially scanning. From them, the states of the power system are estimated. Depending on the intended functions, actions may be taken at a regional control centre.

A global vision of the network situation, is only possible by considering a combination of the measurements taken at different geographical locations. They are processed at the central/national control centre. Implementation results in a hierarchy of the

control centres. There are several supervising levels, from the local RTUs, to, the central host. The chain of command follows a tree topology. The control centres with a higher hierarchical level can supervise similar, or, lower level, control centres. Within each centre, information is passed around different processing units. Analyzes are conducted to monitor the present grid status and include:

- Generation dispatch
- Line/corridor loading
- Transmission capacity
- Equipment settings

Historically, the transient instability caused by, the faults, or, the outages have been the dominant stability problem on most systems. Those potential disruptions, are easily noticeable, and usually exist for only a short time. Tracking the operational dynamics is a crucial application, although, it is of a lesser priority during the initial development of a centralized control centre. The transmission capacity in the 1960s was significantly higher than the daily power demand. Therefore, the grid had a larger tolerance, than at present, for dynamic instabilities. Furthermore, long distant power transfer, in terms of over 500 km, was not common and modern dynamic instabilities like inter-area oscillation were rare. Related to those conditions, monitoring the grid performance, based on the steady-state SCADA supervision, was considered sufficient

As the dependency on computer analysis has grown in the last few decades, more applications have been integrated into SCADA systems. These include:

- Operational Planning
- Automatic generation control
- Power flow control
- Transmission constraints management
- Load management
- Load forecast
- Power quality
- Protective relaying

- System reliability analysis

In order to accommodate the growing applications, continuous modifications have been applied to SCADA.

A.3. *SCADA Limitations*

The aging power grids, in the developed countries are often stressed by their operational scenario. The challenges they face were, never envisioned during the initial SCADA design in the 1960s. Those challenges can be summarized as follows:

1) Growth in power demand outweighs the rate of transmission expansion

   Referring to Ruisheng [186], and Figure A-1, the worldwide daily demand for power has doubled since the 1980s. However, during that same period, major transmission expansions were often difficult to proceed with due to, environmental issues and costly projected investments [9, 47]. Instead, the gird was operated towards its theoretical limits. Relaxing security margins became the primary focus of those operations.

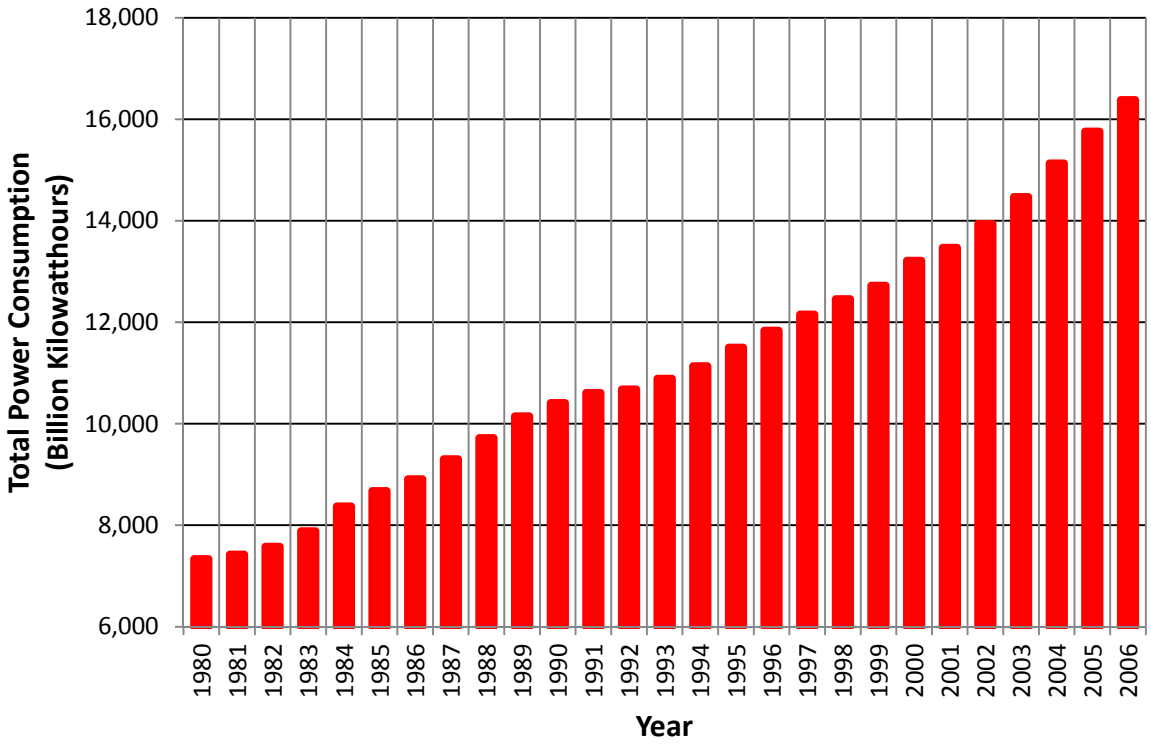

Figure A-1 World's annual power consumption between 1980 to 2006 [186]

2) Unprecedented energy trading across regional power grids

   Since the mid 1990s, the deregulation of energy markets has occurred in many countries. The needs of optimizing the system performance, and minimizing capital investments have became more crucial. Those trends have created power flow scenarios and uncertainties that the existing system was never designed to handle [187, 188].

3) Conservative operational limitations based on worst case scenario

   Restriction to the power flows, and the voltages on the transmissions systems are usually assigned based on: the transmission line thermal limits, offline studies of the voltage, and the transient dynamic stability. Hence, the power flow limits of each transmission line is conservatively determined offline because the operational conditions need to be considered [189]. Dynamic or online modifications of those parameters are not possible.

Due to these challenges, previously unaccounted stability issues have emerged in the past two decades. They are threatening the reliability of the grid operation [190]. Traditionally, only instabilities caused by large disturbances or contingencies were dealt with. However, now, daily events such as; switching of the capacitor banks, or, altering power transfers are enough to generate severe problems to the grid if they are not promptly attended to. Those problems are classified as the small-signal instability. They have become a major concern in modern network supervision [1].

Consequently, new limitations in SCADA systems are being noted. These can be classified into two aspects, namely:

- Lack of dynamic visibility
- Increase in SCADA complexity

The first concern is related to the data acquisition; and the second, to the supervision architecture. In this dissertation, the primary focus is towards the first concern. Therefore, potential monitoring resolutions have been explored.

A.4. *Lack of Dynamic Visibility*

In order to provide adequate security, fast power system dynamics need to be monitored. Although modifying the SCADA system is possible, it is very difficult and challenging compared to any previous upgrades. The fundamental assumption of SCADA, is, that the network is operating under a quasi steady-state. Hence, the static supervision is difficult to track dynamic activity. Also, the small-signal dynamic instabilities, may easily be mistaken as the steady-state, and thus neglected.

RTUs are not synchronized, and the phase angle at the network buses are estimated instead of being measured. Furthermore, aligning those measured data from RTUs into a timely order is difficult and challenging. Consequently, creating a snapshot of the present system state, by building a complete network tree, is a time consuming task. Thus, any early warnings are difficult to be achieved. Therefore, major modifications in the conventional SCADA data acquisition infrastructure are needed. However, such action is equivalent to building a new monitoring architecture.

A.5. *Continuous Build-up in Operational Complexity*

The complexity of present SCADA systems, in terms of: the supervising layers, and the established interconnections between the control centres, have reduced the operating transparency. As more protocols and applications are added, the communication traffic amongst RTUs and control centres is significantly increased. SCADA is unable to provide fast monitoring speeds related to: a hierarchical management style, an increased computation sophistication caused by supervising complexity, and accumulated delays in-between the information transfer. Therefore, it can be foreseen that accommodating the dynamic supervision into SCADA would further amplify the complexity and delay issues.

Currently, the study of the transient and dynamic responses to a large number of potential system disturbances/contingencies in a transient timeframe (about 10 seconds after a disturbance/outage), is computed offline [32, 189]. Since all possible conditions need to be carefully evaluated, a large set of differential algebraic equations needs to be solved, as well as, forming a large admittance matrix to

calculate the stability margins [116]. As a result, the required calculation time usually ranges in the hours for a typically large grid network.

Additionally, the replacement of existing RTUs in a transmission network does not seem to be a realistic expectation for the transmission operators [9]. Therefore, an alternative infrastructure is desired to facilitate the necessary dynamic monitoring applications.

Appendix B. WAMS Experience in New Zealand

B.1. *Limitations in Existing Communication Bandwidths*

Along with an aging transmission network, the present communication infrastructure was also built in the 1960s. Its backbone channel was mainly based on radio links. However, the data bandwidth is now very limited for implementing any modern monitoring strategies [46]. To resolve that issue, existing equipment will be replaced with a higher capacity, and highly resilient network that meets the current and the future needs of the New Zealand grid. Additionally, the modified telecommunication framework will introduce modern IP-based technologies. The total, estimated cost is NZD $269 million. The expected completion date is 2013 [191]. An outline of the new communication infrastructure is shown in Figure B-1. Referring to the diagram, the black lines represent fibre-optic cables, and the yellow represent the radio links. Three regional communication centres will be established: in Hamilton, Wellington and Christchurch. The new telecommunication framework will provide connectivity at Transpower's substations, offices, warehouses and other sites, as required, throughout the country. That will help to pave the way for future WAMS implementations.

B.2. *Installation Procedures*

The selection process for PMU installation sites is based on:

- Regions that are more likely to be vulnerable to the oscillatory instability
- Strategic locations with high observability of the operating dynamics

In terms of the physical installation within the substation, PMU sites are chosen based on the following criteria:

- Access to the instrument transformers for extracting the line voltage and current measurements
- Access to the existing Ethernet communication links

Figure B-1 Outline of the proposed telecommunication network [191]

However, due to the limited broadband availability, and the necessary information management systems, not many nodes in New Zealand are currently installed with PMUs. Furthermore, instead of placing dedicated PMUs for network monitoring, Transpower utilizes the Phasor modules inside the newly upgraded SEL-421 and 451 protection relays as PMUs [55]. That is considered to be a more economical approach, and is part of the protection upgrade project.

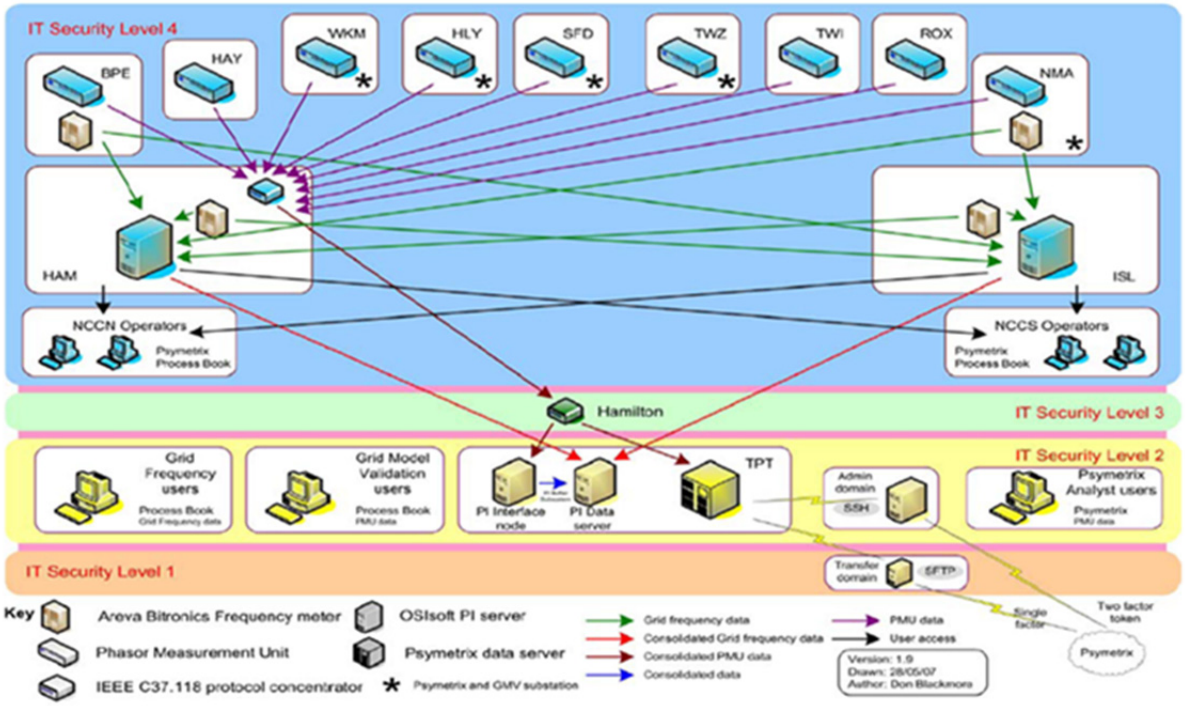

Figure B-2 Outline of the established security level for the New Zealand WAMS network

Apart from installing PMUs across the power grid, Phasor Data Concentrators (PDCs) have also been installed to process the regional Phasor measurements before sending them to the system operators. Currently, Hamilton, located in North Island, and Islington, located in South Island, are the chosen PDC sites. A multi-layered security clearance infrastructure: to provide better security, and prevent any crucial data from leaking to unauthorized parties, has been adopted and shown in Figure B-2 [47]. Each site contains two PDCs with a firewall setup between them. That acts as a buffer and prevents anyone from tempering with the actual PMU's settings or data. Depending on the need, and the position of the users, different IT security levels are issued. This architecture is not the final design because continuous modifications will be carried out to fine-tune the newly established WAMS architecture.

B.3. *Encountered Installation and Testing Issues*

Although installing PMUs at a substation may be considered trivial, several issues were raised during the installations in 2008. They can be summarized into two categories: 1) hardware limitation and 2) Human error. The first: refers to the old telecommunication network used by Transpower, which was built mostly in the 1960s. Consequently, the restricted bandwidth and the limited access to maintenance parts made the task of implementing any real-time Phasor applications challenging. In order to resolve that concern, Transpower has begun upgrading its telecommunication infrastructure with an estimated investment of $NZD 269 millions. The goal is to connect 197 sites with fibre-optic broadband by June 2013. Presently, 31 substations are completed with another 38 in progress [191].

Related to human error, the major challenge was an understanding of the technology. A lack of knowledge has caused minor errors, such as, an incorrect assignment of IP addresses by contractors. Since the PMU is part of the SEL protection relay, assuming that PMU and the actual relay share same IP address, has caused data corruption during the early testing phase of the project. Furthermore, differing standards created synchronization errors between the GPS clock and the data servers. That caused a time offset of 13 hours, and subsequently, most of the recorded Phasor data were discarded by accident.

Although PMUs are now operational, unusual synchronizing errors are still being debugged at Transpower. A recent one occurred in early April 2010, where PMU installed at North Makarewa substation crashed when switching back from daylight saving. The cause may have been due to the internal averaging of ADC in PMU. That could fail when the expected time interval was suddenly pushed back by an hour. Consequently, ADC averaging would have a denominator of zero or negative value and thus, make PMU crash. An appropriate solution would be to adopt a fixed global time instead of, regional time, but the cost would be that of upgrading the existing data acquisition system. The final resolution is not yet decided upon, and the projected maintenance cost could be high due the remote location of that site.

Since PMUs are modules installed inside the line-protection relays, the system operators lose the phasor data when there are line outages. As a result, the purpose

of providing a higher network visibility is not achieved in all cases. Nevertheless, such problems will be fixed as more protection relays are replaced in the future.

B.4. *Overview of Present Synchrophasor Applications*

Since PMUs are being installed into the New Zealand grid for the very first time, the number of initial Wide Area Monitoring System applications are limited. Presently, WAMS are implemented and tested on a central computer. The primary focus is to investigate and identify possible PMU advantages for the NZ grid operation. Therefore, only mature and passive WAMS applications that have been tested to date, are considered for the New Zealand system. Referring to the international developments described by CIGRE working group in [9], two areas were selected: network planning, and operation. The first application focuses on model validation, and the second, on oscillation monitoring. However, results from oscillation monitoring are not directly used in the decision making of the daily operation at present. Instead, they currently act as a validation tool for assessing SCADA performance.

B.5. *Integration of Phasor Information into Network Planning*

Acknowledging the international success in the PMU deployment, one of the initial WAMS applications for the New Zealand grid is the model authentication. The network, in terms of the load flow models, contains more than 400 buses and 800 branches. In addition, the security and economic dispatch model has over 20,000 variables and 12,000 constraints to be validated [5]. In that context, the phasor data are mainly used to: cross-check the dynamic behaviour, the accuracy of the power flow patterns, the load models, the power electronic dynamics, and the transient generator models. One recent example, is the use of phasor measurements to verify the newly installed SVC at the Islington substation in early 2010 [46]. Exhaustive studies were conducted based on data collected by nearby PMUs. Transpower engineers were then able to verify the true dynamic characteristics of the installed SVC. That helped to minimize the testing period and thus, helped to reduce the investment costs.

Furthermore, the adoption of PMU allows a better coordination of the existing assets. That increases the possibility to defer, or, minimize, the future capital investments. Such benefits are crucial for New Zealand as, smart utilization of the existing infrastructure can compensate for a lack of system security related to the relaxation of power transfer margins. Initial benefits identified by Transpower include:

- Enhanced confidence toward the simulated results, allowing a more accurate determination of: the project timing, the control requirements, and the operational regions.
- The ageing equipments with deteriorating performances can be identified more swiftly by monitoring the dynamic performance of their control actions.
- Reductions in the testing, and the commissioning costs, by introducing non-invasive evaluation of the infrastructure performances [43].

Appendix C. Two-Area Network Parameters

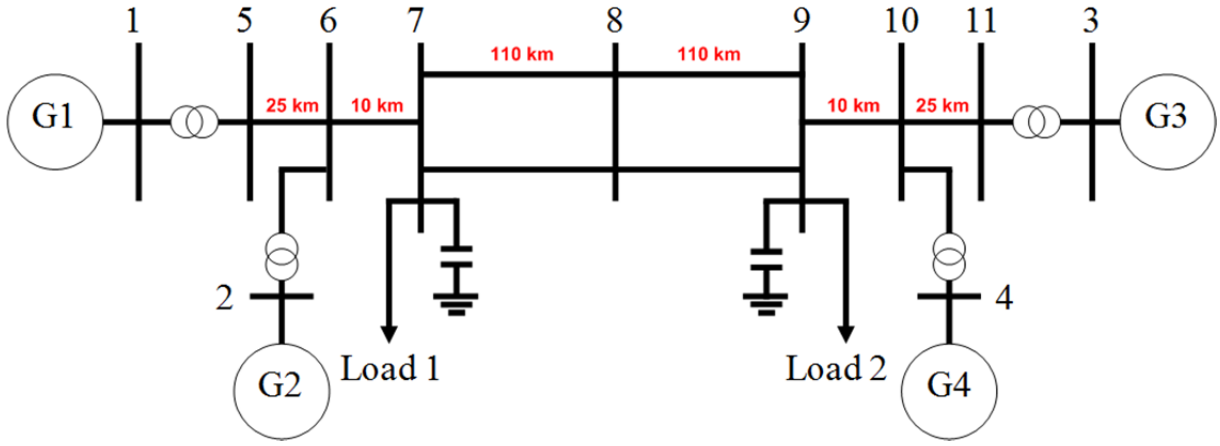

Figure C-1 Overview of Kundur's two-area network [1]

The system is based on Kundur's design from [1]. It consists of two regions that are connected by weak tie-lines as shown in Figure C-1. In each area, are two generating units, each having a rating of 900 MVA and 20 kV. Note that Generator 3, (G3), is set as the reference bus. The generator parameters, are in per unit:

$X_d = 1.8$	$X_q = 1.7$	$X_l = 0.2$	$X_d^{'} = 0.3$	$X_q^{'} = 0.55$
$X_d^{''} = 0.25$	$X_q^{''} = 0.25$	$R_a = 0.0025$	$T_{d0}^{'} = 8.0s$	$T_{q0}^{'} = 0.4s$
$T_{d0}^{''} = 0.03s$	$T_{q0}^{''} = 0.05s$	$S(1.0) = 0.16$	$S(1.2) = 0.57$	$K_D = 0$
$H_{G1,G2} = 6.5$	$H_{G3,G4} = 6.175$			

Every generator is connected to a step-up transformer with an impedance of 0+j0.15 per unit on 900 MVA and 20/230 kV base. In addition, the generators are also equipped with an *IEEEG1* governor with the following parameters:

$K = 15$	$T_1 = 0.01s$	$T_2 = 0s$	$T_3 = 0.025s$	$T_4 = 0s$
$T_5 = 0.2s$	$T_6 = 6s$	$T_7 = 0.4s$	$U_C = -1.139$	$U_O = 0.114$
$K_1 = 0$	$K_2 = 0$	$K_3 = 0.3$	$K_4 = 0$	$K_5 = 0.3$
$K_6 = 0$	$K_7 = 0.4$	$K_8 = 0$	$P_{MAX} = 0.95$	$P_{MIN} = 0$

The static exciter connected to each generator is a standard *EXAC4* model and consists of these settings:

$$T_R = 0.01s \quad T_A = 0 \quad T_B = 0s \quad T_C = 0s$$
$$K_A = 200 \quad K_C = 0 \quad V_{IMAX} = 999 \quad V_{IMIN} = -999$$

Lastly, the lines parameters are defined as:

$$r = 0.0001\ pu/km \quad x_L = 0.001\ pu/km \quad b_C = 0.00175\ pu/km$$

The load is modelled as a static load and the shunt capacitances of 200 MVar and 350 MVar. They are equipped at *Bus7* and *Bus9* respectively. Their magnitudes are set as:

- Load 1 = 967 MW and 100 MVar
- Load 2 = 1767 MW and 100 MVar

References

[1] P. Kundur*, et al.*, *Power System Stability and Control*: McGraw-Hill, 1994.

[2] J. Luque*, et al.*, "Analytic model of the measurement errors caused by communications delay," *IEEE Transactions on Power Delivery,* vol. 17, pp. 334-337, 2002.

[3] "Annual report 2008/9 to the House of Representatives," Electricity Commission, Ministry of Energy, New Zealand , 2009.

[4] "Annual report 2008/9," Transpower New Zealand Limited, 2009.

[5] K. Devine, "The New Zealand power system in balance," in *Otago University Physics Departmental Seminar*, Dunedin, New Zealand, 2009.

[6] "New Zealand Energy Strategy to 2050: Powering Our Future," Ministry of Economic Development, New Zealand, 2007.

[7] Census. (20 March, 2011). *2006 Quick Stats*. Available: http://www.stats.govt.nz/census/2006censushomepage/quickstats/quickstats-about-a-subject/housing.aspx

[8] "Briefing to the incoming government September 2008: key issues and challenges," Transpower New Zealand Limited, 2008.

[9] P. Pourbeik and C. Rehtanz, "Wide area monitoring and control for transmission capability enhancement " CIGRE Working Group, January 2007.

[10] D. Novosel*, et al.*, "Dawn of the Grid Synchronization," *IEEE Power and Energy Magazine,* vol. 6, pp. 49-60, 2008.

[11] K. E. Holbert*, et al.*, "Use of satellite technologies for power system measurements, command, and control," *Proceedings of the IEEE,* vol. 93, pp. 947-955, 2005.

[12] C. W. Taylor*, et al.*, "WACS-wide-area stability and voltage control system: R&D and online demonstration," *Proceedings of the IEEE,* vol. 93, pp. 892-906, 2005.

[13] A. G. Phadke and J. S. Thorp, "History and applications of phasor measurements," in *IEEE PES Power Systems Conference and Exposition*, Atlanta, USA, 2006.

[14] K. E. Martin*, et al.*, "IEEE standard for synchrophasors for power systems," *IEEE Transactions on Power Delivery,* vol. 13, pp. 73-77, 1998.

[15] K. Martin*, et al.*, "Phasor measurements in the WECC," in *North American Synchrophasor Initiative Meeting*, Scottsdale, USA, 2009.

[16] IEEE, "IEEE standard for synchrophasors for power systems," in *IEEE Std C37.118-2005 (Revision of IEEE Std 1344-1995)*, ed, 2006.

[17] S. Horowitz*, et al.*, "The Future of Power Transmission," *IEEE Power and Energy Magazine,* vol. 8, pp. 34-40, 2010.

[18] K. Martin and J. Carroll, "Phasing in the Technology," *IEEE Power and Energy Magazine,* vol. 6, pp. 24-33, 2008.

[19] G. Ledwich*, et al.*, "Phasor measurement units for system diagnosis and load identification in Australia," in *IEEE Power Engineering Society General Meeting*, Pittsburgh, USA, 2008.

[20] R. Agha Zadeh*, et al.*, "Analysis of phasor measurement method in tracking the power frequency of distorted signals," *IET Generation, Transmission & Distribution,* vol. 4, pp. 759-769 2010.
[21] D. Karlsson, "Synchrophasor activities in CIGRE countries," in *North American Synchrophasor Initiative Meeting*, Vancouver, Canada, 2010.
[22] G. Ledwich, "PMU in use in Australia," in *North American Synchrophasor Initiative Meeting*, Vancouver, Canada, 2010.
[23] A. G. Phadke and R. M. de Moraes, "The Wide World of Wide-Area Measurement," *IEEE Power and Energy Magazine,* vol. 6, pp. 52-65, 2008.
[24] I. C. Decker*, et al.*, "Performance of a synchronized phasor measurements system in the Brazilian power system," in *IEEE Power and Energy Society General Meeting*, Montreal, Canada, 2006.
[25] I. C. Decker*, et al.*, "System wide model validation of the Brazilian interconnected power system," in *IEEE Power and Energy Society General Meeting*, Minneapolis, USA, 2010.
[26] I. Kamwa*, et al.*, "Wide-area monitoring and control at Hydro-Quebec: past, present and future," in *IEEE Power Engineering Society General Meeting*, Montreal, Canada, 2006.
[27] T. Bi, "WAMS implementation in China," in *North American Synchrophasor Initiative Meeting*, Vancouver, Canada, 2010.
[28] J. Wu, "New implementations of wide area monitoring system in power grid of China," in *IEEE/PES Transmission and Distribution Conference and Exhibition: Asia and Pacific*, Dalian, China, 2005.
[29] X. Xie*, et al.*, "WAMS Applications in Chinese Power Systems," *IEEE Power and Energy Magazine,* vol. 4, pp. 54-63, 2006.
[30] Y. Xue, "Some viewpoints and experiences on wide area measurement systems and wide area control systems," in *IEEE Power and Energy Society General Meeting* Pittsburgh, USA, 2008.
[31] O. Hernández, "Using PMUs to manage governor stability issues within the Colombian power system," in *North American Synchrophasor Initiative Meeting*, Vancouver, Canada, 2010.
[32] D. H. Wilson*, et al.*, "Control centre applications of integrated WAMS-based dynamics monitoring and Energy Management Systems," in *CIGRE Session*, Paris, France, 2008.
[33] C. Candia*, et al.*, "PMU location and parameter identification techniques for the Italian wide-area measurement system," in *International World Energy System Conference*, Torino, Italy, 2006.
[34] K. Saarinen, "Applications of phasor measurement units and wide-area measurement systems in Finland," in *North American Synchrophasor Initiative Meeting*, Vancouver, Canada, 2010.
[35] S. K. Soonee*, et al.*, "Application of phase angle measurement for real time security monitoring of Indian electric power system - an experience," in *CIGRE Session*, Paris, France, 2008.
[36] N. S. Sodha, "Smart grid initiatives in EHV transission in Indian power sector," in *North American Synchrophasor Initiative Meeting*, Vancouver, Canada, 2010.

[37] M. Hojo*, et al.*, "Observation of frequency oscillation in western Japan 60 Hz power system based on multiple synchronized phasor measurements," in *IEEE Power Tech Conference Proceedings*, Bologna, Italy, 2003.
[38] N. Kakimoto*, et al.*, "Monitoring of interarea oscillation mode by synchronized phasor measurement," *IEEE Transactions on Power Systems,* vol. 21, pp. 260-268, 2006.
[39] T. Hashiguchi*, et al.*, "Power system dynamic performance measured by phasor measurement unit," in *IEEE Power Tech Conference Proceedings*, Lausanne, Switzerland, 2007.
[40] S. T. Kim*, et al.*, "Development of K-WAMS for monitoring Korean power grid security, and applications to the future IT infrastructure," in *CIGRE Session*, Paris, France, 2008.
[41] E. Martinez, "Mexico's wide area measurement systems," in *North American Synchrophasor Initiative Meeting*, Vancouver, Canada, 2010.
[42] E. M. Martinez, "Wide area measurement & control system in Mexico," in *Third International Conference on Electric Utility Deregulation and Restructuring and Power Technologies*, Nanjing, China, 2008.
[43] P. Griffiths and R. Sherry, "Applications of synchronous phasor measurements systems in the New Zealand grid," in *Electricity Engineers' Association Conference*, Christchurch, New Zealand, 2008.
[44] J. C.-H. Peng and N. K. C. Nair, "Monitoring electromechanical oscillations in New Zealand grid using phasor measurement units," in *The Asia-Oceania Top University League on Engineering, Postgraduate Student Conference*, Tapei, Taiwan, 2009.
[45] N. K. C. Nair*, et al.*, "Syncrhophasors in the New Zealand grid," in *North American SynchroPhasor Initiative Meeting*, Vancouver, Canada, 2010.
[46] J. C.-H. Peng*, et al.*, "Phasor measurement network and its applications in the New Zealand grid: overview and experiences," in *IEEE Power and Energy Society General Meeting*, Detroit, USA, 2011.
[47] N. K. C. Nair*, et al.*, "Synchrophasors and supporting infrastructure in New Zealand transmission grid," in *IEEE Power and Energy Society General Meeting*, Detroit, USA, 2011.
[48] J. F. Hauer*, et al.*, "Integrated monitor facilities for the western power system: WAMS analysis " *The Electrical Power Engineering Handbook,* December 2005.
[49] D. Hawkins, "Synchrophasor update success story," in *North American Synchrophasor Initiative Meeting*, Bellevue, USA, 2008.
[50] D. Carty and M. Atanacio, "PMUs and their potential impact on real-time control center operations," in *IEEE Power and Energy Society General Meeting*, Minneapolis, USA, 2010.
[51] B. Bhargava*, et al.*, "Phase angle based lining study Eastern Interconnections," in *North American Synchrophasor Initiative Meeting*, Vancouver, Canada, 2010.
[52] M. Bianco and V. Madani, "Western Electricity Coordinating Council western interconnection synchrophasor program (WISP)," in *North American Synchrophasor Initiative Meeting*, Vancouver, Canada, 2010.
[53] V. Madani, "PG&E ARRA synchrophasor project: project update," in *North American Synchrophasor Initiative Meeting*, Vancouver, Canada, 2010.

[54] K. Tomsovic*, et al.*, "Designing the next generation of real-time control, communication, and computations for large power systems," *Proceedings of the IEEE,* vol. 93, pp. 965-979, 2005.
[55] "Transmission 2040 (grid development strategy): work package 6 – grid communications, control and protection technology," Transpower New Zealand Limited, 2008.
[56] "A guide for PMU installation, commissioning and maintenance. part II: PMU installation procedures," North American Synchrophasor Initiative, 2007.
[57] Z. Huang, "Performance evaluation of phasor measurement systems," in *IEEE Power and Energy Society General Meeting*, Montreal, Canada, 2006.
[58] M. Larsson*, et al.*, "Monitoring and operation of transmission corridors," in *IEEE Power Tech Conference Proceedings*, Bologna, Italy, 2003.
[59] B. Bhargava and J. Minnicucci, "Synchornized phasor measurement system at Southern California Edison Co.," in *EIPP Meeting*, 2006.
[60] M. Larsson and C. Rehtanz, "Predictive frequency stability control based on wide-area phasor measurements," in *IEEE Power Engineering Society Summer Meeting*, Chicago, USA, 2002.
[61] M. Weibel*, et al.*, "Overhead line temperature monitoring pilot project," in *CIGRE Session*, Paris, France, 2006.
[62] D. Cirio*, et al.*, "Wide area monitoring and control system: the Italian research and development," in *CIGRE Session*, Paris, France, 2006.
[63] T. Ohno*, et al.*, "Islanding protection system based on synchronized phasor measurements and its operational experiences," in *IEEE Power and Energy Society General Meeting*, Pittsburgh, USA, 2008.
[64] F. Galvan*, et al.* (2008) The Role of Phasor Data in Emergency Operations. *Transmission & Distribution World*. Available: http://tdworld.com/overhead_transmission/role_phasor_data_emergency_operations_1208/
[65] V. Venkatasubramanian and R. Carroll, "Oscillation monitoring system at TVA," in *North American Synchrophasor Initiative Meeting*, New Orleans, USA, 2008.
[66] A. B. Leirbukt*, et al.*, "Wide area monitoring experiences in Norway," in *IEEE PES Power Systems Conference and Exposition*, Atlanta, USA, 2006.
[67] J. Lehner*, et al.*, "Monitoring of inter-area oscillations within the european interconnected network based on a wide area measuring system," in *IEEE Transmission and Distribution Conference and Exposition*, New Orleans, USA, 2010.
[68] I. Kamwa, "Wide-area monitoring and control at Hydro Quebec," in *North America Synchrophasor Initiative Meeting*, 2006.
[69] S. Corsi and G. N. Taranto, "A real-time voltage instability identification algorithm based on local phasor measurements," *IEEE Transactions on Power Systems,* vol. 23, pp. 1271-1279, 2008.
[70] D. J. Trudnowski*, et al.*, "WECC dynamic probing tests: purpose and results," in *North American Synchrophasor Initiative Meeting*, Charlotte, USA, 2008.
[71] BPA, "BPA power system stability controls," in *North American Synchrophasor Initiative Meeting*, Charlotte, USA, 2008.
[72] H. Huang*, et al.*, "Model parameter calibration using recorded dynamics," in *North American Synchrophasor Initiative Meeting*, Charlotte, USA, 2008.

[73] D. Novosel and J. Cole, "Phasor measurement application study," California Institute for Energy and Environment 2006.
[74] C. B. Denegri*, et al.*, "Perturbation identification via voltage phasor monitoring in transmission systems," in *IEEE Power Tech Conference Proceedings*, Bologna, Italy, 2003.
[75] W. Sattinger, "Wide area monitoring in the middle of the central European system: four years of practical experience," in *North American Synchrophasor Initiative Meeting*, Montreal, Canada, 2007.
[76] Y. Liu*, et al.*, "On-line event location determination and reporting using distribution level synchro-phasor measurement," in *North American Synchrophasor Initiative Meeting*, New Orleans, USA, 2007.
[77] N. Voraphonpiput and C. Chaonirattisai, "Application of wide area monitoring system in Thailand transmission system " in *Asian Power and Energy Systems Conference*, Phuket, Thailand, 2007.
[78] I. Kamwa and C. Cyr, "WACS design at Hydro Quebec " in *IEEE Power and Energy Society General Meeting - Tutorial Workshop*, Minneapolis, Canada, 2010.
[79] R. Avila-Rosales*, et al.*, "Impact of PMU technology in state estimation," in *CIGRE Session*, Paris, France, 2008.
[80] B. Xu and A. Abur, "Observability analysis and measurement placement for systems with PMUs," in *IEEE PES Power Systems Conference and Exposition*, New York, USA, 2004.
[81] Z. Liang and A. Abur, "Multi area state estimation using synchronized phasor measurements," *IEEE Transactions on Power Systems,* vol. 20, pp. 611-617, 2005.
[82] A. G. Phadke*, et al.*, "Recent developments in state estimation with phasor measurements," in *IEEE PES Power Systems Conference and Exposition*, Seattle, USA, 2009.
[83] R. Emami and A. Abur, "Robust measurement design by placing synchronized phasor measurements on network branches," *IEEE Transactions on Power Systems,* vol. 25, pp. 38-43, 2010.
[84] I. Kamwa*, et al.*, "Robust design and coordination of multiple damping controllers using nonlinear constrained optimization," *IEEE Transactions on Power Systems,* vol. 15, pp. 1084-1092, 2000.
[85] A. Messina, *Inter-area Oscillations in Power Systems: A Nonlinear and Nonstationary Perspective*: Springer, 2009.
[86] N. R. Chaudhuri*, et al.*, "Wide-area power oscillation damping control in Nordic equivalent system," *IET Generation, Transmission & Distribution,* vol. 4, pp. 1139-1150, 2010.
[87] B. Marinescu and J. M. Coulondre, "A coordinated phase shifting control and remuneration method for a zonal congestion management scheme," in *IEEE PES Power Systems Conference and Exposition*, New York, USA, 2004.
[88] X. Zhang*, et al.*, *Flexible AC Transmission Systems: Modelling and Control*: Springer, 2006.
[89] D. Andersson*, et al.*, "Intelligent load shedding to counteract power system instability," in *IEEE/PES Transmission and Distribution Conference and Exposition: Latin America*, San Paulo, Brazil 2004.

[90] B. Yinger*, et al.*, "Load modeling and control," in *Transmission Research Colloquium*, Sacramento, USA, 2008.
[91] S. Corsi, "Wide area voltage protection," *IET Generation, Transmission & Distribution,* vol. 4, pp. 1164-1179, 2010.
[92] A. Johnson*, et al.*, "Static VAR controlled compensation via synchrophasors," Schweitzer Engineering Laboratories, 2009.
[93] M. Glavic and T. Van Cutsem, "Wide-area detection of voltage instability from synchronized phasor measurements. part I: principle," *IEEE Transactions on Power Systems,* vol. 24, pp. 1408-1416, 2009.
[94] M. Glavic and T. Van Cutsem, "Wide-area detection of voltage instability from synchronized phasor measurements. part II: simulation results," *IEEE Transactions on Power Systems,* vol. 24, pp. 1417-1425, 2009.
[95] D. Q. Zhou*, et al.*, "Online monitoring of voltage stability margin using an artificial neural network," *IEEE Transactions on Power Systems,* vol. 25, pp. 1566-1574, 2010.
[96] J. C.-H. Peng and N. K. C. Nair, "Comparative assessment of Kalman Filter and Prony methods for power system oscillation monitoring," in *IEEE Power and Energy Society General Meeting*, Calgary, Canada, 2009.
[97] Q. Ao*, et al.*, "Sampling effects in monitoring power system low frequency oscillations using Prony Analysis and Kalman Filter," in *Australasian Universities Power Engineering Conference*, Brisbane, Australia, 2011.
[98] R. W. Kulp, "An optimum sampling procedure for use with the Prony method," *IEEE Transactions on Electromagnetic Compatibility,* vol. EMC-23, pp. 67-71, 1981.
[99] J. C.-H. Peng and N. K. C. Nair, "Effects of sampling in monitoring power system oscillations using on-line Prony analysis," in *Australasian Universities Power Engineering Conference*, Sydney, Australia, 2008.
[100] J. C.-H. Peng and N. K. C. Nair, "Adaptive sampling scheme for monitoring oscillations using Prony analysis," *IET Generation, Transmission & Distribution,* vol. 3, pp. 1052-1060, 2009.
[101] J. C.-H. Peng*, et al.*, "Detection of lightly damped inter-area power oscillations using extended complex Kalman filter," in *IEEE Region 10 Conference*, Singapore, 2009.
[102] J. C.-H. Peng*, et al.*, "Parallel computing for smart power oscillation monitoring using synchrophasor meausrements," in *IEEE Region 10 Conference*, Fukuoka, Japan, 2010.
[103] J. C.-H. Peng*, et al.*, "Exploring the potential of parallel processing for smart grid montioring applications," in *IEEE Power and Energy Society General Meeting*, Detroit, USA, 2011.
[104] M. Klein*, et al.*, "A fundamental study of inter-area oscillations in power systems," *IEEE Transactions on Power Systems,* vol. 6, pp. 914-921, 1991.
[105] J. H. Chow*, et al.*, "Power system damping controller design-using multiple input signals," *IEEE Control Systems Magazine,* vol. 20, pp. 82-90, 2000.
[106] J. C.-H. Peng and N. K. C. Nair, "Effects of load characteristics on the damping performance of power system stabilizers for inter-area oscillations," in *Australasian Universities Power Engineering Conference*, Adelaide, Australia, 2009.

[107] J. C.-H. Peng*, et al.*, "Adaptive Power System Stabilizer tuning technique for damping inter-area oscillations," in *IEEE Power and Energy Society General Meeting*, Minneapolis, USA, 2010.
[108] G. Rogers, *Power System Oscillations*: Kluwer Academic, 2000.
[109] B. Pal and B. Chaudhuri, *Robust Control in Power Systems*: Springer, 2005.
[110] H. Wu, "Robust Control Design Considering Time Delay for Wide Area Power Systems," PhD thesis, Arizona State University, Phoenix, USA, 2004.
[111] J. Quintero, "A Real-Time Wide-Area Control for Mitigating Small-Signal Instability in Large Electric Power Systems," PhD thesis, Washington State University, Seattle, USA, 2005.
[112] D. P. Sengupta and I. Sen, "A tensor approach to understand dynamic instability in a power system and design a stabilizer," in *IEEE Region 10 Conference*, Bombay, India, 1989.
[113] Y. Zhang, "Design of Wide-Area Damping Control Systems for Power System Low-Frequency Inter-Area Oscillations," PhD thesis, Washington State University, Seattle, USA, 2007.
[114] C.-L. Chang*, et al.*, "Experience with power system stabilizers in a longitudinal power system," *IEEE Transactions on Power Systems,* vol. 10, pp. 539-545, 1995.
[115] G. Liu, "Oscillation Monitoring System Based on Wide Area Phasor Measurements in Power Systems," PhD thesis, Washington State University, Seattle, USA, 2010.
[116] J. Grainger and W. Stevenson, *Power System Analysis*: McGraw-Hill, 1994.
[117] A. R. Bergen and V. Vittal, *Power Systems Analysis*: Prentice Hall, 2000.
[118] D. I. Trudnowski, "Order reduction of large-scale linear oscillatory system models," *IEEE Transactions on Power Systems,* vol. 9, pp. 451-458, 1994.
[119] J. W. Pierre*, et al.*, "Initial results in electromechanical mode identification from ambient data," *IEEE Transactions on Power Systems,* vol. 12, pp. 1245-1251, 1997.
[120] R. W. Wies*, et al.*, "Use of ARMA block processing for estimating stationary low-frequency electromechanical modes of power systems," *IEEE Transactions on Power Systems,* vol. 18, pp. 167-173, 2003.
[121] J. F. Hauer*, et al.*, "Initial results in Prony analysis of power system response signals," *IEEE Transactions on Power Systems,* vol. 5, pp. 80-89, 1990.
[122] D. J. Trudnowski*, et al.*, "Making Prony analysis more accurate using multiple signals," *IEEE Transactions on Power Systems,* vol. 14, pp. 226-231, 1999.
[123] T. J. Browne*, et al.*, "A comparative assessment of two techniques for modal identification from power system measurements," *IEEE Transactions on Power Systems,* vol. 23, pp. 1408-1415, 2008.
[124] J.-Z. Yang*, et al.*, "A hybrid method for the estimation of power aystem low-frequency oscillation parameters," *IEEE Transactions on Power Systems,* vol. 22, pp. 2115-2123, 2007.
[125] D. J. Trudnowski*, et al.*, "Performance of three mode-meter block-processing algorithms for automated dynamic stability assessment," *IEEE Transactions on Power Systems,* vol. 23, pp. 680-690, 2008.
[126] G. Liu*, et al.*, "Oscillation monitoring system based on wide area synchrophasors in power systems," in *iREP Symposium*, Charleston, USA, 2007.

[127] N. Zhou*, et al.*, "Electromechanical mode online estimation using regularized robust RLS methods," *IEEE Transactions on Power Systems,* vol. 23, pp. 1670-1680, 2008.
[128] A. R. Messina and V. Vittal, "Nonlinear, non-stationary analysis of interarea oscillations via Hilbert spectral analysis," *IEEE Transactions on Power Systems,* vol. 21, pp. 1234-1241, 2006.
[129] P. Korba, "Real-time monitoring of electromechanical oscillations in power systems: first findings," *IET Generation, Transmission & Distribution,* vol. 1, pp. 80-88, 2007.
[130] S. Bruno*, et al.*, "Taking the pulse of power systems: monitoring oscillations by Wavelet analysis and wide area measurement system," in *IEEE PES Power Systems Conference and Exposition*, Atlanta, USA, 2006.
[131] D. Tufts and R. Kumaresan, "Singular value decomposition and improved frequency estimation using linear prediction," *IEEE Transactions on Acoustics, Speech and Signal Processing,* vol. 30, pp. 671-675, 1982.
[132] G. Ledwich and E. Palmer, "Modal estimates from normal operation of power systems," in *IEEE Power Engineering Society Winter Meeting*, Singapore, 2000.
[133] N. Zhou*, et al.*, "Automatic implementation of Prony analysis for electromechanical mode identification from phasor measurements," in *IEEE Power and Energy Society General Meeting*, Minneapolis, USA, 2010.
[134] Y. Hua and T. K. Sarkar, "Matrix pencil method for estimating parameters of exponentially damped/undamped sinusoids in noise," *IEEE Transactions on Acoustics, Speech and Signal Processing,* vol. 38, pp. 814-824, 1990.
[135] Y. Hua, "Parameter estimation of exponentially damped sinusoids using higher order statistics and matrix pencil," *IEEE Transactions on Signal Processing,* vol. 39, pp. 1691-1692, 1991.
[136] S. Van Huffel, "Enhanced resolution based on minimum variance estimation and exponential data modeling," *Signal Processing,* vol. 33, pp. 333-355, 1993.
[137] R. Kumaresan and D. W. Tufts, "Improved spectral resolution III: efficient realization," *Proceedings of the IEEE,* vol. 68, pp. 1354-1355, 1980.
[138] R. E. Kalman, "A new approach to linear filtering and prediction problems," *Transactions of the ASME-Journal of Basic Engineering,* vol. 82, pp. 35-45, 1960.
[139] S. Haykin, *Adaptive Filter Theory*: Prentice Hall, 2002.
[140] P. Zarchan and H. Musoff, *Fundamentals of Kalman Filtering: a Practical Approach*: American Institute of Aeronautics and Astronautics, 2005.
[141] P. Goupillaud*, et al.*, "Cycle-octave and related transforms in seismic signal analysis," *Geoexploration,* vol. 23, pp. 85-102, 1984.
[142] M. Bronzini*, et al.*, "Power system modal identification via wavelet analysis," in *IEEE Power Tech*, 2007.
[143] J. Turunen*, et al.*, "Selecting wavelets for damping estimation of ambient-excited electromechanical oscillations," in *IEEE Power and Energy Society General Meeting*, Minneapolis, USA, 2010.
[144] G. Box*, et al.*, *Time Series Analysis: Forecasting and Control*: Prentice Hall, 1994.
[145] P. Stoica and R. Moses, *Introduction to Spectral Analysis*: Prentice Hall, 1997.

[146] N. Zhou*, et al.*, "Robust RLS methods for online estimation of power system electromechanical modes," *IEEE Transactions on Power Systems,* vol. 22, pp. 1240-1249, 2007.
[147] N. E. Huang*, et al.*, "The empirical mode decomposition and the Hilbert spectrum for nonlinear and non-stationary time series analysis," *Proceedings of the Royal Society of London. Series A: Mathematical, Physical and Engineering Sciences,* vol. 454, pp. 903-995, 1998.
[148] D. S. Laila*, et al.*, "A refined Hilbert-Huang transform with applications to interarea oscillation monitoring," *IEEE Transactions on Power Systems,* vol. 24, pp. 610-620, 2009.
[149] A. T. Connie*, et al.*, "Identification of AR parameters at a very low SNR using estimated spectral distribution in DCT domain," *IEE Proceedings - Vision, Image and Signal Processing,* vol. 153, pp. 95-100, 2006.
[150] J. G. Proakis, *Algorithms for Statistical Signal Processing*: Prentice Hall, 2002.
[151] J. Xiao*, et al.*, "Dynamic tracking of low-frequency oscillations with improved Prony method in wide-area measurement system," in *IEEE Power Engineering Society General Meeting*, Denver, USA, 2004.
[152] J.-H. Lee and H.-T. Kim, "Selecting sampling interval of transient response for the improved Prony method," *IEEE Transactions on Antennas and Propagation,* vol. 51, pp. 74-77, 2003.
[153] D. B. Rao, "An explanation to the limitation observed in the Kumaresan-Prony algorithm," *IEEE Transactions on Acoustics, Speech and Signal Processing,* vol. 34, pp. 1338-1340, 1986.
[154] M. L. Van Blaricum and R. Mittra, "Problems and solutions associated with Prony's method for processing transient data," *IEEE Transactions on Electromagnetic Compatibility,* vol. EMC-20, pp. 174-182, 1978.
[155] A. J. Poggio*, et al.*, "Evaluation of a processing technique for transient data," *IEEE Transactions on Electromagnetic Compatibility,* vol. EMC-20, pp. 165-173, 1978.
[156] A. Bracale*, et al.*, "Adaptive Prony method for waveform distortion detection in power systems," *International Journal of Electrical Power & Energy Systems,* vol. 29, pp. 371-379 2007.
[157] C. Lawson and R. Hanson, *Solving Least Squares Problems*: SIAM, 1995.
[158] G. H. Golub and C. F. V. Loan, *Matrix Computations*: Johns Hopkins University Press, 1996.
[159] E. Kreyszig, *Advanced Engineering Mathematics*: John Wiley, 2006.
[160] J. Zhang*, et al.*, "Parameter estimation of exponentially damped sinusoids using HSVD based extended complex Kalman filter," in *IEEE Region 10 Conference* Hyderabad, India, 2008.
[161] K. Nishiyama, "A nonlinear filter for estimating a sinusoidal signal and its parameters in white noise: on the case of a single sinusoid," *IEEE Transactions on Signal Processing,* vol. 45, pp. 970-981, 1997.
[162] S. Y. Kung*, et al.*, "State-space and singular-value decomposition-based approximation methods for the harmonic retrieval problem," *Journal of the Optical Society of America,* vol. 73, pp. 1799-1811, 1983.
[163] D. J. Tylavsky and A. Bose, "Parallel processing in power systems computation," *IEEE Transactions on Power Systems,* vol. 7, pp. 629-638, 1992.

[164] J. M. Campagnolo*, et al.*, "Fast small-signal stability assessment using parallel processing," *IEEE Transactions on Power Systems,* vol. 9, pp. 949-956, 1994.
[165] T. Oyama*, et al.*, "Parallel processing for power system analysis using band matrix," *IEEE Transactions on Power Systems,* vol. 5, pp. 1010-1016, 1990.
[166] C. Lemaitre and B. Thomas, "Two applications of parallel processing in power system computation," *IEEE Transactions on Power Systems,* vol. 11, pp. 246-253, 1996.
[167] J. Sanders and E. Kandrot, *CUDA by Example: An Introduction to General-Purpose GPU Programming*: ADDISON WESLEY (PEAR, 2010.
[168] C. L. Chang*, et al.*, "Oscillatory stability analysis using real-time measured data," *IEEE Transactions on Power Systems,* vol. 8, pp. 823-829, 1993.
[169] S. Yan, "High speed signal processing system," in *Proceedings of the IEEE International Conference on Industrial Technology*, Guangzhou, China, 1994.
[170] M. O. Tokhi*, et al.*, *Parallel Computing for Real-Time Signal Processing and Control*: Springer, 2003.
[171] A. Grama, *Introduction to Parallel Computing*: Addison-Wesley, 2003.
[172] L. S. Blackford*, et al.*, "An updated set of basic linear algebra subprograms (BLAS)," *ACM Trans. Math. Softw.,* vol. 28, pp. 135-151, 2002.
[173] T. H. Cormen, *Introduction to Algorithms*: MIT Press, 2001.
[174] P. Kundur*, et al.*, "Power system stabilizers for thermal units: abalytical techiques and on-site validation," *IEEE Transactions on Power Apparatus and Systems,* vol. PAS-100, pp. 81-95, 1981.
[175] E. V. Larsen and D. A. Swann, "Applying power system stabilizers part I: general concepts," *IEEE Transactions on Power Apparatus and Systems,* vol. PAS-100, pp. 3017-3024, 1981.
[176] E. V. Larsen and D. A. Swann, "Applying power system stabilizers part III: practical considerations," *IEEE Power Engineering Review,* vol. PER-1, pp. 63-63, 1981.
[177] E. V. Larsen and D. A. Swann, "Applying power system stabilizers part II: performance objectives and tuning concepts," *IEEE Power Engineering Review,* vol. PER-1, pp. 63-63, 1981.
[178] B. Chaudhuri and B. C. Pal, "Robust damping of multiple swing modes employing global stabilizing signals with a TCSC," *IEEE Transactions on Power Systems,* vol. 19, pp. 499-506, 2004.
[179] Z. Yang and A. Bose, "Design of wide-area damping controllers for interarea oscillations," *IEEE Transactions on Power Systems,* vol. 23, pp. 1136-1143, 2008.
[180] P. Kundur*, et al.*, "Application of power system stabilizers for enhancement of overall system stability," *IEEE Transactions on Power Systems,* vol. 4, pp. 614-626, 1989.
[181] P. Kundur, "Effective use of power system stabilizers for enhancement of power system reliability," in *IEEE Power Engineering Society Summer Meeting*, Edmonton, Canada, 1999.
[182] H. Ni, "Robust Damping Controller Design for Larger Power Systems using Wide Area Measurements," PhD thesis, Arizona State University, Phoenix, USA, 2002.

[183] C. He*, et al.*, "Wide-area robust H infinity control with pole placement for damping inter-area oscillations," in *IEEE PES Power Systems Conference and Exposition*, Seattle, USA, 2006.
[184] W.-S. Kao, "The effect of load models on unstable low-frequency oscillation damping in Taipower system experience w/wo power system stabilizers," *IEEE Transactions on Power Systems,* vol. 16, pp. 463-472, 2001.
[185] DIgSILENT, "DIgSILENT technical documentation ver. 13.2," DIgSILENT GmbH, 2007.
[186] D. Ruisheng, "Power System Online Security Assessment using Synchronized Phasor Measurements and Decision Trees " PhD thesis, Arizona State University, Phoenix, USA, 2009.
[187] L. Lai, *Power System Restructuring and Deregulation: Trading, Performance and Information Technology*: John Wiley, 2001.
[188] A. Mazer, *Electric Power Planning for Regulated and Deregulated Markets*: IEEE Press, 2007.
[189] R. Schainker*, et al.*, "Real-Time Dynamic Security Assessment: Fast Simulation and Modeling Applied to Emergency Outage Security of the Electric Grid," *IEEE Power and Energy Magazine,* vol. 4, pp. 51-58, 2006.
[190] E. Santacana*, et al.*, "Getting Smart," *IEEE Power and Energy Magazine,* vol. 8, pp. 41-48, 2010.
[191] "Telecommunications and networking programme (TNP)," Transpower New Zealand Limited, 2010.